INFORMATION TO USERS

The most advanced technology has been used to photograph and reproduce this manuscript from the microfilm master. UMI films the original text directly from the copy submitted. Thus, some dissertation copies are in typewriter face, while others may be from a computer printer.

In the unlikely event that the author did not send UMI a complete manuscript and there are missing pages, these will be noted. Also, if unauthorized copyrighted material had to be removed, a note will indicate the deletion.

Oversize materials (e.g., maps, drawings, charts) are reproduced by sectioning the original, beginning at the upper left-hand corner and continuing from left to right in equal sections with small overlaps. Each oversize page is available as one exposure on a standard 35 mm slide or as a 17″ × 23″ black and white photographic print for an additional charge.

Photographs included in the original manuscript have been reproduced xerographically in this copy. 35 mm slides or 6″ × 9″ black and white photographic prints are available for any photographs or illustrations appearing in this copy for an additional charge. Contact UMI directly to order.

UMI
Accessing the World's Information since 1938

300 North Zeeb Road, Ann Arbor, MI 48106-1346 USA

Order Number 8825918

Formation of bcc non-equilibrium La, Gd and Dy alloys and the magnetic structure of Mg-stabilized βGd and βDy

Herchenroeder, James W., Ph.D.

Iowa State University, 1988

U·M·I
300 N. Zeeb Rd.
Ann Arbor, MI 48106

Formation of bcc non-equilibrium La, Gd and Dy alloys and the magnetic structure of Mg-stabilized βGd and βDy

by

James W. Herchenroeder

A Dissertation Submitted to the
Graduate Faculty in Partial Fulfillment of the
Requirements for the Degree of
DOCTOR OF PHILOSOPHY

Department: Materials Science and Engineering
Major: Metallurgy

Approved:

Signature was redacted for privacy.

In Charge of Major Work

Signature was redacted for privacy.

For the Major Department

Signature was redacted for privacy.

For the Graduate College

Iowa State University
Ames, Iowa

1988

TABLE OF CONTENTS

INTRODUCTION

The rare earth metals are known to exhibit complex magnetic character, especially below room temperature. Ferromagnetism, ferrimagnetism and antiferromagnetism all exist in one or more rare earth element. One reason for this diversity is that at these temperatures most of the rare earths have an anisotropic crystal field produced by a hexagonal close-packed (or dhcp) crystal structure. The crystal field interacts with the orbital magnetic moment of the electrons to produce the varied magnetic alignments.

In the absence of crystal field - orbital interactions one might expect simpler magnetic structures. Gd, which has the hcp structure, has no orbital magnetic moment (L=0), and therefore no crystal field interactions, which results in a simple ferromagnetic structure. Divalent Eu, which is bcc at all temperatures, also has L=0, but is a spiral antiferromagnet. A third case of interest would be a more symmetrical structure like bcc Eu but with a nonzero L.

One way to achieve this third combination is found in the allotropy of the rare earth metals. While the rare earths (excluding Eu and Sm) are hcp or dhcp at room temperature and below, nearly all of them transform just below the melting point to a bcc structure. The magnetic ordering is destroyed at these higher temperatures, yet the bcc structure can be stabilized at room temperature by alloying and rapid cooling from the high temperature regions.

The stabilization of a rare earth bcc allotrope was first done by Gibson and Carlson[1] by quenching a Y-Mg alloy from the high temperature bcc solid. Later, Miller and Daane[2] showed that the bcc allotropes of

other heavy rare earths could be retained with Mg alloying and ice water quenching from the liquid state. They were even successful in obtaining bcc structures for rare earths subsequently shown[3] not to have a bcc allotrope in the pure elemental form. Finally, Manfrinetti[4] was able to produce bcc La-Mg and Gd-Mg alloys by ice water quenching from the solid state.

In order to approximate the magnetic properties of a pure bcc rare earth metal, the amount of alloying should be minimized. This goal can be achieved in two basic ways. The first method involves searching for the alloying element(s) that stabilizes the bcc phase at the lowest concentration. A prerequisite for alloying is high solubility in the bcc phase. Group II metals, e.g., Mg, have extensive solubilities in the rare earth bcc phase, and these solubilities are the highest of all the elements. Other elements (e.g., Group IIIB metals) also have extensive solubilities, as well, which suggest their use as bcc stabilizers. By varying the alloying element, one can vary the electronic structure (different valence) or the atomic spacing (different size) both of which will affect the degree of stabilization.

The second method is to vary the type of quench. The rate of quench is probably the most important variable and can vary from ~10^2 K/s (ice-water) to ~10^5 K/s (melt spinning). The starting state can be either a liquid melt or a solid bcc alloy which also affects the quenching characteristics. The best quench is not necessarily the fastest, but the one that allows retention of the bcc phase to the lowest composition.

This study is divided in two parts. Part I is devoted to the metallurgy involved in forming stabilized bcc rare earth alloys. The effects of alloying element, M, and quench are reported for La-M binary

alloys. The techniques developed are then extended to two systems, Gd-Mg and Dy-Mg, that include a magnetic rare earth element. The thermal stability of the non-equilibrium bcc phase is also discussed.

The Gd-Mg and Dy-Mg alloys show surprisingly complex behavior combining ferromagnetism, antiferromagnetism and spin glass orderings due to the change of crystal structure plus Mg dilution. Part II describes low temperature (4-300 K) magnetic susceptibility and heat capacity (1.5-60 K) measurements which distinguish between the different ordering types. Bcc Gd-Mg alloys show reentrant spin glass behavior with a mixed ferromagnetic and spin glass structure. The Dy-Mg alloys have a mixed antiferromagnetic and spin glass structure.

Bcc La-Mg alloys are superconducting below 5 K and are discussed in Appendix A.

EXPERIMENTAL PROCEDURES

Alloy Preparation

Materials

Alloys were made from the pure starting materials. The rare earth metals --La, Gd and Dy-- were produced by the Materials Preparation Center at the Ames Laboratory. Generally, the total transition metal impurity content was less than 30 ppm atomic. The total rare earth impurity was less than 10 ppm atomic. Depending on the metal, total interstitial impurities (O, N, and H) ranged from approximately 500 to 1000 ppm atomic. Sometimes different lots were used, but the amount of impurities was always similar. Complete impurity tables are in Appendix B.

The alloying metals were obtained from various sources. Cd, Zn, In and Tl were obtained from commercial sources reported to be at least 99.995 at.% pure. Mg and Ca were sublimed from commercial stock and were 99.998 at.% pure. Hg was not analyzed but was triply distilled.

Usually the materials as procurred were not in a readily usable form. The shape of the material had to be modified to fit into a tantalum capsule (see below) 6 mm in diameter. La and Dy were available in large bulk form. The proper diameter for these materials was obtained by cutting and grinding, by swaging, or by drop casting in an arc melter. Gd was only available in beads larger than 6 mm in diameter, so the beads were drop cast to the proper diameter. In all cases the final pieces were electropolished in a methanol/6% perchloric bath at -60°C before use in an alloy.

Mg and Ca were available as small sublimed crystals and could be used directly as obtained. Tl, In, Cd and Zn were rolled into thin sheets that

could be easily cut by scissors into small pieces. These metals were cleaned prior to weighing with a solution containing 45 ml H_2O_2 and 7.5 ml H_2SO_4 in 100 ml of water. Hg in liquid form was dispensed using micro-pipettes.

Melting and annealing

Alloys were made by melting the pure components, approximately 3 g total weight, in sealed thin-walled (0.2 mm) tantalum under a helium partial pressure. The small sample mass was used to maximize heat removal during the quenching step. The capsules were cylindrical with a diameter of 6 mm and about 35 mm long so that the sample occupied from one third to one half of the available volume. This shape was used as a compromise between convenience and the importance of having a large surface to volume ratio for rapid ice water quenching. The alloy name and actual composition for the Gd and Dy alloys are listed in Table I.

Table I. Overall compositions of βGd and βDy alloys (atomic percent)

Alloy	%Mg
Gd-23Mg	23.64
Gd-26Mg	25.97
Gd-28Mg	27.47
Gd-29Mg	29.02
Dy-27Mg	27.25
Dy-28Mg	27.96
Dy-29Mg	28.99

Actual melting was done in one of two ways. The capsules with La alloys were sealed in quartz tubes under a partial pressure of He and melted in a resistance furnace. Because of their higher melting points, the Gd and Dy alloys were melted in a vacuum induction furnace. In both cases, the alloys were heated to 100°C above the melting point of the rare

earth metal. Then the alloys were cooled, inverted and remelted to insure homogeneity.

Annealing prior to quenching in ice water was done in the same tantalum capsules (sealed in a quartz tube) used for melting. Twenty to thirty minutes at temperature was sufficient to provide a single phase starting material. Some annealing (for thermal analysis) was done on samples cut from the melted alloys. These samples were electropolished and enclosed in quartz before heating in a resistance furnace.

Quenching

Three types of quenching were used: ice water, liquid metal and melt spinning. For a quench from the liquid state, the alloy was heated to at least 25°C above the alloy's melting point. The temperatures were determined from phase diagrams when available. For unknown systems, the melting points could be determined visually, and the bcc phase field was estimated from known systems. The quench was accomplished by quickly breaking the quartz tube such that the capsule would fall into an ice water or ice water/acetone bath.

The liquid metal quench is based on the presumption that better thermal contact is achieved between two metals than a metal and water. In this case a Ga-In eutectic melt, liquid at 16°C, was used as the quench bath. A thin slice (1 mm thick) cut from the premelted alloy was suspended in a specially constructed vacuum furnace. The slice was heated into the bcc phase field and then rapidly pushed into the Ga-In bath while still under vacuum. This method is restricted to solid state quenching because of the high solubility of Ga and In in the rare earth metals.

Melt spinning is a much faster technique than the other two reaching cooling rates of 10^5 K/s. In the basic form a molten alloy is forced

through a small orifice onto a rotating copper wheel which provides the rapid cooling. This method is severely limited in this study because the alloying elements have low boiling points and consequently high vapor pressure. Often the melting point of an alloy is higher than the boiling point of the stabilizing element. Melt spinning by necessity has an open melting chamber, so volatilization of the stabilizing element occurs, effectively undoing the alloying process. Melt spinning was used successfully in the La-Mg system (low melting point) but could not be used with the higher melting Gd and Dy alloys.

Typical cooling curves for these three types of quenching might schematically look like Fig. 1. The slowest quench would be the ice water quench from either the solid or liquid state. Some heat is lost transferring a sample from the furnace to the quench bath, and some slow cooling occurs during quartz breakage before the sample becomes completely immersed. This slow cooling is depicted by the initial transients on the schematic curves. For a liquid quench, the transient allows the bcc phase to form from the liquid, but for a solid quench this slow cooling step may drop the temperature below the eutectoid temperature allowing the equilibrium transformation to begin. The maximum rate of cooling for the ice water quenches and the Ga-In quench should be similar, although the Ga-In quench is advantageous because of the lack of the initial transient.

Sample Preparation

Tantalum removal

During melting a degree of bonding takes place between the alloy and the tantalum walls. For the La alloys this bond is relatively weak (the melting temperature is lower than the Gd and Dy alloys), so the tantalum

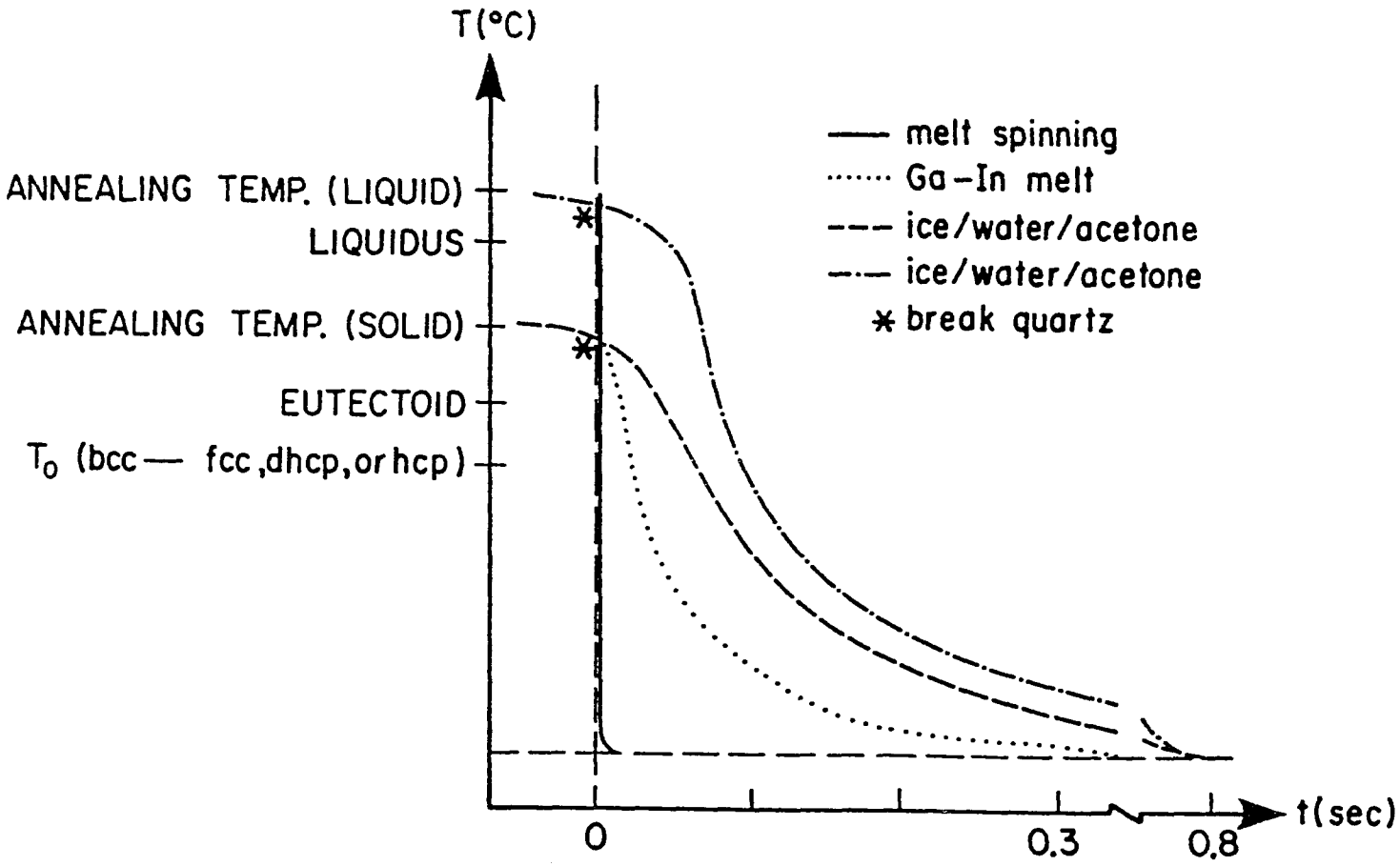

Figure 1. Typical cooling curves for quenching La-M alloys.

can be peeled off the alloy after the end caps are cut off and a cut along the length of the capsule is made. The bonding is stronger for the Gd and Dy alloys, so grinding is the only method of tantalum removal. There was some concern that this extensive cold work might cause the nonequilibrium bcc phase to revert to the equilibrium close-packed phase, but no evidence of this type of reversion was found. Finally the alloys were electropolished to to remove any surface damage.

Sectioning

Alloy ingots were 6 mm in diameter and 10 to 20 mm long. A thin slice for x-ray diffraction analysis was cut using a low speed diamond saw from the center of the ingot parallel to the cylindrical axis. This same slice was used for metallography as well. The remaining pieces were used for magnetic susceptibility, heat capacity, DTA or annealing samples.

Handling

All the alloys had some degree of air sensitivity. The alloys containing Mg could be passivated by electropolishing and be stored in air for long periods. The La-M alloys where M is Zn, Cd, In and Tl were all air sensitive. None of these alloys could be passivated by electropolishing, so vacuum storage was required although the alloys could be handled in air for short periods (< 1 hour). La-Hg alloys exhibited surface oxidation after one minute in air, and samples would completely oxidize in a matter of hours. A clean surface could be obtained by electropolishing using a methanol rinse at -60°C. After rinsing, the alloy was immediately placed in a bath of outgassed diffusion pump oil and taken into a He dry box. Even with these precautions, some surface oxidation occurred.

Apparatus

A variety of equipment was used in this study, and for most only brief descriptions are necessary.

Ga-In quench furnace

A special furnace was designed and built to perform quenches into a Ga-In liquid metal bath (Fig. 2). The heater was a tungsten wound alumina tube surrounded by tantalum radiation shields. At ten amps (110 V) the heater would reach 1100°C. Temperature measurement was made by a chromel/alumel thermocouple. The temperature was uniform along the length of the heating element so sample contact was not required for temperature measurement. The heater was suspended in a vacuum chamber that reaches a maximum vacuum of 10^{-6} torr with a diffusion pump.

The sample was suspended by 10 mil tantalum wire from a stainless steel rod. After an appropriate anneal at the temperature of interest the rod was pushed down submersing the sample in the Ga-In bath. The bath was about one cubic inch in volume and was contained in a large brass cup. The cup was kept cool externally with chilled water.

X-ray diffractometer

X-ray diffraction was done on a standard rotating diffractometer using Cu Kα radiation. Bulk samples were used instead of powders because powder formation would introduce extensive cold work which could not be annealed out without transforming the alloys to the equilibrium state. The surface of the slices were prepared by grinding through 600 grit paper and then electropolishing. The samples were spun during the diffraction scans to minimize preferred orientation effects.

A special sample holder was designed for the air sensitive samples.

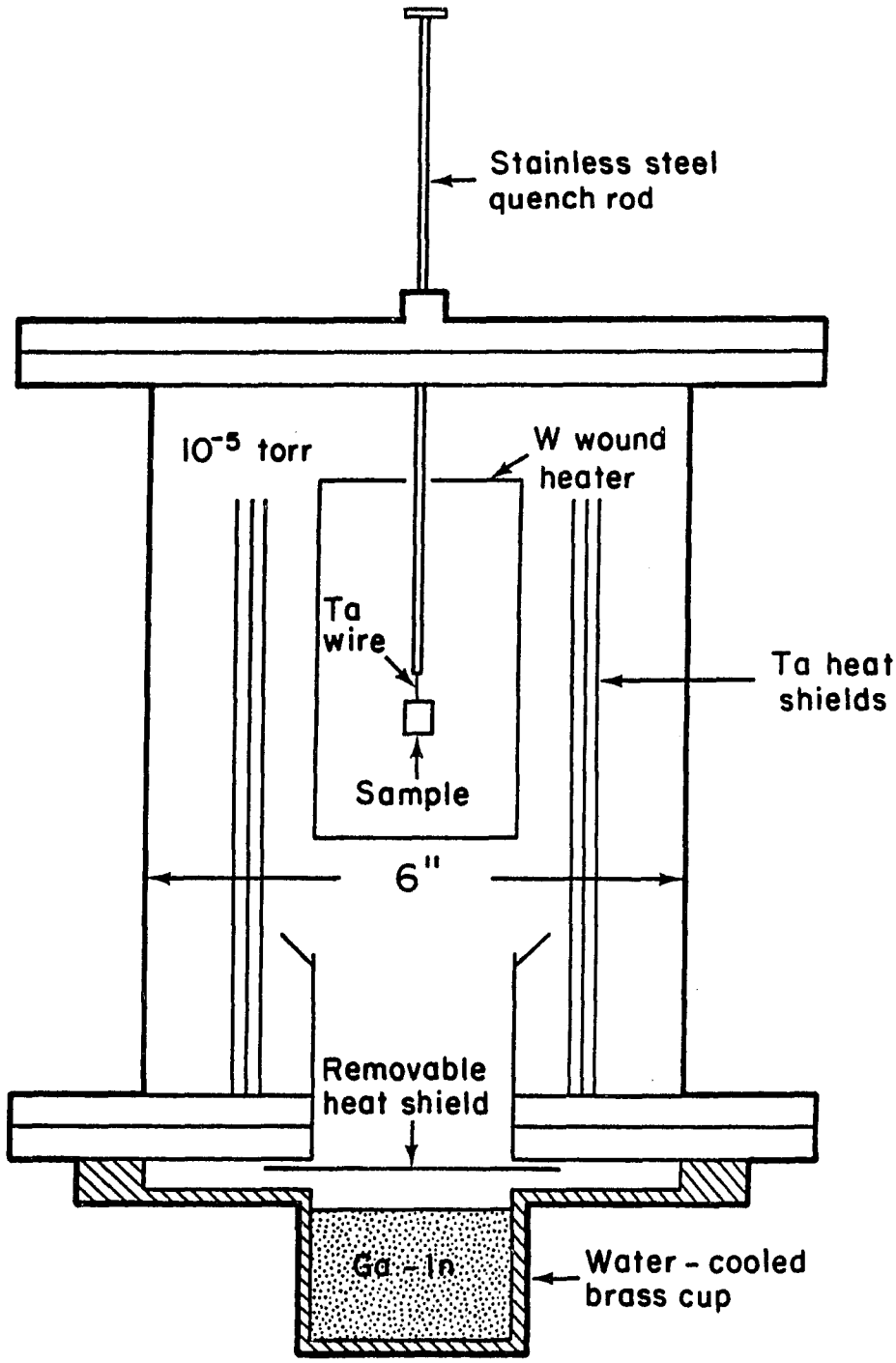

Figure 2. Vacuum quenching furnace with Ga-In quench bath.

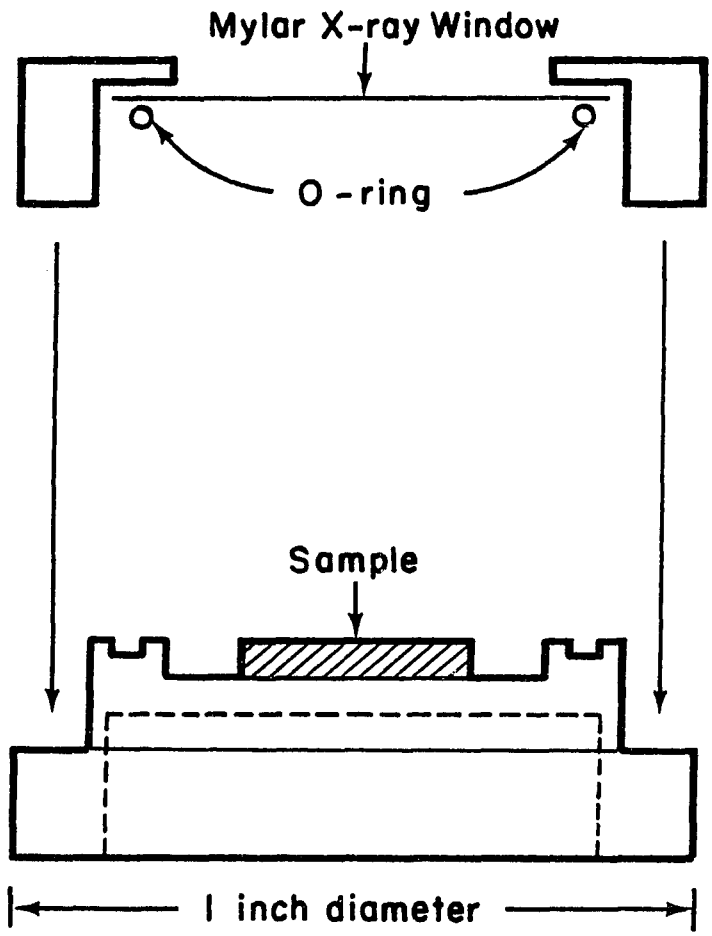

Figure 3. Airtight sample holder for x-ray diffraction.

A closed chamber was built (Fig. 3) using an O-ring seal. An aluminized Mylar film was used as the x-ray window. Tests on quartz powder showed that intensity of the diffraction peaks with the film decreased little (0 to 10 %) compared to scans without the film. Air sensitive samples were loaded into the sample holder in a glove box to eliminate surface oxidation. The He (from the glove box) atmosphere inside the holder would remain overnight.

Differential Thermal Analysis

Some differential thermal analysis was done on a Perkin-Elmer system in Dr. McCallum's group. The thermocouples are calibrated with melting point standards at various temperatures. Reproducibility is generally ±2°C. Other measurements were done on a DuPont system at the ISU Engineering Research Institute Materials Lab. Both systems are comparable.

Magnetic Susceptibility

Magnetic susceptibility was measured with three devices. High field (0.5 to 1.4 T) measurements were made in a Faraday balance rig described elsewhere.[5,6] The accuracy of the Faraday rig depends on knowing the field gradient which in this case is produced by specially machined pole faces.[5] A complete calibration is described in Appendix C.

Low field measurements (< 0.05 T) were made on the Quantum Design SQUID magnetometer in Dr. Johnston's group. In this case, volume susceptibility is measured instead of gram susceptibility so direct comparison of the two types of data requires a density factor. The number used is the density calculated from x-ray lattice parameters.

AC susceptibility was measured at extremely low fields (2.5×10^{-6} T) at 100 Hz in the rig in Dr. Finnemore's group between 4.2 and 200 K.

Calorimeter

Heat capacity was measured from 1.2 to 60 K in a semi-adiabatic pulse calorimeter described in detail elsewhere.[7] The sample size for all the alloys was approximately 1 gram. The rare earth-Mg alloys have poor thermal conductivity, so in order to reach thermal equilibrium at temperatures above 30 K a delay of up to 40 seconds was used between the heat pulse and temperature measurement. No delay was needed at lower temperatures.

PART I. FORMATION OF BCC NON-EQUILIBRIUM La, Gd AND Dy ALLOYS

BCC PHASE RETENTION

In the rare earth metals the bcc phase occurs just below the melting point of the metal. In addition the range of temperature in which the bcc allotrope exists is narrow, e.g., ΔT_{bcc} for La is just 53°C. Rapid cooling of the pure element is insufficient to retain the bcc structure at room temperature. The most viable alternative is to alloy the rare earth metal with another metal which stabilizes the bcc structure.

Potential Bcc stabilizers

A good bcc stabilizer is one that expands the bcc phase field in much the same way that Ni stabilizes the γFe fcc structure in steels. One measure of stabilization is the maximum solubility of the stabilizer in the bcc phase. High solute concentrations is an indication that the bcc structure is becoming more preferred and will make bcc retention by quenching easier. In addition high solubility allows a wide range of alloy compositions from which the composition effect can be determined.

A second desirable property of a bcc stabilizer would be to lower the bcc to close packed phase transformation temperature. As this transformation temperature is lowered, diffusion processes slow down which makes suppression of the transformation by quenching easier.

Third, ideally the bcc stabilizer would have low chemical reactivity with the rare earth solvent; e.g., the rare earth and the stabilizer should form few compounds. Assuming extensive solubility exists, the formation of compounds and their stoichiometry limit what the maximum solubility will be. If the two elements have a high affinity for each other, then a high driving force for the nucleation and precipitation of

the compound during quenching will exist which may trigger the equilibrium transformation.

Finally, the stabilizer should increase the temperature width, ΔT_{bcc}, of the bcc phase. From a practical standpoint, this type of expansion makes the formation of the bcc phase by annealing or by cooling from the liquid much easier. Not all the potential stabilizers meet all the above criteria. For example, Hg does not appreciably expand the bcc phase field as discussed below, and it is highly reactive, but it does have high solubility and does well in lowering the bcc to close packed transition termperature.

Which elements would make good stabilizers? For high solubility, there must be size compatibility. The classical Hume-Rothery rule is still a good measure of size effects. Elements with size differences of 15% or less, as measured by the atomic radii, will be the best candidates.

Electron concentration is another important factor. Divalent Eu is bcc at all temperatures while the other rare earth metals all have close packed room temperature structures. One might expect then that elements that reduce the electron concentration of the alloy, i.e., Groups I and II, would be good stabilizers. However, Yb which is also divalent, is fcc at room temperature, so decreasing electron concentration is not a sufficient condition.

As discussed above chemical reactivity should be limited. A convenient scale is electronegativity. To avoid compound formation, electronegativities of the elements should be similar. In terms of the Periodic table, the elements should be close to each other, so Group IIA elements would be preferred over Group IIB with regard to reactivity. Table II summarizes size and electronegativity differences for seven

potential stabilizers.

Using these arguments, elements from Groups II and III plus monovalent Au and tetravalent Pb were considered. La was chosen as the initial solvent because of its comparatively low melting point and because of the high proportion of known phase diagrams. The best bcc stabilizer for La would then be used to stabilize bcc Gd and Dy.

Table II. Size, r, and electronegativity, e, for seven potential stabilizers with respect to La (from ref. 8)

Element	e	Δe	r	Δr (%)
La	1.12	0.00	1.877	0.000
Ca	1.02	-0.10	1.974	0.052
Mg	1.23	0.11	1.602	-0.147
Zn	1.66	0.54	1.394	-0.257
Cd	1.58	0.46	1.568	-0.165
Hg	1.78	0.66	1.594	-0.153
Tl	1.86	0.74	1.716	-0.086
In	1.82	0.70	1.666	-0.112

The phase diagrams for the La-M systems are shown in Figs. 4-11 where M is a potential bcc stabilizer. Four of the La-M systems are not well known so the Pr-M phase diagrams have been substituted in these cases (M=Au, Zn, Hg and Ga). No substitute could be found for Ca. Pr and La are similar metals (e.g., melting points are 931 and 918°C, respectively) so despite some small differences in equilibrium features such as solubility limits and critical temperatures, the general thermodynamic considerations for a given M obtained from phase diagrams should be similar whether La or Pr is the actual solvent. La has three allotropes. At room temperature the α structure is dhcp which transforms on heating to fcc β at 310°C. At 865°C La transforms to bcc γ before melting at 918°C. Pr has only two allotropes, bcc β at higher temperatures and dhcp α at

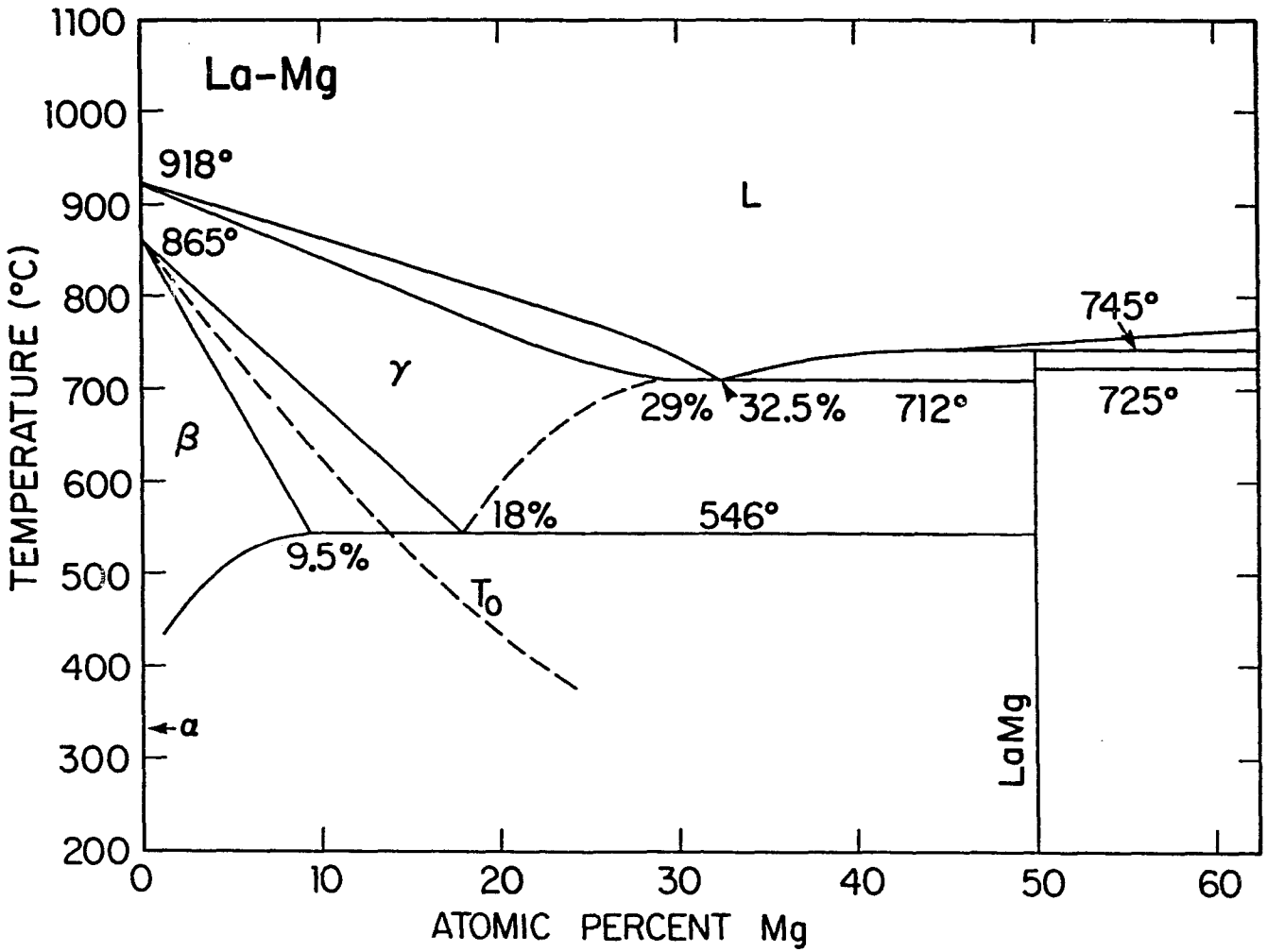

Figure 4. The La-rich end of the La-Mg system.[9]

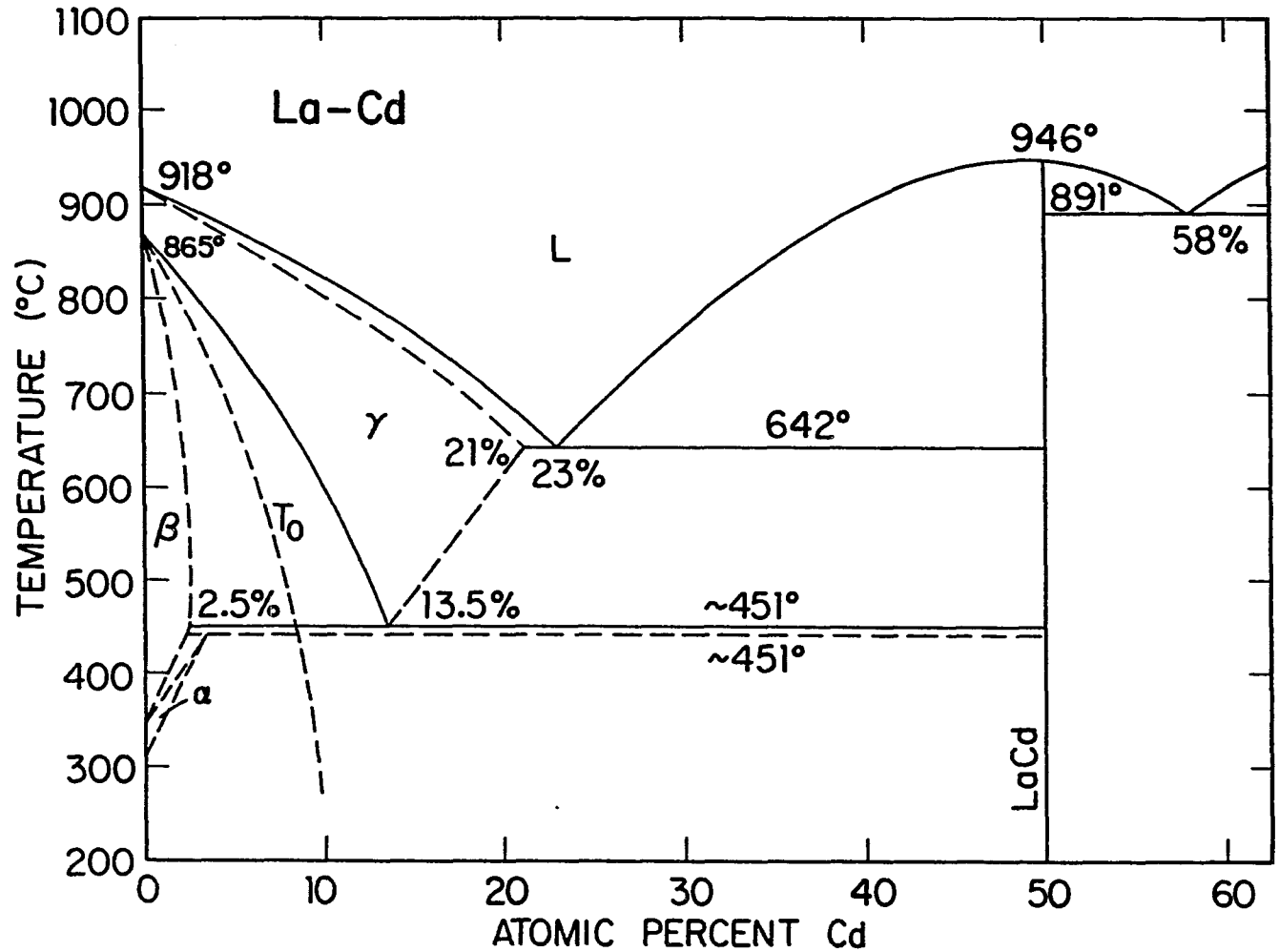

Figure 5. The La-rich end of the La-Cd system.[10]

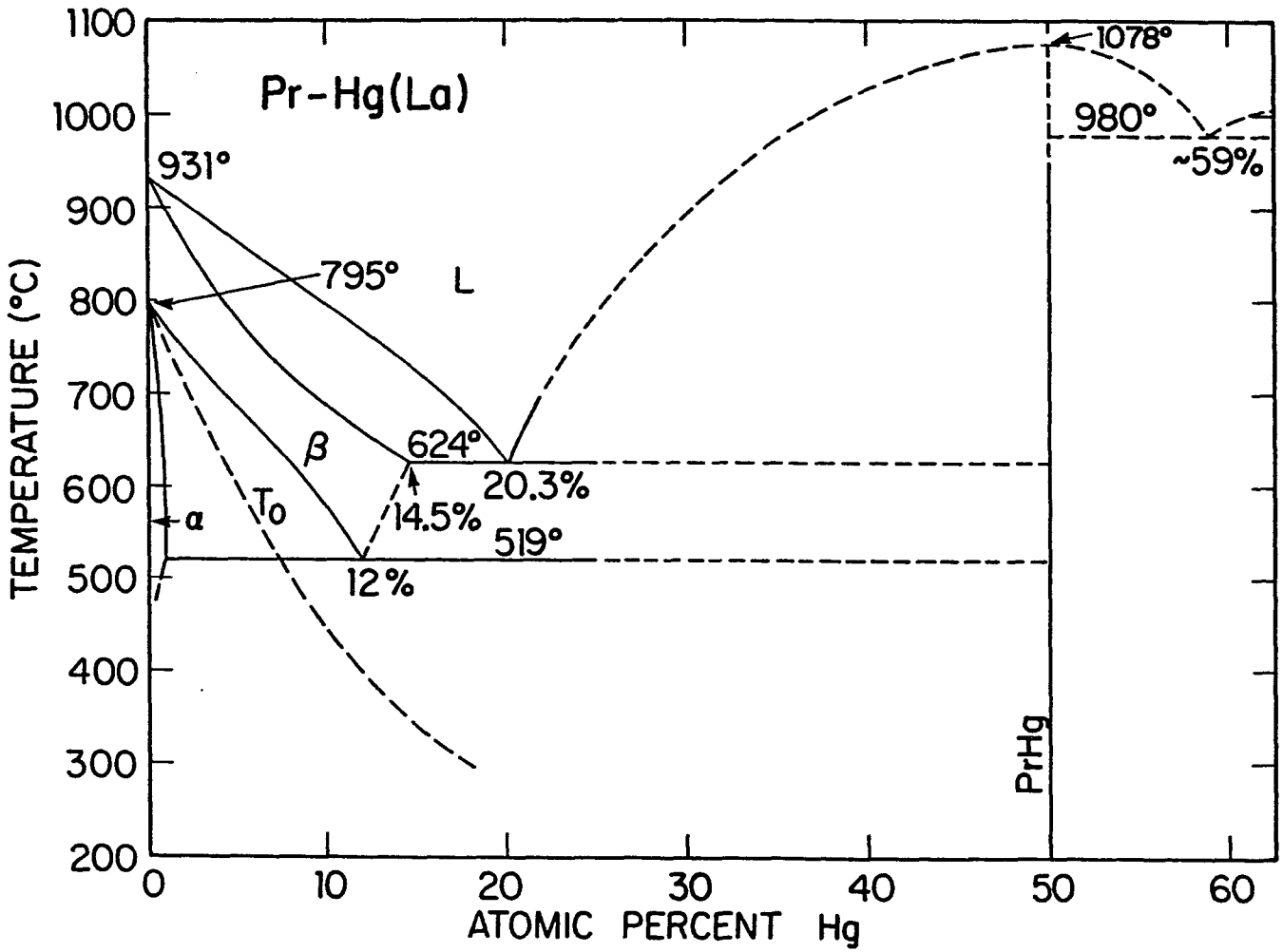

Figure 6. The Pr-rich end of the Pr-Hg system.[11] The phase relationships at concentrations greater the 30% Hg are taken from the known Hg-rich La-Hg system.[12]

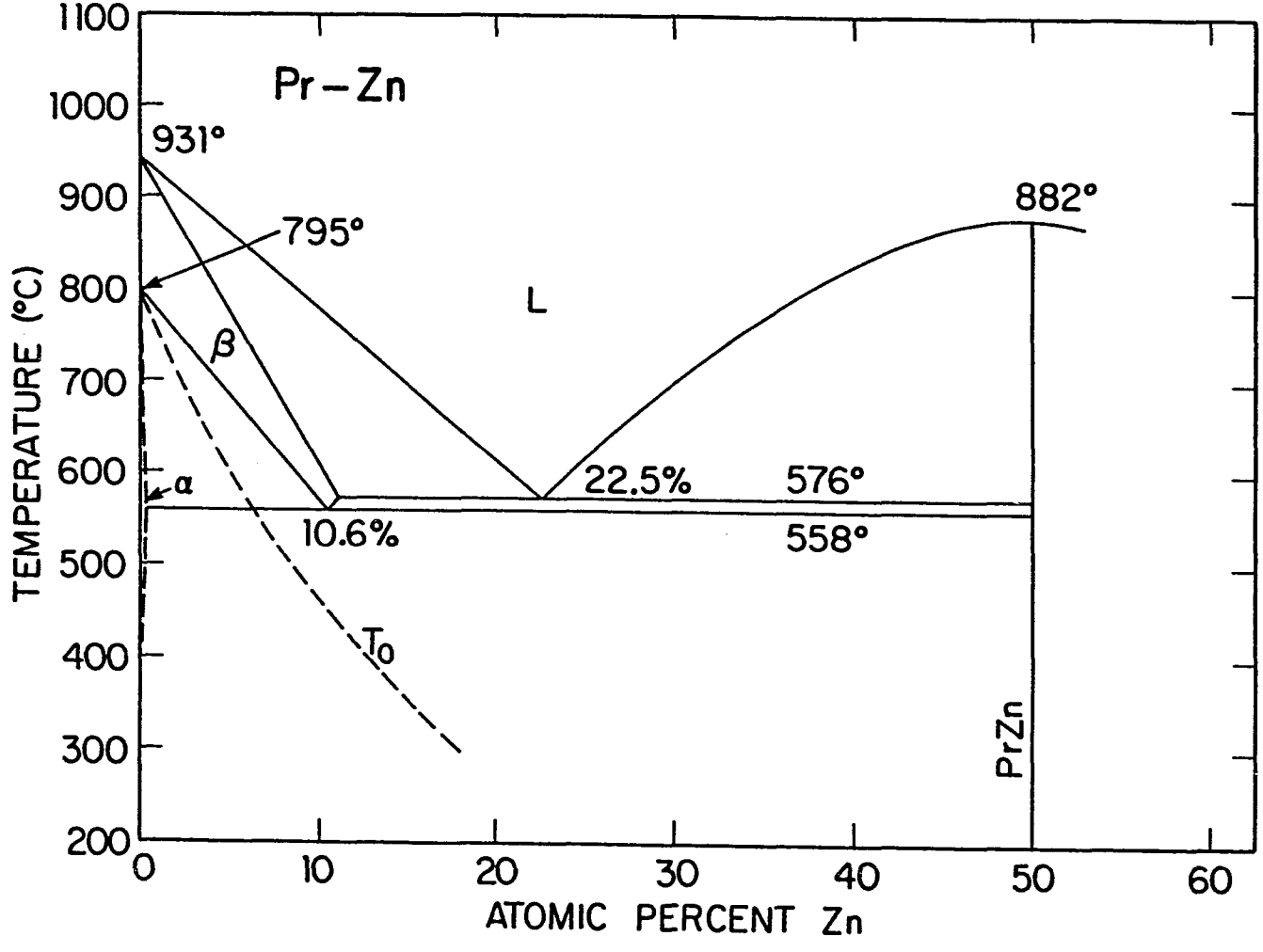

Figure 7. The Pr-rich end of the Pr-Zn system.[13]

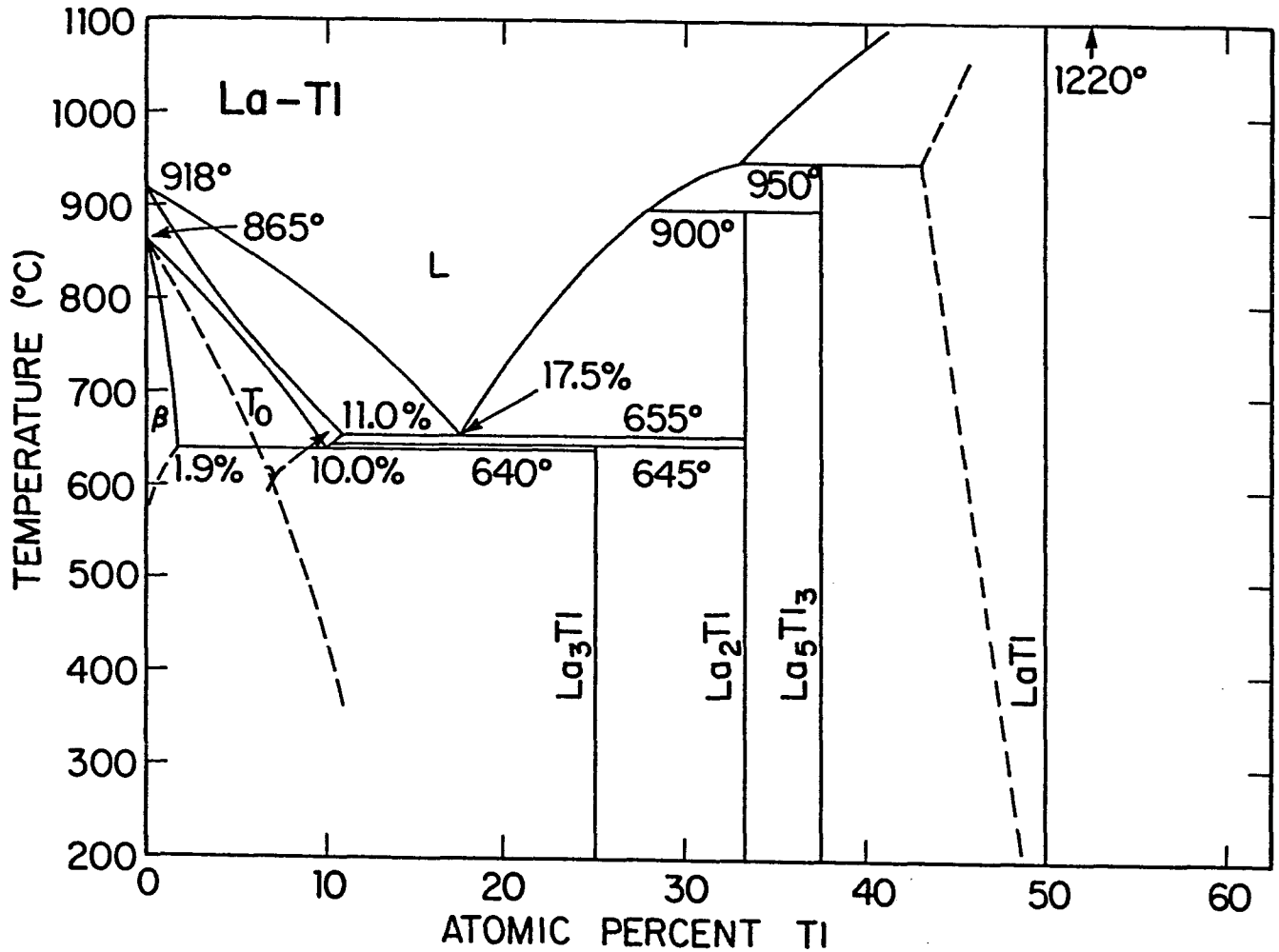

Figure 8. The La-rich end of the La-Tl system.[14]

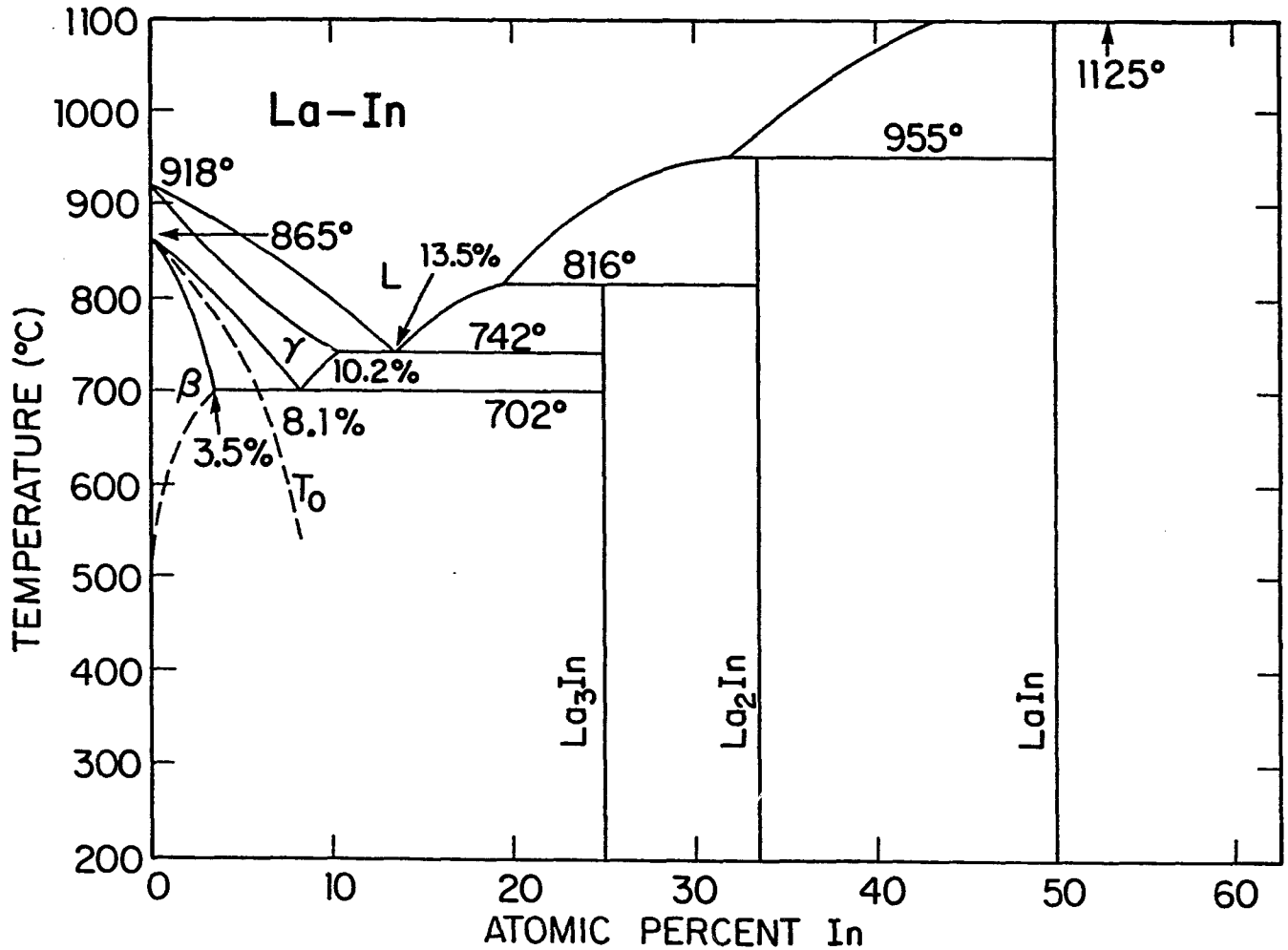

Figure 9. The La-rich end of the La-In system.[15]

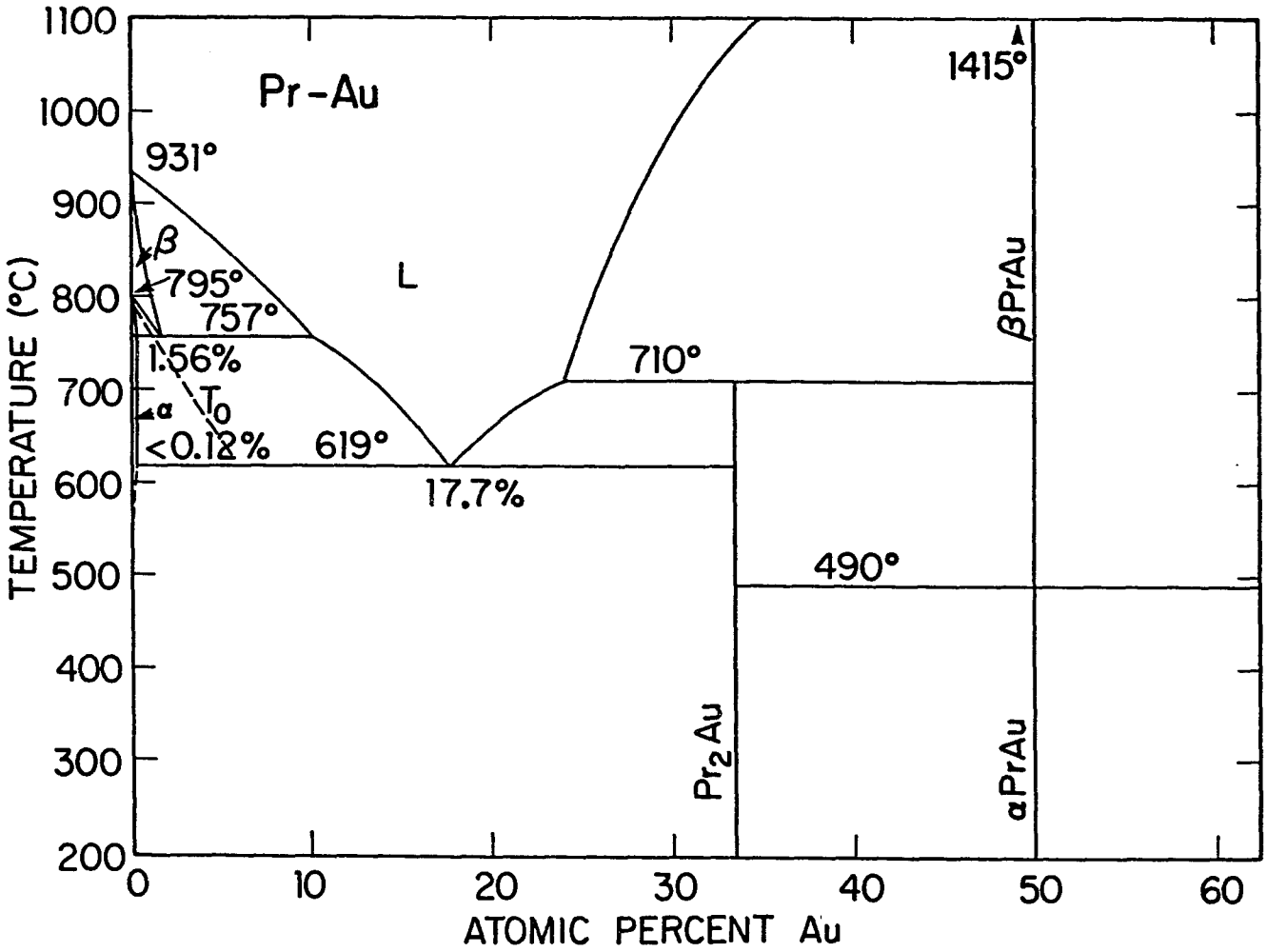

Figure 10. The Pr-rich end of the Pr-Au system.[16]

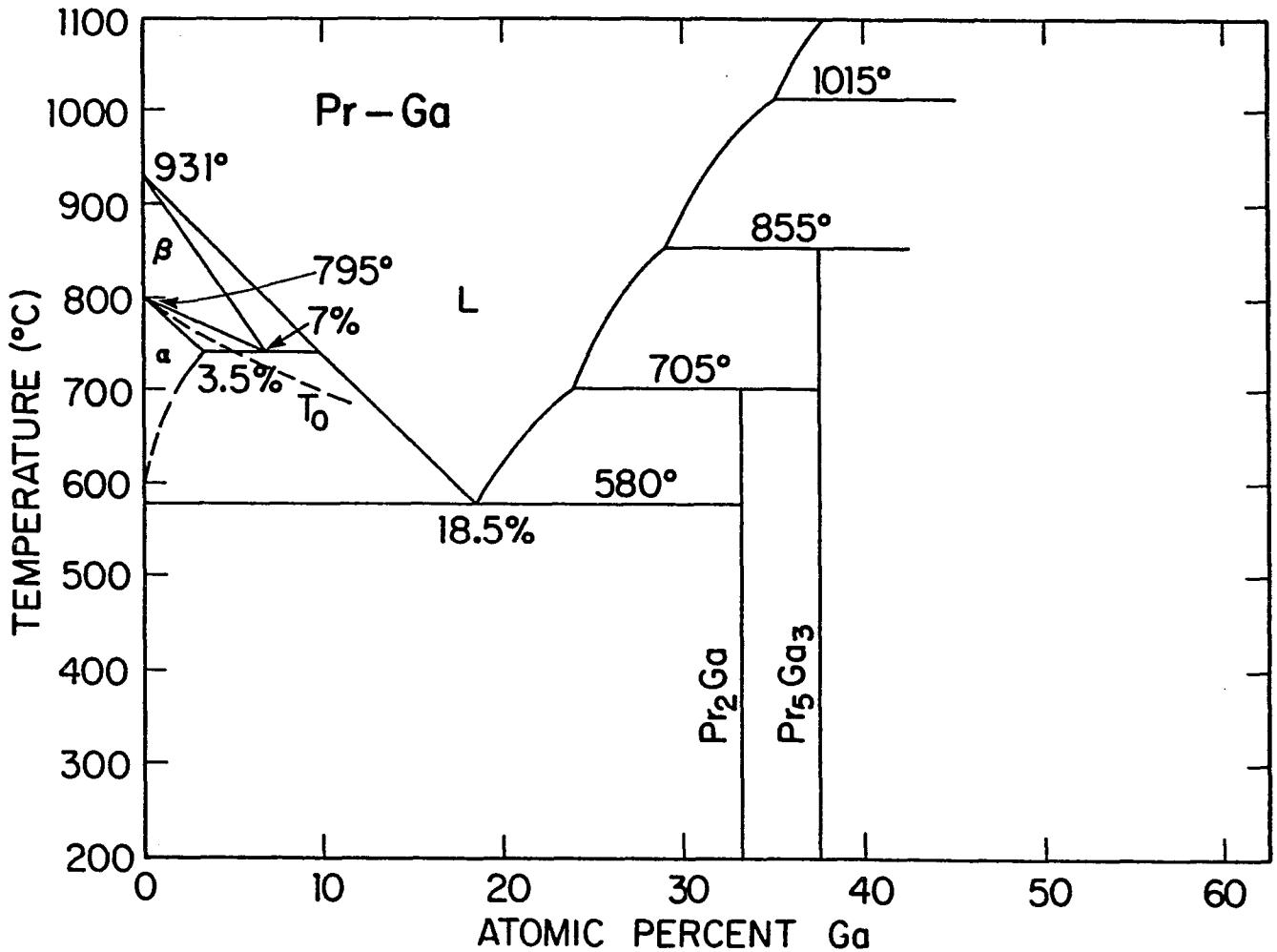

Figure 11. The Pr-rich end of the Pr-Ga system.[17]

room temperature.

Not surprisingly, the divalent metals Mg, Zn, Cd and Hg are the most effective stabilizers of γ-La (β-Pr) having the best combination of size, reactivity and electron count. These metals form eutectoid systems with a eutectoid composition greater than 10 at.%. All of these elements lower the $\gamma \rightarrow \beta$ transformation temperature by over 300°C at the eutectoid composition. Only two of the elements, Cd and Mg, expand the γ region as measured by ΔT_{bcc} where for the alloy systems $\Delta T_{bcc} = T_{eutectic} - T_{eutectoid}$ (Fig. 12, ΔT_{bcc}=53°C for pure La). With this rough measure of phase field width, it can be seen that Mg and Cd both greatly expand the bcc field (ΔT = 166 and 191°C, respectively), Hg has little effect, and Zn although it has 10% solubility actually closes up the γ field. In these systems the first compound is at 50 at.% M which helps increase the maximum solubility.

Trivalent Tl and In also form eutectoid phase diagrams but are not as effective as the divalent metals. The atomic sizes meet the Hume-Rothery criterion, but the alloy electron concentration remains constant. In addition Tl and In are more reactive as illustrated by larger electronegativity differences. The transformation temperature depressions are on the order of 150-200°C while the eutectoid solubility also decreases compared to Group II metals. Both systems have narrow bcc fields with ΔT_{bcc} decreasing indicating γ closure. Tl and In also have a greater tendency to form compounds. The closest compound contains 75 at.% La which cuts down on bcc solubility.

Trivalent Ga, as well as Pb and Au form inverted peritectics instead. These three metals all close off the bcc region and are not stabilizers. Pb probably fails because it increases the electron concentration. Both

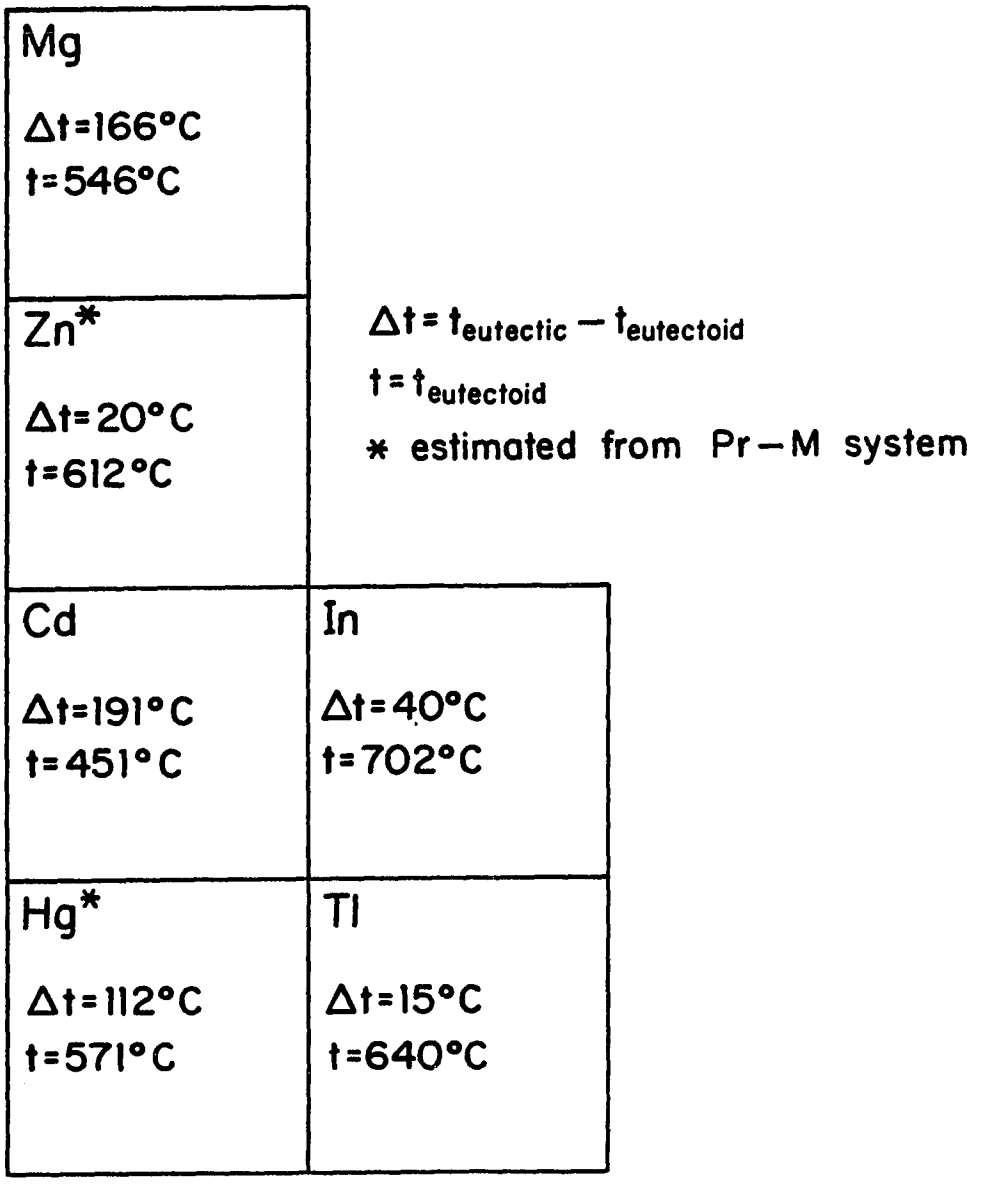

Figure 12. Summary of the important parameters for the γLa phase region for the La-M systems (M = Mg, Zn, Cd, Hg, In and Tl). Δt is the effective width of the γLa solid solution region and t is the eutectoid temperature (taken from the preceding phase diagrams).

Ga and Au are too small by the Hume-Rothery criterion to have extensive solubility. In addition, Ga does not decrease the electron concentration, and although Au does, it has a strong tendency to form compounds.

Only the eutectoid systems were investigated as possible bcc retainers. These systems include five divalent metals -- Mg, Ca, Zn, Cd and Hg -- plus trivalent In and Tl.

Kinetic Considerations

Diffusion

In the pure metal only short range atom movements are needed for the bcc to close packed transition. In the La-M systems described above there is extensive solubility of M in the bcc phase, but there is virtually no solubility of M in the room temperature α phase. For the eutectoid transformation to occur a great amount of solute must diffuse out of the the bcc phase (forming LaM) so that α can form. Just the presence of the solute element slows down the transformation by introducing long range diffusion in to the kinetic processes.

There is most likely a size effect on the diffusion rate. All the potential stabilizers used in the study are smaller than La except for Ca. The slowest diffusers will be the elements with the largest atomic mismatch due to the increase of strain energies in the materials. However too large of a mismatch will enhance diffusion by interstitial means.

Equilibrium

To retain the bcc phase at room temperature, the quench must be rapid enough to suppress the equilibrium eutectoid transformation. As in any such transformation there are two processes, nucleation and growth. Suppression of either process or both will enable bcc retention.

The nucleation rate depends on the formation free energy driving force for the formation of the transformation product. For hypoeutectoid alloys nucleation of the α phase should dominate and compound (LaM or La_3M) nucleation should be stronger in hypereutectoid alloys. The driving force for α nucleation is small as $\Delta H_{\gamma\rightarrow\alpha}$ is on the order of 3.5 kJ/mole for pure La. The driving force for nucleating compounds, in the absence of thermodynamic data, can be qualitatively compared between alloying elements in two ways. A large electronegativity difference between La and solute implies a high chemical reactivity and hence a large driving force for nucleation. Alternatively, one can compare melting points of compounds assuming that a higher melting point corresponds to a high formation free energy. For example one might expect that LaHg (m.p. = 1078°C) to have a larger driving force for nucleation than LaMg (m.p. = 745°C).

The growth rate depends on the diffusion rate discussed above. Any nucleation of α or a compound will require some undercooling. The amount of undercooling required for nucleation may bring the temperature to a region where diffusion controlled growth is too slow to form the equilibrium phases. On the other hand, if nucleation embryos do form, rapid cooling may suppress the growth of the nucleii simply by allowing little time for diffusional processes to occur.

Non-equilibrium

During quenching equilibrium considerations as just described may be invalid. Instead of γ transforming to equilibrium α + LaM, during rapid cooling γ may transform to a supersaturated β solid solution (for hypoeutectoid alloys only). This type of reaction can take place at a temperature T_0 where at a composition x_0 the free energies of the γ and β

phases are equal. Because the two phases have identical compositions, only short range atomic rearrangements are necessary to complete the transformation which is inherently a faster process. As before, however, some undercooling of T_o is necessary to form β nucleii, and then there must be some time, albeit short, for growth of β from the γ matrix which will still depend on the diffusion rate which is time and temperature dependent. To retain γ, a critical temperature must be reached at some point below T_o where diffusion is slowed with the constraint that a minimum of time be spent between the critical temperature and T_o to suppress β formation.

T_o curves have been drawn on the phase diagrams based on a regular solution model[18] (see Appendix D for complete derivation). The actual reaction temperature will be somewhat lower depending on the undercooling necessary to achieve nucleation. At a given composition, if the quench rate below the undercooling temperature is rapid enough the actual temperature becomes less important as there is no time for β growth. If the undercooling is low enough, the temperature where nucleation of β occurs may be too low to allow atomic movement necessary for β growth. From these arguments and the calculated T_o curves, it is evident that bcc retention is going to be favored at higher compositions where T_o is lower. As the composition of the bcc stabilizing agent is lowered, faster and faster quenching rates will be needed to meet the conditions for retention.

Quench Results

La-Mg and La-Cd

Of the seven potential stabilizers, only Mg and Cd were successful in stabilizing single phase γ at room temperature, Mg alloys between 13 and 20 at.% Mg and Cd alloys between 11 and 13.5 at. % Cd. For most of the Mg and Cd alloys, an ice water quench from the liquid state was sufficiently fast to metastably retain γ, but an ice water quench from the solid state tended to be ineffective, most likely due to the aforementioned initial cooling transient, except for alloys near the eutectoid composition.

Below 16 at.% Mg, a faster quench was needed for the La-Mg alloys. Both the Ga-In bath (from the solid) and melt spinning (from the liquid) enabled γ retention at concentrations down to 13 at.% Mg. At compositions below 13 at.% Mg, a Ga-In quench yielded $\beta + \alpha$, and melt spinning produced amorphous alloys. The Ga-In bath was not rapid enough to suppress the T_o reaction (and the subsequent precipitation of α) while melt spinning was so rapid that the bcc phase could not form from the liquid state during freezing. Above 20 at.% Mg the compound LaMg would precipitate from the bcc phase.

La-Cd alloys at 8 and 10 at.% Cd (ice water quench) were two phase mixtures of γ and α where both phases probably had the same composition (that of the overall alloy). The occurrence of two phases at the low end of the retention composition range indicates that the growth of the equilibrium phase had started but could not be completed because of the quench thus setting the lower limit for ice water quenching. Melt spinning was not attempted on La-Cd alloys because of the high degree of surface reactivity which would severely limit phase analysis by x-ray

diffraction or metallographic techniques. Like the La-Mg system, hypereutectoid alloys precipitated the LaCd compound. The superconducting transition temperatures of the hypereutectoid alloys remained constant[19] suggesting that the composition of the γ phase remained constant at a value near the eutectoid composition although the overall alloy concentration may be higher.

βGd and βDy

Gd and Dy have only two allotropes, hcp α at low temperatures which transforms on heating to the bcc structure. The melting points of both Gd and Dy are considerably higher than for La which means that the critical transformations will occur at higher temperatures, the main effect being that the bcc phase is more difficult to retain. Mg was chosen as the bcc stabilizer for βGd and βDy over Cd because the Mg alloys are not air sensitive and because the the Gd-Mg phase diagram is known (Fig. 13).[9]

Single phase bcc Gd-Mg could be retained by ice water quenching containing 23.6 to 29 at.% Mg while βDy could be retained from just 27 to 29 at.% Mg. A two phase $\alpha + \beta$ mixture was obtained at 22 at.% Mg in the Gd alloys and down to 24 at.% Mg in Dy alloys. Alloys containing more than 29 at.% Mg precipitated GdMg (DyMg). Melt spinning was attempted for the Gd-Mg alloys (the lower melting of the two), but Mg was volatilized before melting was achieved.

X-ray diffraction analysis

The primary means of phase identification used in this study was x-ray diffraction. Alloys were said to be single phase if only a single diffraction pattern was observable. The accepted rule is that a second phase would be observable if the volume fraction of that phase is greater than 5%, so a single phase pattern is at least 95% one phase.

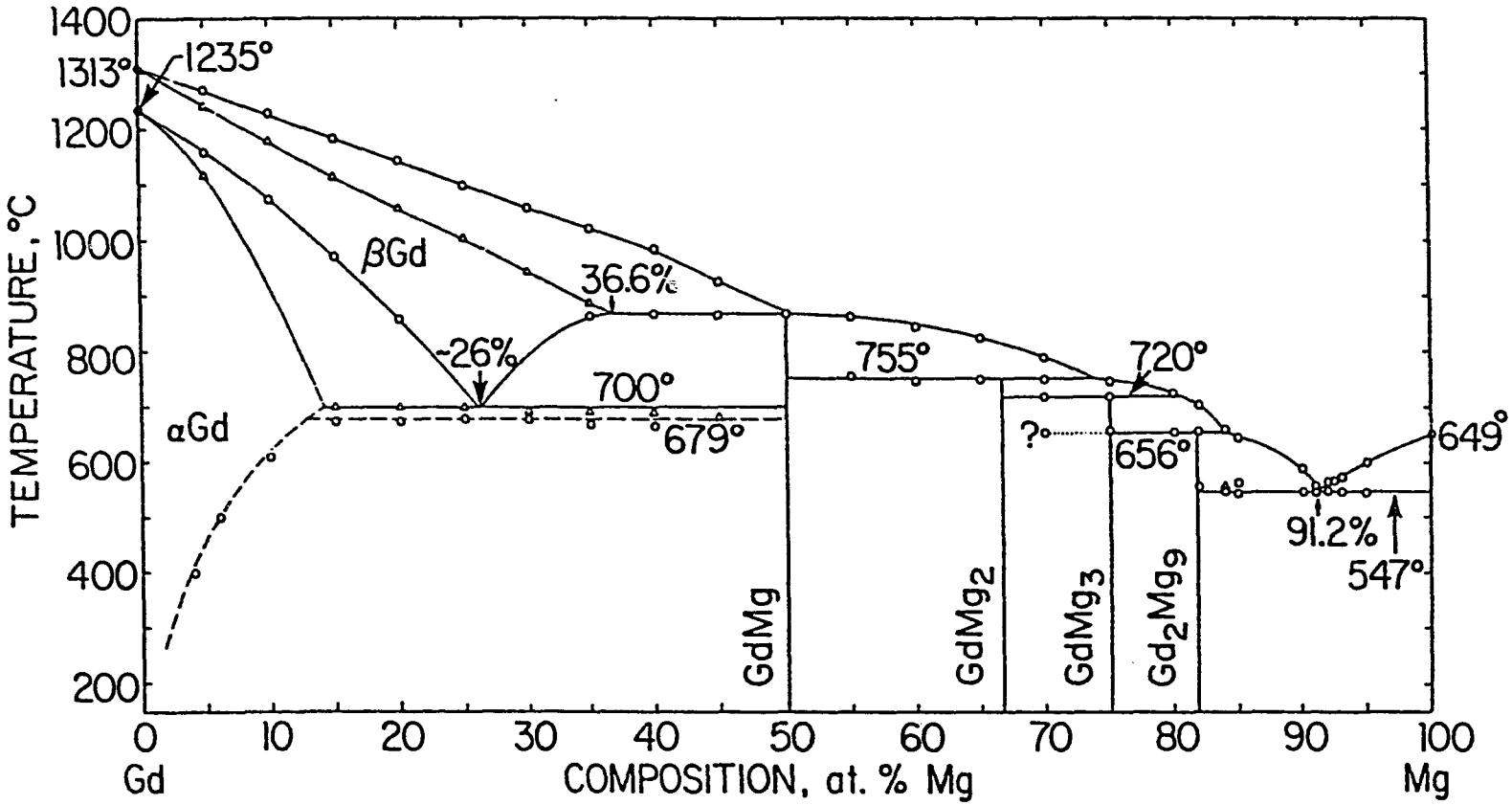

Figure 13. The Gd-Mg system.[9]

A diffraction pattern for a typical retained bcc structure near the eutectoid composition is shown in Fig. 14. The peaks are sharp and narrow like what one would expect for a well annealed bcc structure. Above the upper end of the retention range peaks of an intermetallic compound are observed with little change in the bcc pattern (Fig. 15) indicating that compound precipitated from the bcc phase as opposed to being part of the eutectoid transformation.

Conversely, at the low end of the composition range, the bcc peaks broaden and become less intense (Fig. 16). This indicates that the bcc structure is transforming to the room temperature close packed structure, but the transformation could not be completed due to the quench.

Lattice parameters provided a check on alloy composition. Because Mg is smaller than the rare earth atoms, one would expect a decrease in a_o with increasing Mg content. While this relationship may not follow Vegard's Law, some systematic relationship should be seen. The lattice parameters for the Gd and Dy alloys are shown in Fig. 17a. For comparison the lattice parameters for the Gd-Mg alloys of Manfrinetti[4] are also shown in Fig. 17a while the lattice parameters for La-Mg alloys are in Fig. 17b.

The lattice parameters in Fig. 17 were not obtained in the usual way (e.g., a Nelson-Riley extrapolation). Preferred orientation in the sample limits the number of quality peaks, so an extrapolated value is no improvement over the values calculated from each peak. Therefore the 211 peak was arbitrarily chosen as the peak giving the best a_o because it repeatedly was the highest angle, high intensity peak. There is some scatter in the a_o versus %Mg plot due to the quench, but a linear extrapolation is in good agreement with the previous work. No large anomalies were observed suggesting that the nominal alloy concentration is

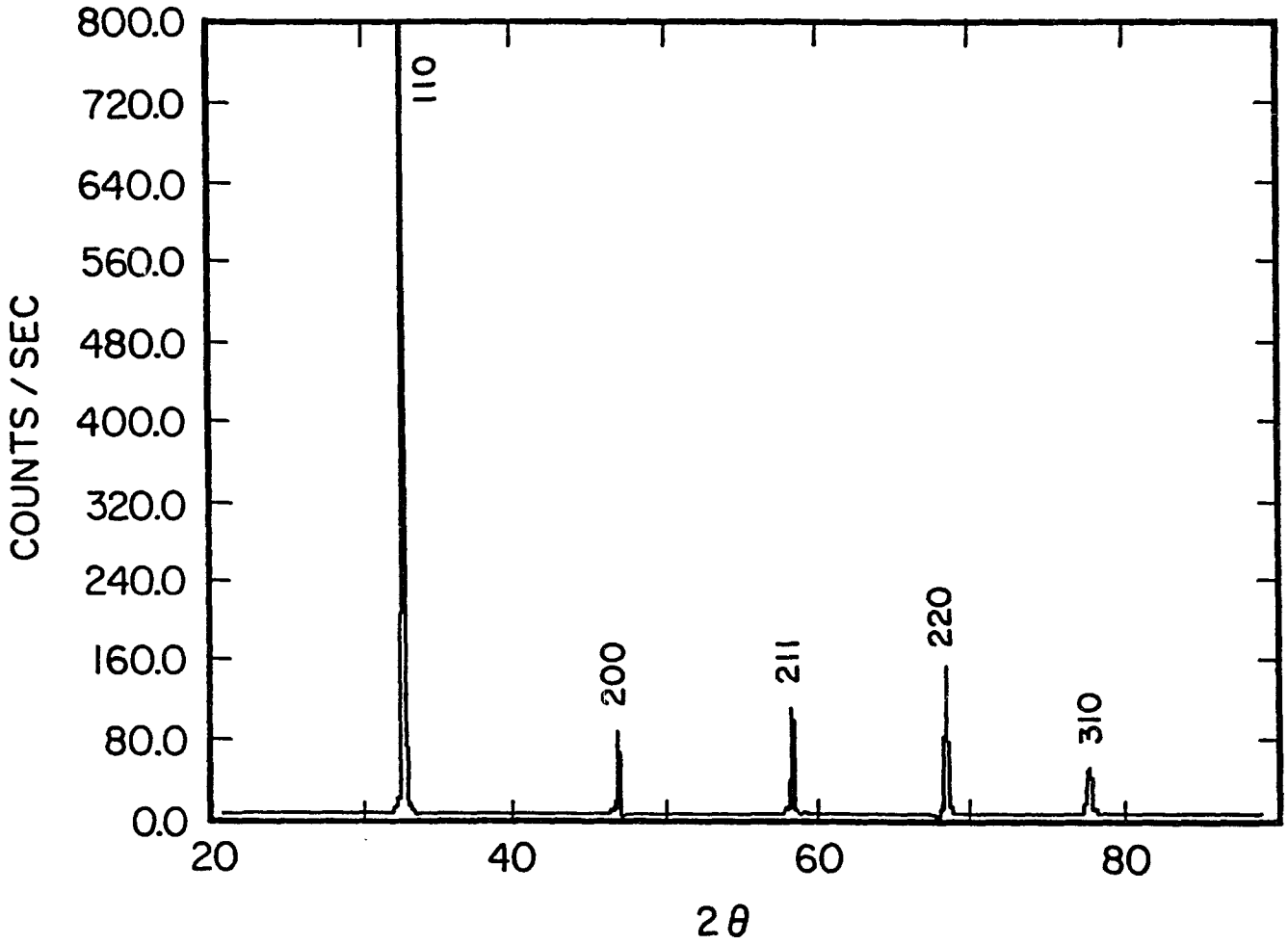

Figure 14. X-ray diffraction pattern for bcc Dy-27Mg quenched from the liquid.

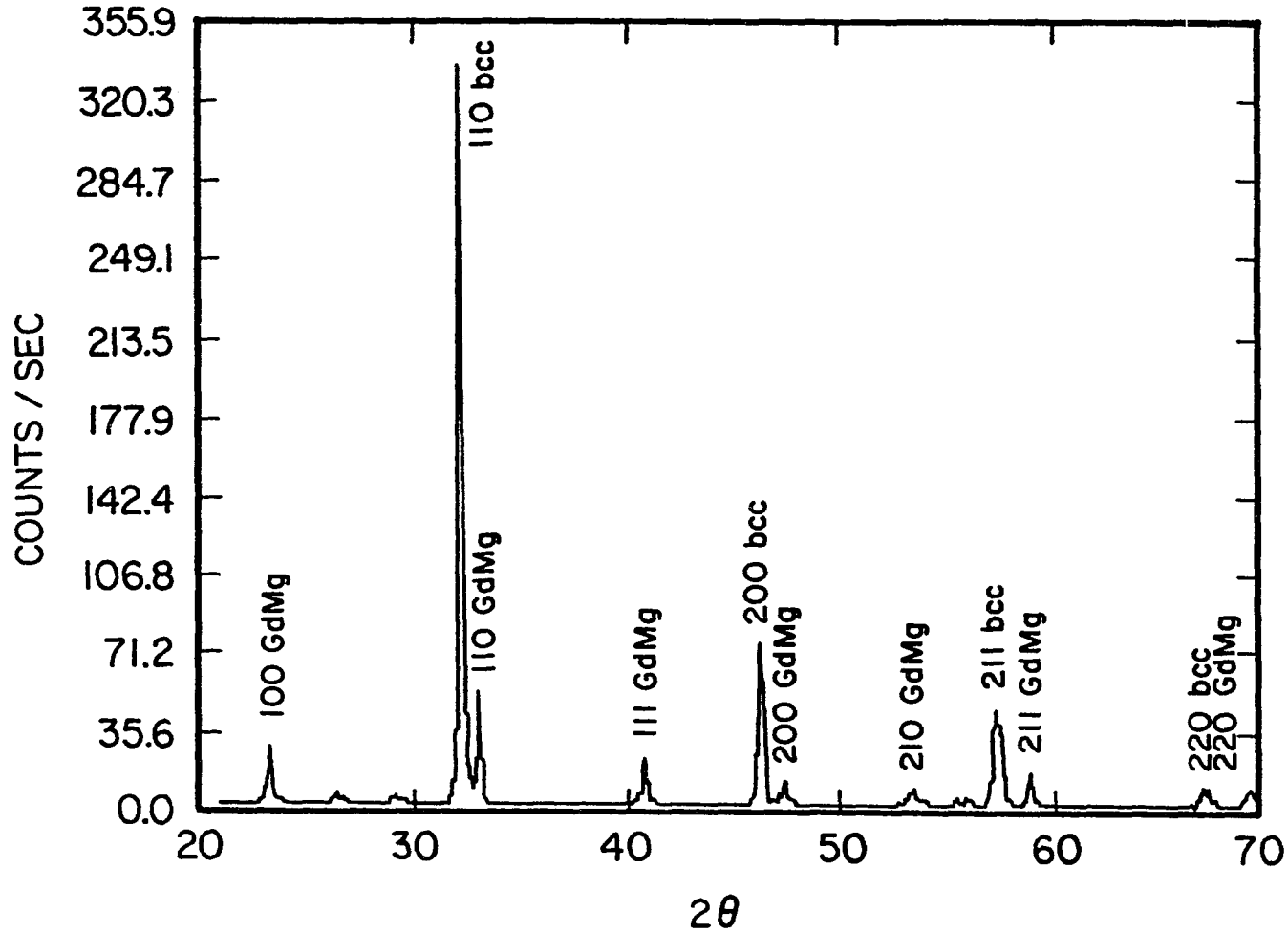

Figure 15. X-ray diffraction pattern for Gd-31Mg quenched from the liquid showing both a bcc phase and GdMg precipitates.

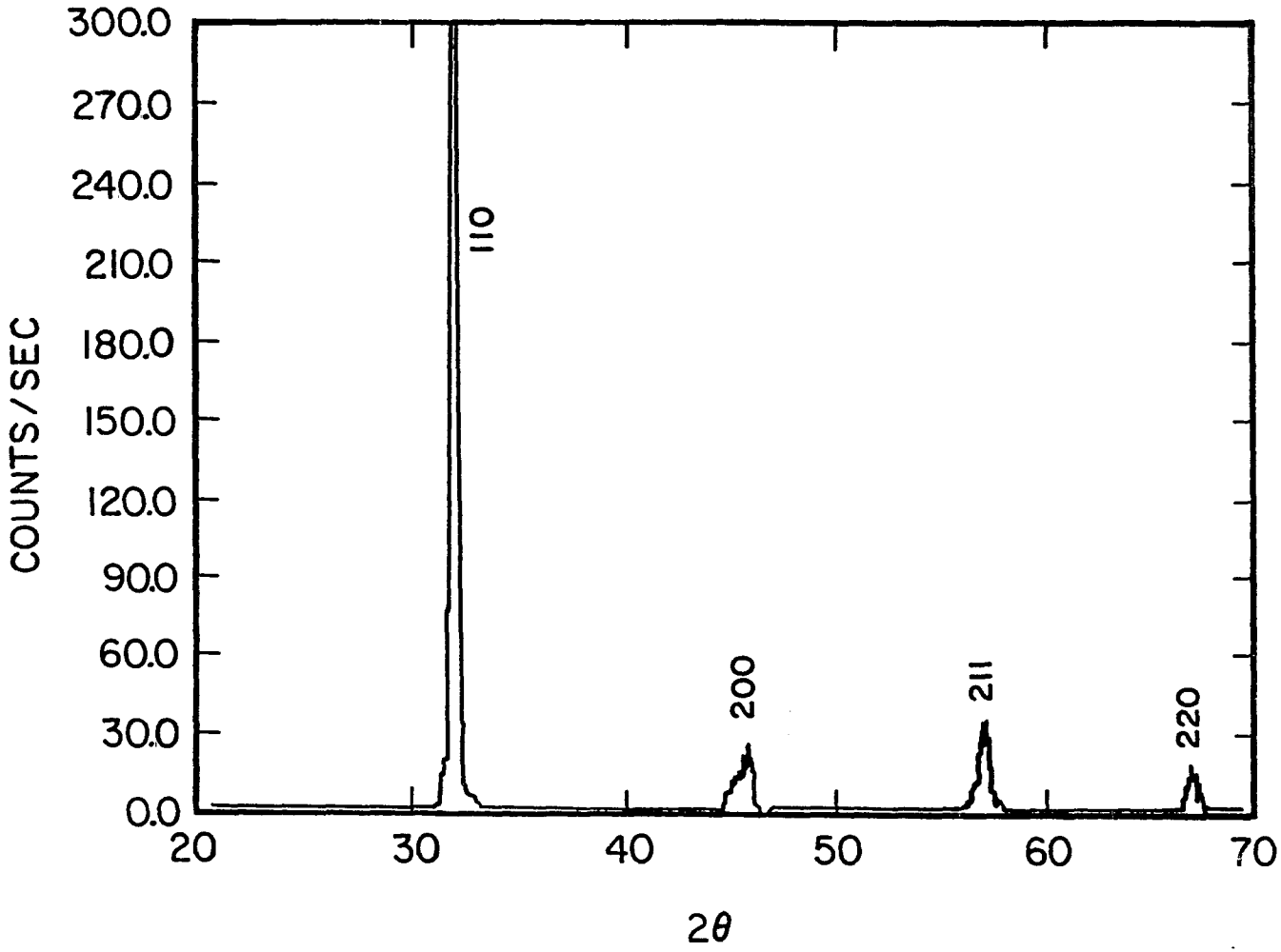

Figure 16. X-ray diffraction pattern for bcc Gd-23Mg quenched from the liquid.

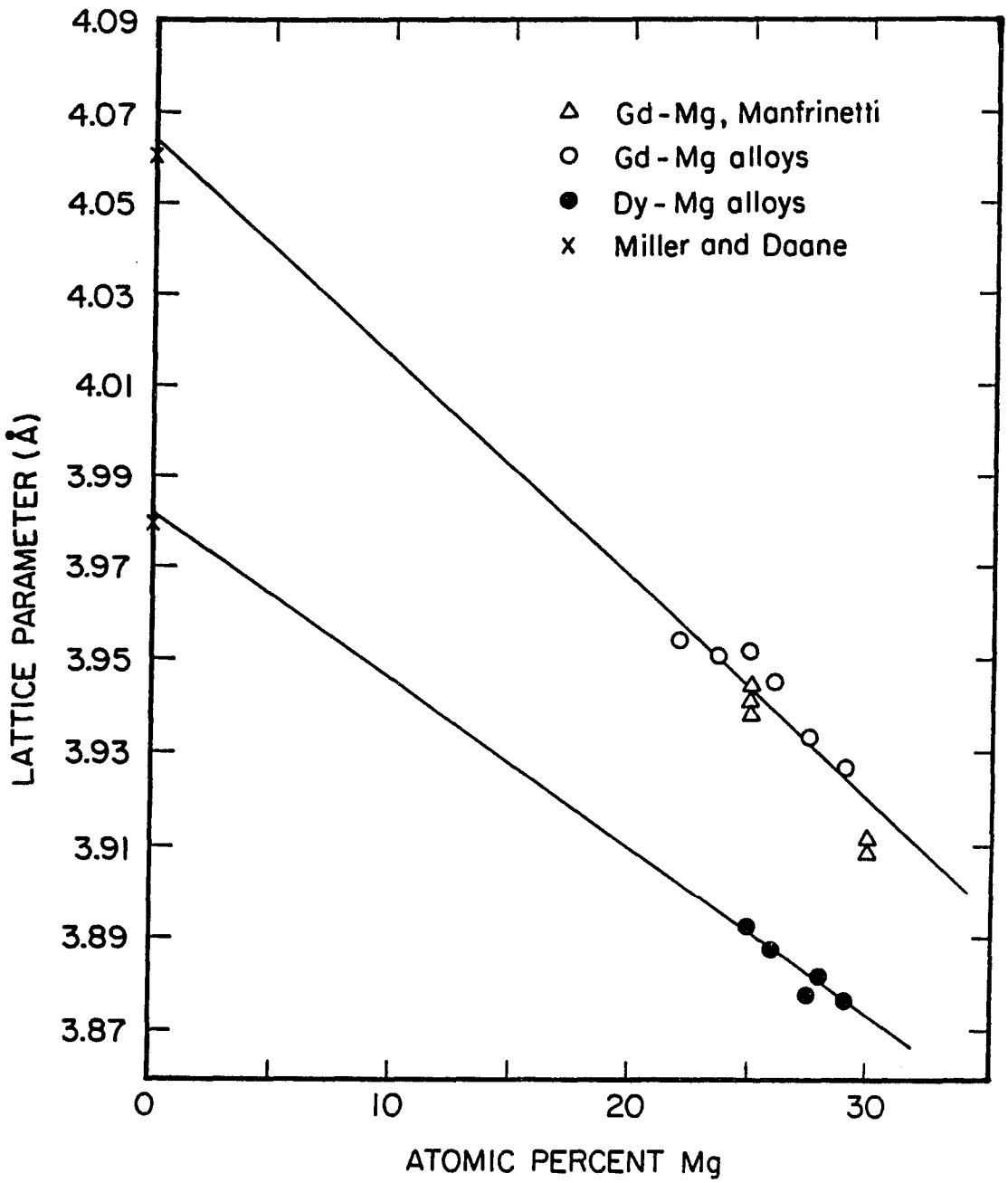

Figure 17a. Lattice parameters of bcc Gd-Mg and Dy-Mg alloys. Literature values are included for comparison.

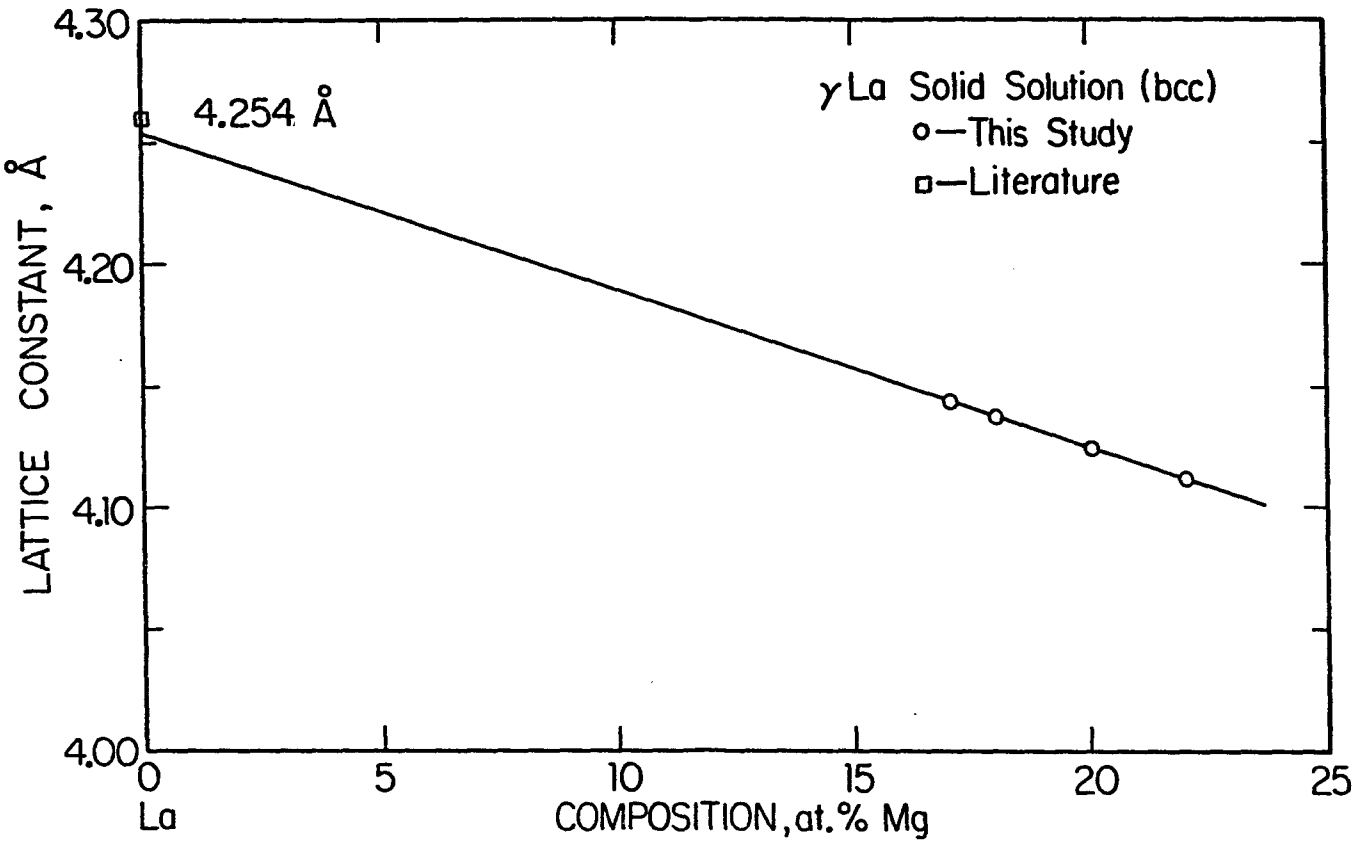

Figure 17b. Lattice parameters of bcc La-Mg alloys after Manfrinetti.[4]

close to the actual composition of the bcc phase.

Microstructures

The La-Mg alloys were the only alloys to have really clean microstructures. Fig. 18a of a La-Mg alloy near the eutectoid quenched from the solid shows no evidence of a second phase. Fig. 18b at 20% Mg begins to show precipitation of the LaMg intermetallic. A two phase microstructure can also be produced by quenching from too low of a temperature as illustrated by Fig. 19 quenched from the β + L two phase region. The large grains are the existing β phase while the intergranular phase freezes from the liquid.

All Gd and Dy alloys show evidence of dendritic growth from the liquid phase on quenching. Fig. 20a is a micrograph of an alloy that exhibits only a bcc x-ray diffraction pattern with no evidence of a second phase in the pattern. However, the micrograph clearly has contrasting regions which is sometimes evidence of a two phase microstructure. This same type of contrast is also observed in alloys (Fig. 20b) that are known to have both a bcc and hcp phase by x-ray diffraction. Here however, the second phase (inside the dendrite arms) is clearly identifiable as a eutectoid transformation product that consists of the hcp phase and quite likely some of the RMg compound. There are also indications of another phase between the dendrite arms.

The most likely possibility is Mg segregation caused by dendritic cooling through the β + L two phase region; that is, the center of the dendrites are at a lower composition than the final surface due to Mg gradients that occur during solidification. This composition variance, in itself is sufficient to cause the contrast. Because this center region has less Mg it is more susceptible to the eutectoid transformation during

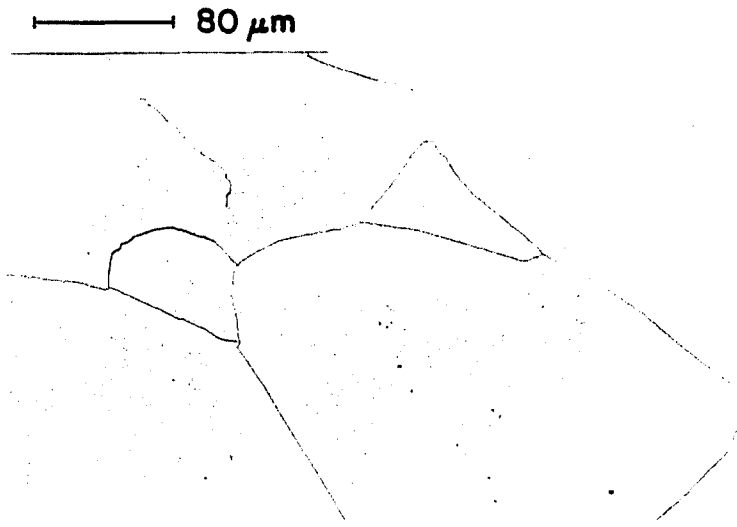

a)

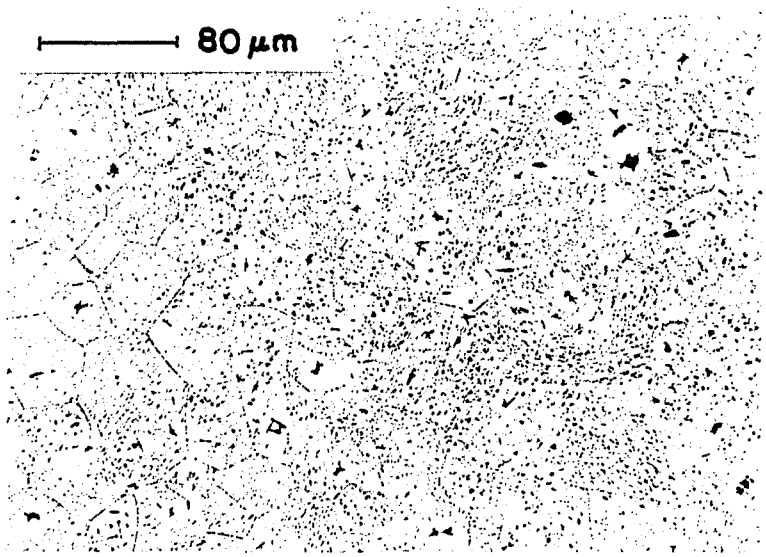

b)

Figure 18. Optical micrographs of a) single phase La-20Mg quenched from the solid and b) La-20Mg quenched from the liquid showing no dendrites, but precipitation of LaMg.

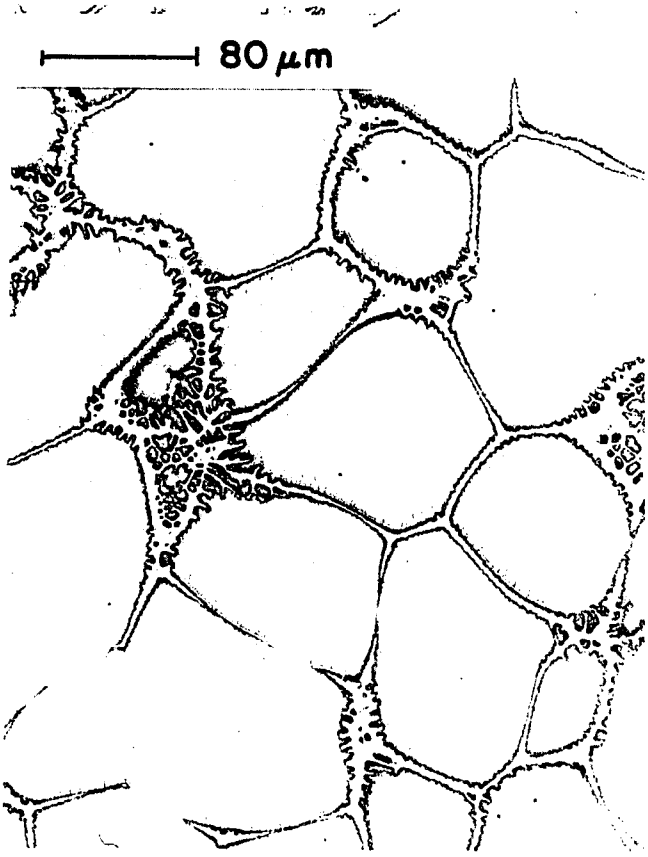

Figure 19. Optical micrograph of Gd-25Mg quenched from two phase L + β region.

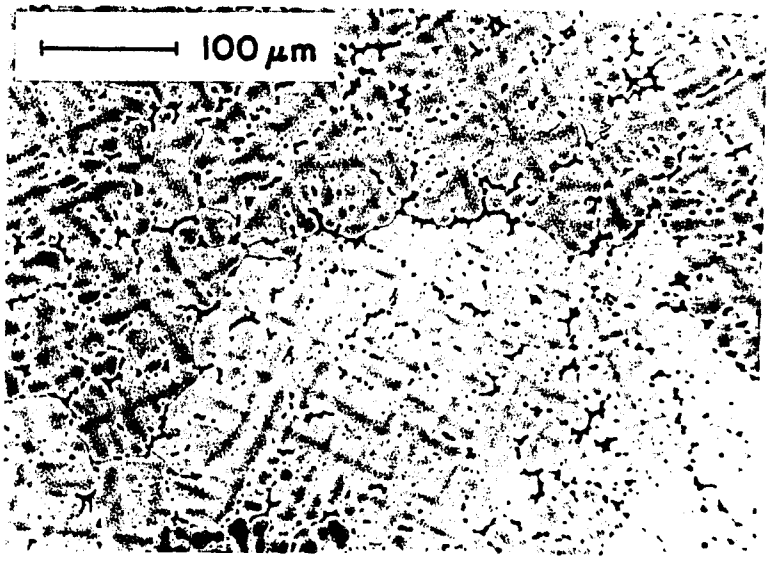

a)

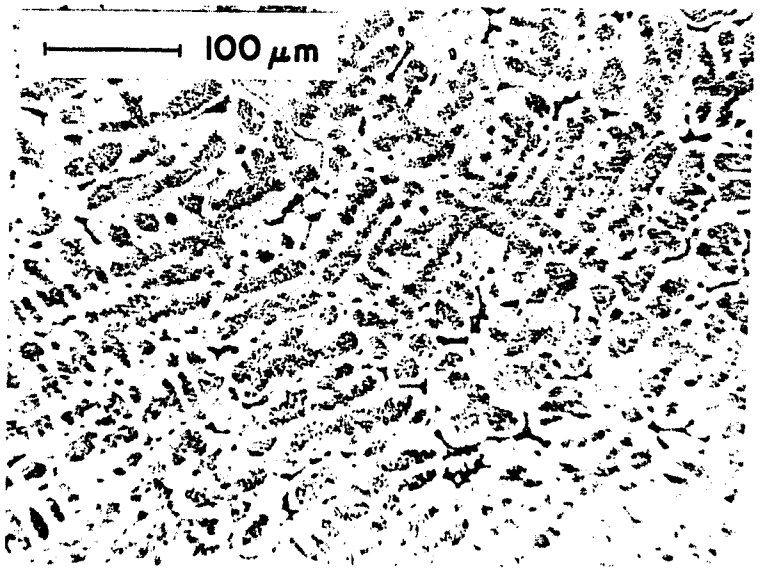

b)

Figure 20. Optical micrograph of a) "single phase" Dy-29Mg and b) two phase Gd-22Mg.

the quench, so the possibility that some transformation has occurred can not be ruled out. If the eutectoid transformation has started it will still be proceeding slowly, and it is stopped by the quench before it can reach completion. The resulting product is then either amorphous or microcrystalline (no x-ray diffraction pattern) and would also appear as the dark phase in Fig. 20a. Any such phase must closely resemble the bcc phase because these "single phase" alloys have only one magnetic transition as discussed later.

Another type of microstructure (Fig. 21a) was observed in one other alloy. This particular micrograph shows no evidence of a dendritic structure and no transformation products similar to the La-Mg system. An SEM micrograph at twice the magnification (Fig. 21b), however shows remnants of dendritic arms. What has probably happened is that during the quench, this alloy stayed longer in the bcc one phase region. This extra time would allow some annealing and homogenization to take place. That would also tend to eliminate any Mg segregation from freezing as in Fig. 20 as well allowing time for grain growth. For physical measurements such as heat capacity and magnetic susceptibility, this would be the preferred microstructure, but reproducibility is a problem.

Discussion

As expected, the best bcc stabilizers were the γ retainers. Mg and Cd are both divalent with large depressions in the bcc to close packed transition temperature. They have the largest bcc solubility and the lowest chemical affinity for La of all the metals considered. In addition, Mg and Cd are the only two metals that expand the γ field; the others have little effect or contract the γ field. However, some of the

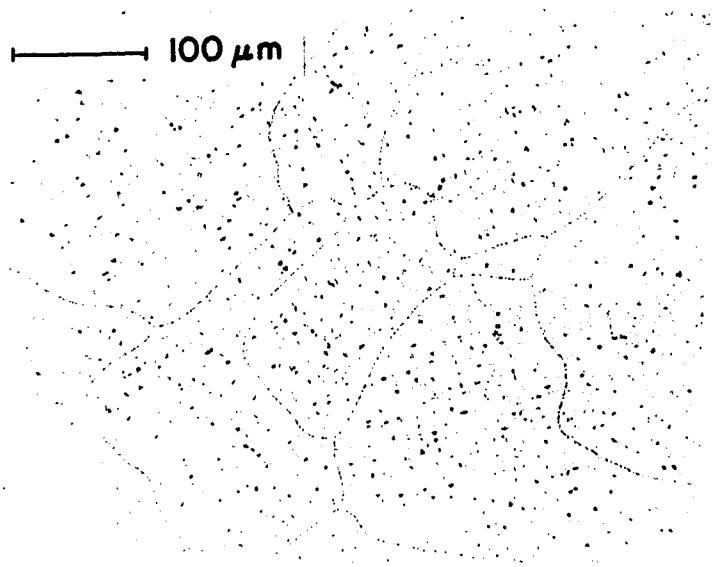

a)

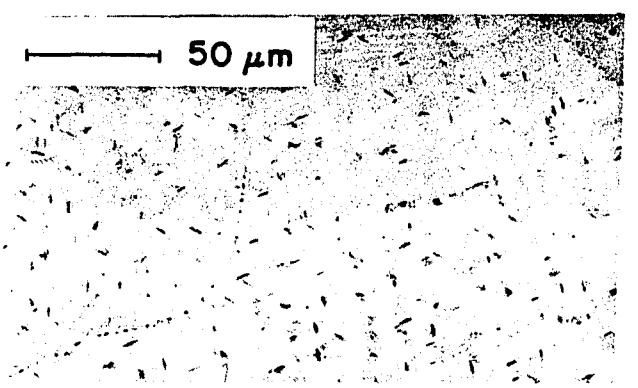

b)

Figure 21. a) Optical micrograph of Gd-25Mg quenched from the liquid state and b) SEM micrograph at higher magnification showing evidence of dendritic freezing.

other metals, most notably Hg, also have favorable characteristics although they are not γ retainers. To understand these other systems the reaction kinetics must be considered.

Critical temperatures

A simultaneous plot (Fig. 22) of the T_o curves for each alloy system shows that a low T_o is not a sufficient condition for γ retention. (T_o data obtained from Pr diagrams were normalized to La with respect to the close packed to body-centered transition temperatures.) The La-Cd T_o is the lowest curve, and the only other γ retainer, Mg, has the highest T_o curve. The other elements all have similar T_o curves, but they fail to provide γ retention. The advantage that Cd and Mg share is a high eutectoid solubility that allow alloy compositions far out on the T_o curves where the temperature is lower. This low temperature region is where diffusion starts to become slow and γ retention can occur. Also of importance is the relative diffusion rate of the solute element with respect to La. The slower the solute diffusion rate, the higher the T_o can be and still get γ retention.

From this same plot a critical T_o temperature, $T_{o,c}$, can be determined which defines the temperature below which diffusion processes become slow enough so that the γ to β transition is inhibited. This temperature is the T_o temperature at the lowest composition at which the γ phase can be stabilized. For the Cd and Mg systems, $T_{o,c} \simeq 500$ and 525°C, respectively, for ice water quenching. These $T_{o,c}$'s are remarkably similar and indicate some average value of $T_{o,c}$=515°C for the La systems. The importance of this critical temperature is that if it is above the eutectoid temperature, the equilibrium transformation can be repressed. If $T_{o,c}$ is below the eutectoid temperature, then the equilibrium

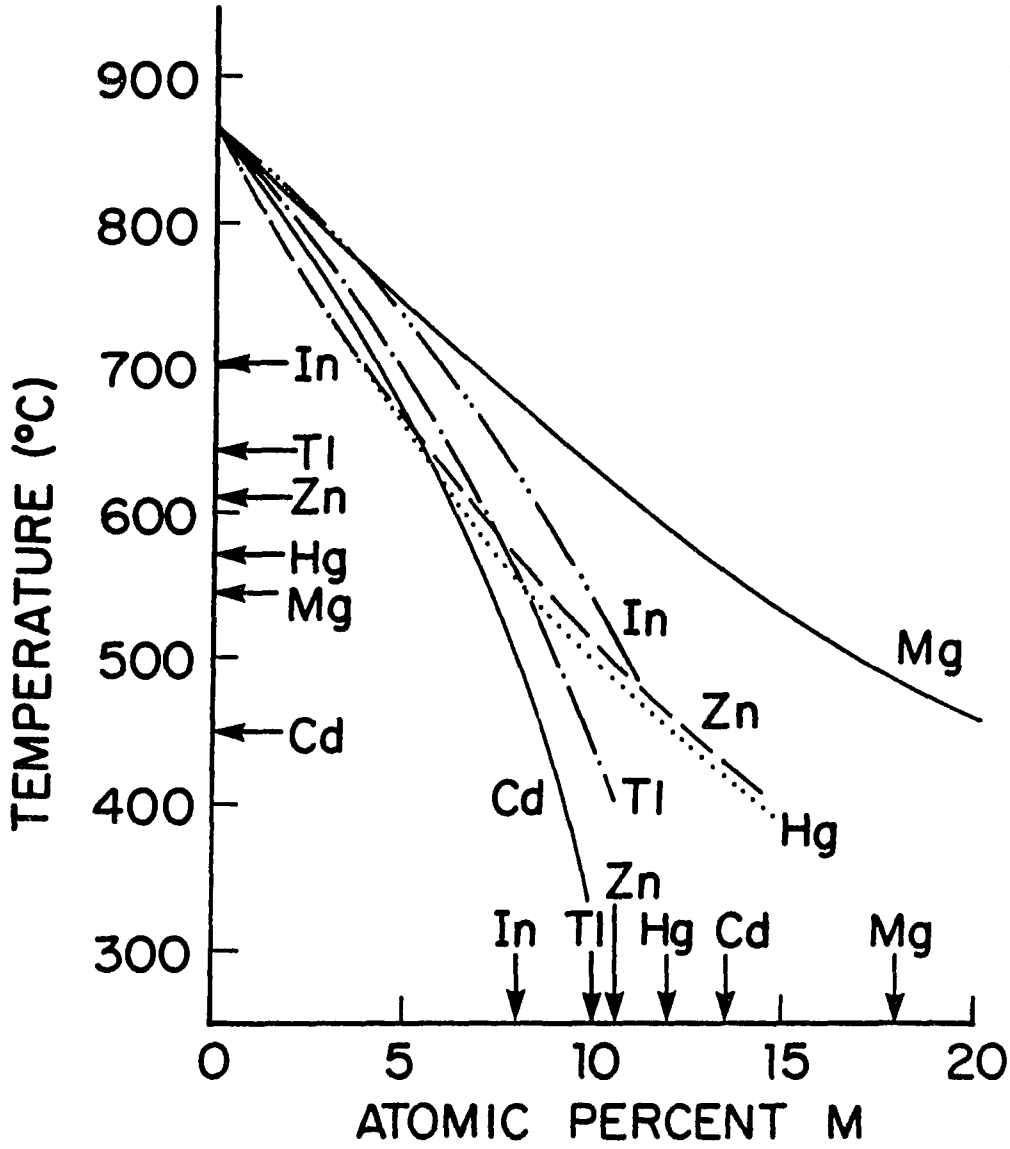

Figure 22. Composite of the La-M T_0 curves. The arrows on the temperature axis indicate the eutectoid temperature, and the arrows on the composition axis indicate the eutectoid composition.

transformation will be favored. The value of $T_{o,c}$ can be increased by increasing the quenching rate as illustrated by the extension of the lower concentration limit by melt spinning in the La-Mg system.

The La-Cd system is the only system where the eutectoid temperature is less than $T_{o,c}$, and this factor overwhelms the eutectoid equilibrium transformation. The eutectoid temperature in the La-Mg system is higher than $T_{o,c}$ but only by a few degrees which may be enough to suppress the eutectoid reaction. In addition, Mg is probably a slow diffuser in La. Differential thermal analysis (DTA) in the La-Mg system shows that the equilibrium transition from γ to β (or α) and LaMg are sluggish even under slow cooling (10°C/min), especially near the eutectoid composition.[9]

Failed La-M systems

The other alloying elements were not γ retainers. In all these systems, the eutectoid temperature is higher than $T_{o,c}$ by at least 50°C. There is no composition where the T_o curve is less than $T_{o,c}$ because of the eutectoid composition upper limit. This would indicate that γ retention is not favored in these systems.

Quenched alloys in the La-Ca system resulted in only the α phase (La and Ca form no compounds). Ca is slightly larger (+5%) than La which would result in little diffusion inhibition. Ca is the only M in which there is an atomic mismatch of this small magnitude.

Both La-Hg and La-Zn quenched alloys were generally β phase or a mixture of β and LaHg (LaZn) despite favorable eutectoid solubilities and relatively low eutectoid temperatures. The fact that β was the quench product indicates that T_o reaction took place as opposed to the eutectoid reaction which supports the critical T_o argument. The formation of the compound probably takes place at the eutectoid temperature. The chemical

reactivity of Hg and Zn with La is much greater than for Mg or Cd using either the electronegativity or compound melting point criteria.

The trivalent metals Tl and In form many compounds including one at 25 at.% Tl, La_3Tl (La_3In). Quenched alloys contained a mixture of β and the compound formed in the same way as the Hg and Zn alloys. The presence of a La-rich compound effectively decreases the solubility limit while increasing the eutectoid temperature which in turn forces low alloy compositions at high T_o temperatures. Another consideration is the narrowness of the γ phase field in these systems. While the divalent metals generally expand the γ field, Tl and In contract the field with $\Delta T_{bcc} < 50°C$. If one is quenching from the liquid, the γ phase may not form at all due to the narrowness of the field and β may be the first solid formed instead.

THERMAL STABILITY OF BCC ALLOYS

The thermal stability of the bcc phase can be measured by isothermal annealing or by controlled heating, i.e., differential thermal analysis (DTA). Throughout this analysis it is assumed that the small composition variance from sample to sample will have only small effects on the thermodynamic stability of the quenched phase. Therefore, all the Gd-Mg alloys will be considered without regard to composition with the same procedure being used for Dy-Mg alloys. These types of experiments have been done on La-Mg by Manfrinetti.[4] He finds an exothermic DTA reaction at about 350°C on heating at 10°/min which he describes as the bcc to hcp + LaMg reversion temperature. He also reports complete reversion to αLa + LaMg after heating to 420°C at 20°C/min, isothermal annealing for 1 day at 300°C, or 2 days at 250°C.

DTA analysis of 3 Gd-Mg alloys of different compositions ranging from 25% to 29% Mg heated at 10°/min show essentially the same behavior regardless of composition. The DTA trace (Fig. 23) shows two exothermic reactions, the lower temperature peak being much larger than the higher temperature peak. The first peak is centered just below 400°C for all three alloys, but the second transitions ranges from 470°C to 490°C with a larger breadth than height. A strong endothermic reaction is observed between 705 and 710°C corresponding to the eutectoid transformation. Manfrinetti and Gschneidner report 700°C for this reaction, so there is reasonable agreement. The βDy alloys have almost the same trace (Fig. 24). The first exothermic reaction is again at 400°C, but the second one is somewhat lower at 435°C. The eutectoid transformation is at 720°C and is nearly identical to that of the Gd-Mg system.

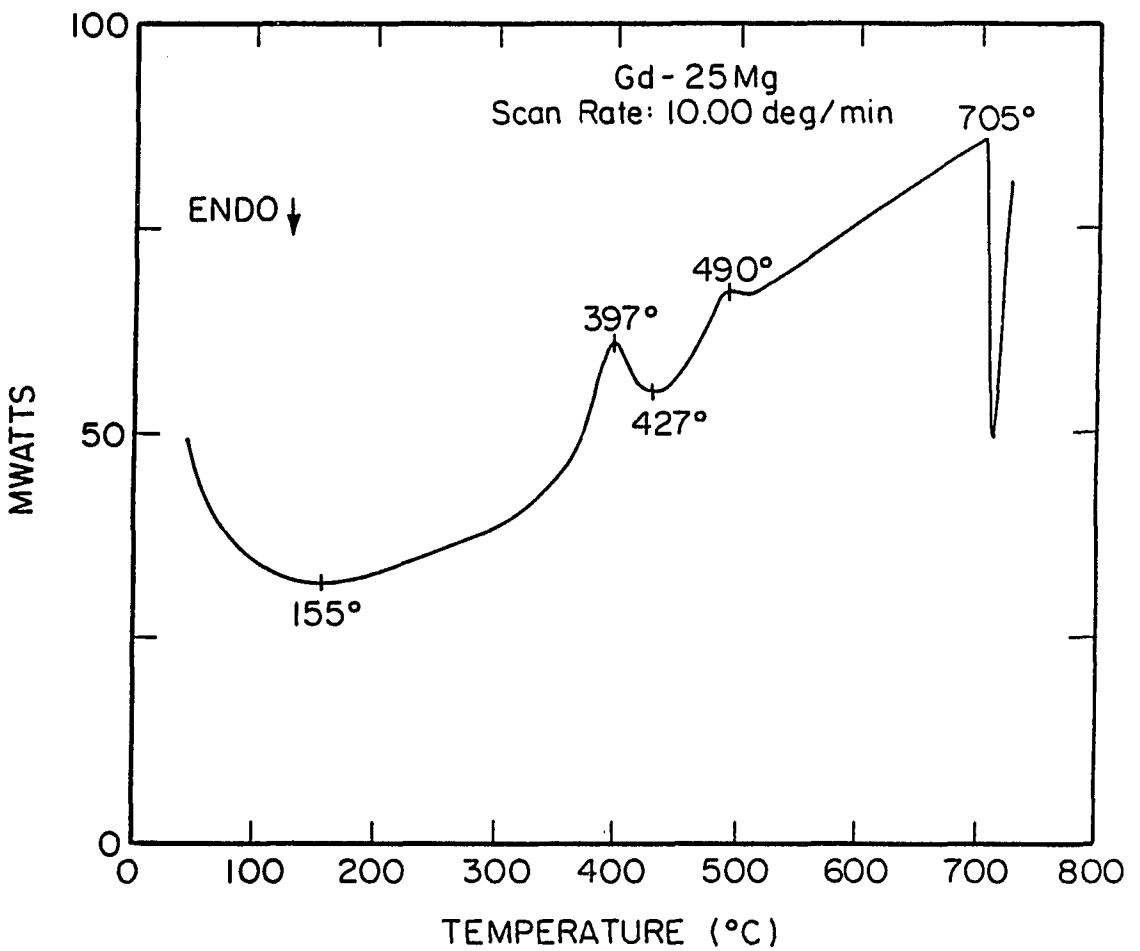

Figure 23. DTA trace for Gd-25Mg.

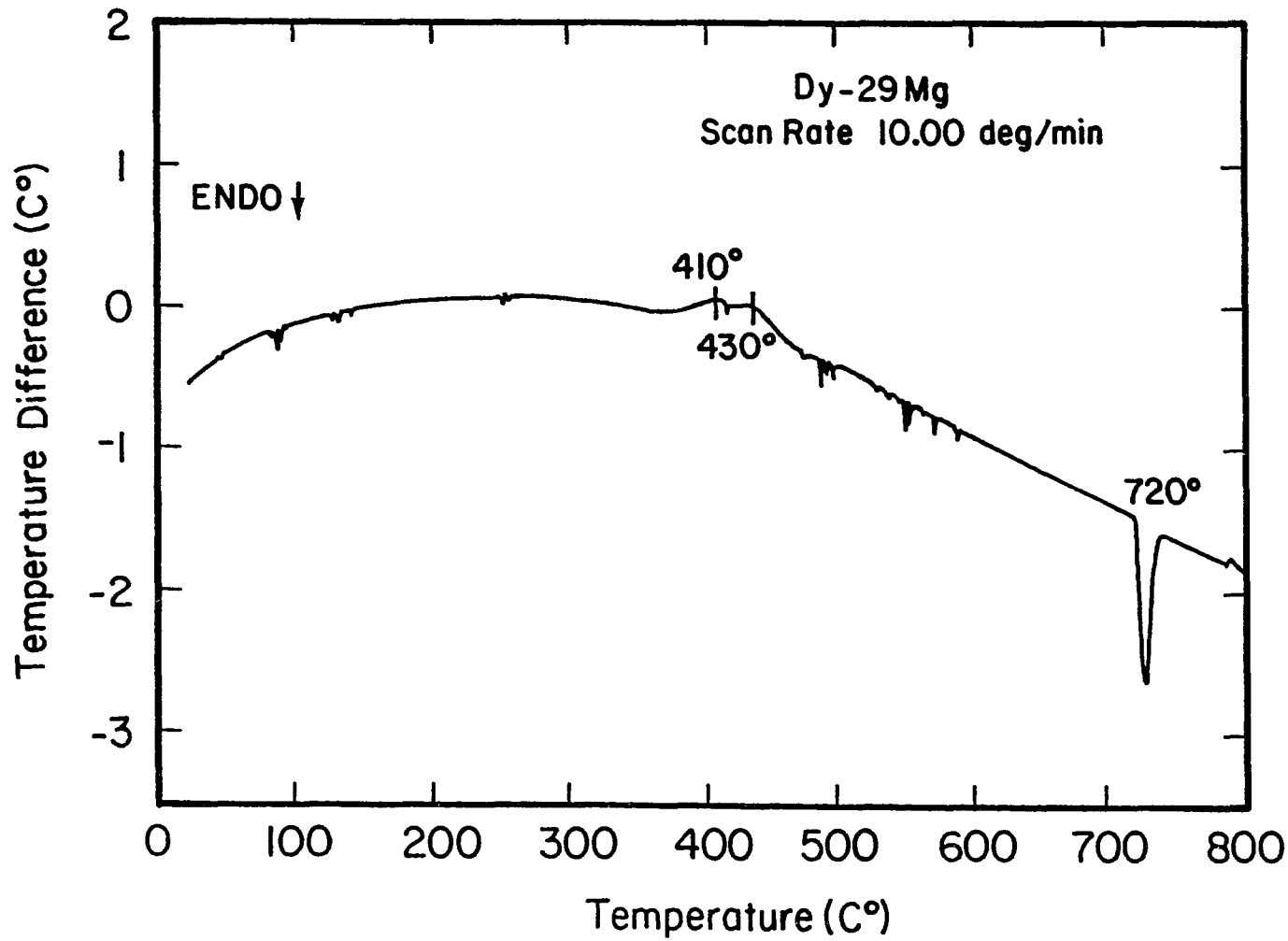

Figure 24. DTA trace for Dy-29Mg.

Another βGd sample was put into a high temperature diffractometer and heated at 10°/min. During heating the bcc 110 peak was scanned repeatedly in such a way that the peak was scanned every 25°C (Fig. 25). From room temperature to 300°C, no hcp peaks are observed, and the bcc 110 peak gradually loses intensity due to increased thermal vibrations. At about 300°C, just below the onset of the first exothermic reaction, the hcp 002 and 101 peaks become visible. The 101 peak is very broad and may have obscured the bcc 110 reflection, but later annealing experiments show that the bcc phase no longer exists at this temperature. Simultaneously, the hcp peaks increase in intensity until the 375-400°C interval and then level off matching exactly the peak of the first exothermic reaction. At 490°C, the hcp peaks increase in intensity matching the second exothermic reaction.

Still another βGd sample was heated at the same rate and then quickly cooled from 385°C (Fig. 26a). Figure 26b shows a well annealed sample for comparison. The dendritic structure is still intact, but the contrast is more uniform than the quenched state indicating some homogenization. X-ray diffraction analysis over a complete 2θ range showed only a noisy, weak peak centered at the hcp 101 diffraction angle as if there was a wide range of atomic spacings. No bcc or GdMg peaks were observable at any angle. Therefore, the first reaction is a reversion of the bcc phase to a highly saturated and distorted hcp phase. The second reaction is a relaxation of this intermediate phase (the upturn in Fig. 25) accompanied by the precipitation of GdMg.

A series of isothermal anneals was done to determine the bcc stability at lower temperatures. It was assumed that the Dy and Gd would behave similarily because of the DTA traces and will be treated together.

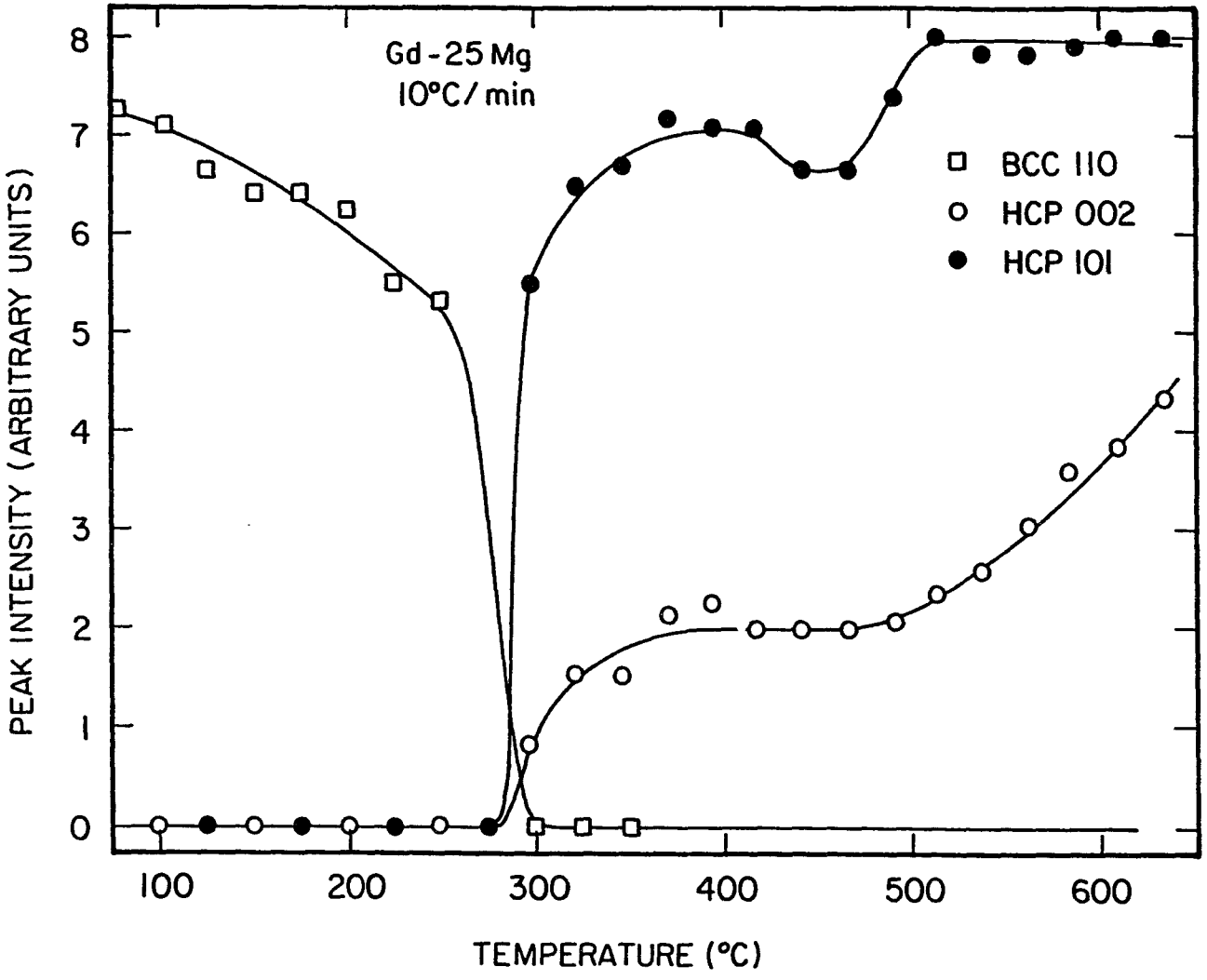

Figure 25. Intensity of three x-ray diffraction peaks of a quenched Gd-25Mg sample taken during heating.

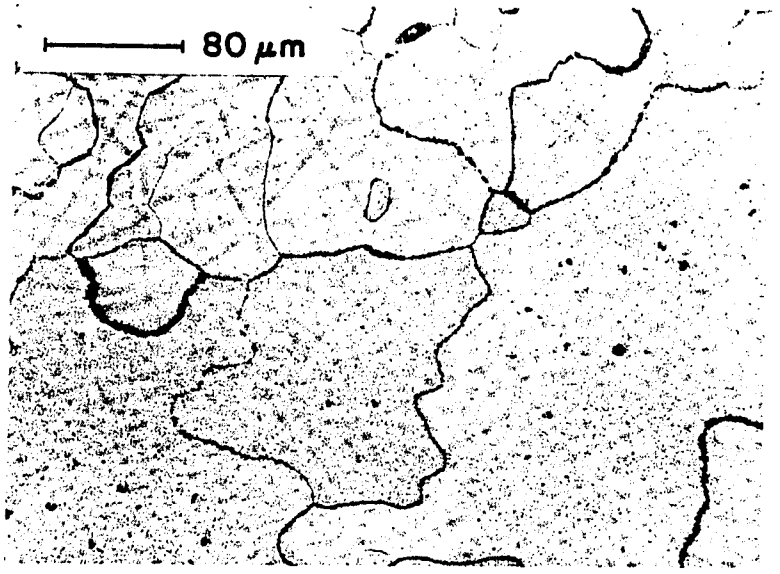

a)

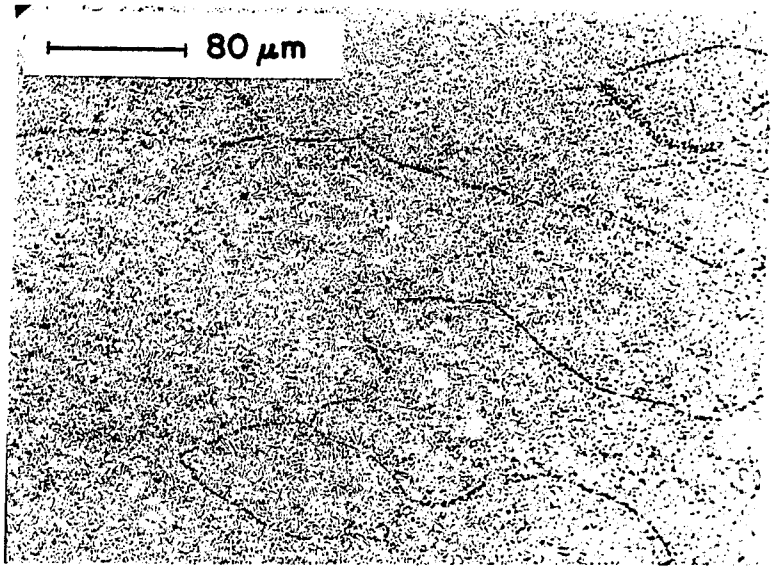

b)

Figure 26. Optical micrographs for a) Gd-25Mg heated to 385°C at 10°/min and quenched and b) Dy-28Mg annealed at 680°C for one hour.

The samples were put into a heated furnace and then periodically removed from the furnace to check the structure by x-ray diffraction. In all the samples the bcc phase had disappeared before the first check: 15 min at 400°C, 90 min at 325°C, six hours at 260°C, and one day at 200°C indicating the relative stability of the bcc phase.

Only the 400° (Fig. 27a) sample showed an αGd + GdMg diffraction pattern after this first check. The other samples all had the distorted hcp 101 type peak of the intermediate phase. The relaxation and precipitation reaction takes much longer to occur. A complete αGd + GdMg pattern was first observed after 28 hours at 325°C and 119 hours at 260°C. After two weeks at 200°C the transformation had not yet occurred.

Optical micrographs of these samples after annealing are Figs. 27a-d. The 325° (Fig. 27b) sample shows almost a complete transformation. Some of the intermediate phase (light colored) is still untransformed. The growth of the eutectoid colonies appears to be coupled growth radially outward from grain boundaries and surface irregularities. The alternating light and dark contrast within each colony denote the hcp and GdMg phases respectively.

The 260° sample (Fig. 27c) shows very little transformation compared to the 325° sample. The transformation structure from this temperature is much finer and can be seen as short dark lines especially at the grain boundaries. The dendritic structure from the quench can still be seen although some homogenization seems to have occurred. The grain boundaries are marked by dark precipitates of GdMg. Some small eutectoid colonies are also seen.

The 200° sample (Fig. 27d) x-ray diffraction pattern shows no GdMg phase, but the structure may be too fine. The micrograph shows a fine

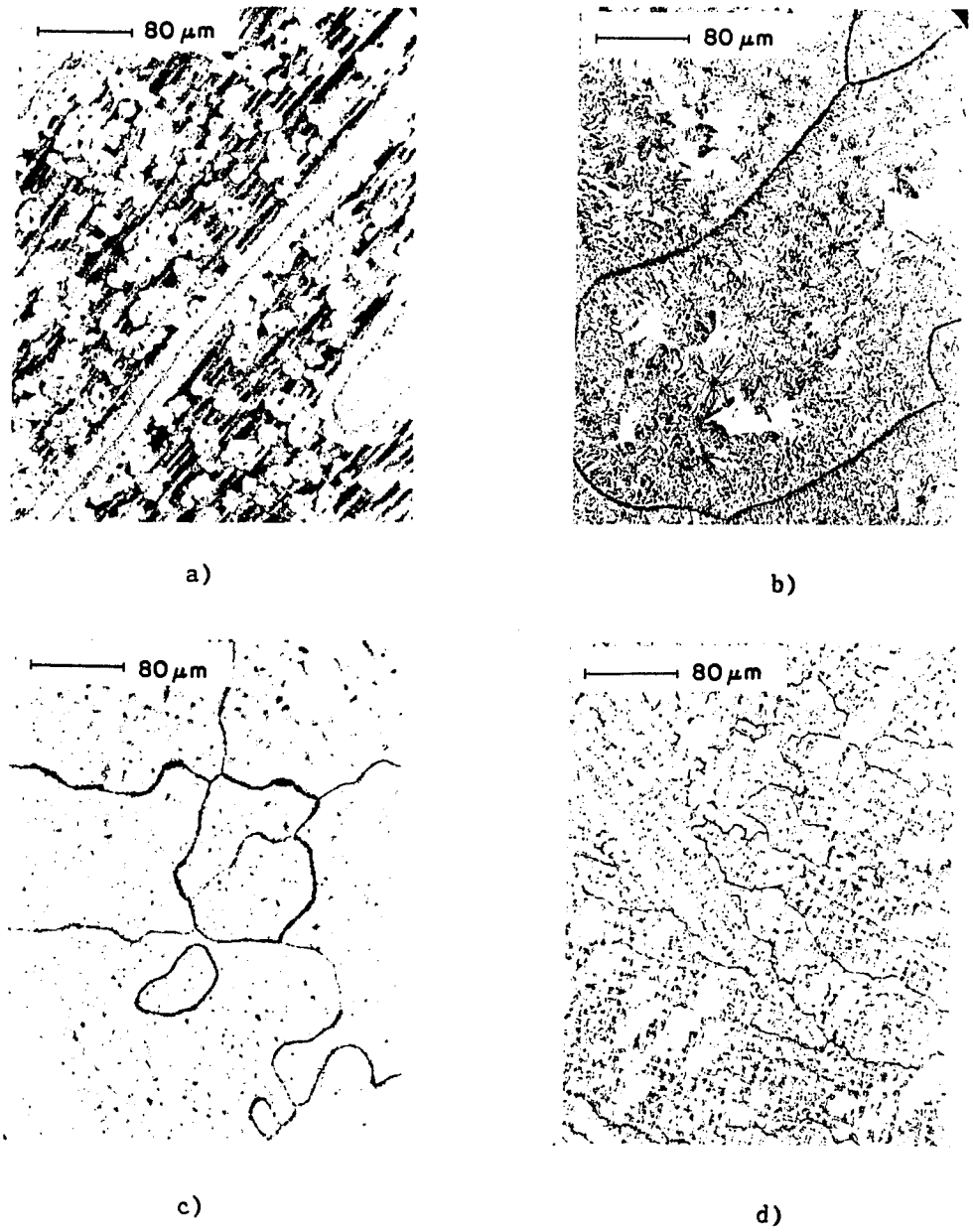

Figure 27. Optical micrographs of annealed alloys: a) 15 minutes at 400°C, b) 28 hours at 325°C, c) 119 hours at 260°C and d) 14 days at 200°C.

precipitate in grain boundaries and in between dendrite arms where the Mg concentration should be locally higher as this is the last liquid to freeze. Coupled eutectoid growth appears to be growing away from the grain boundaries and the interdendritic areas. The grain boundaries have diffusion enhanced growth while the interdendritic initiated growth is favored by the locally high Mg concentrations.

The behavior of the Gd and Dy alloys is significantly different from the La-Mg alloys. The reversion reaction in the La alloys is a one step process while the Gd (Dy) alloys follow a two step process featuring an intermediate distorted phase. Consequently the bcc phase has less stability in the Gd (Dy) systems because the intermediate phase is easily reached without diffusion. The La system seems to require a coupled growth for the reversion and hence is more stable because diffusion is now required. This difference may be a size effect. Mg is closer in size to Gd (Dy) than to La and so a saturated closepacked hcp lattice in the Gd (Dy) system may be more easily accommodated than for La.

It appears that the intermediate Gd (Dy) phase is more stable than the La bcc phase based on the higher temperatures and longer times needed for transformation. On a relative basis, however, the La alloys are more stable. Fig. 28 shows a plot of annealing temperature normalized to the eutectoid temperature versus the time at which the hcp phase was first observed (about 10% transformation). The La curve lies everywhere above the Gd curve meaning that for a given time the La alloys have to be brought relatively nearer to the equilibrium eutectoid temperature before transformation occurs. Therefore γLa is more stable than βGd (Dy) with respect to relative temperature as well as to retention of a bcc phase at elevated temperatures [as opposed to the Gd (Dy) intermediate state].

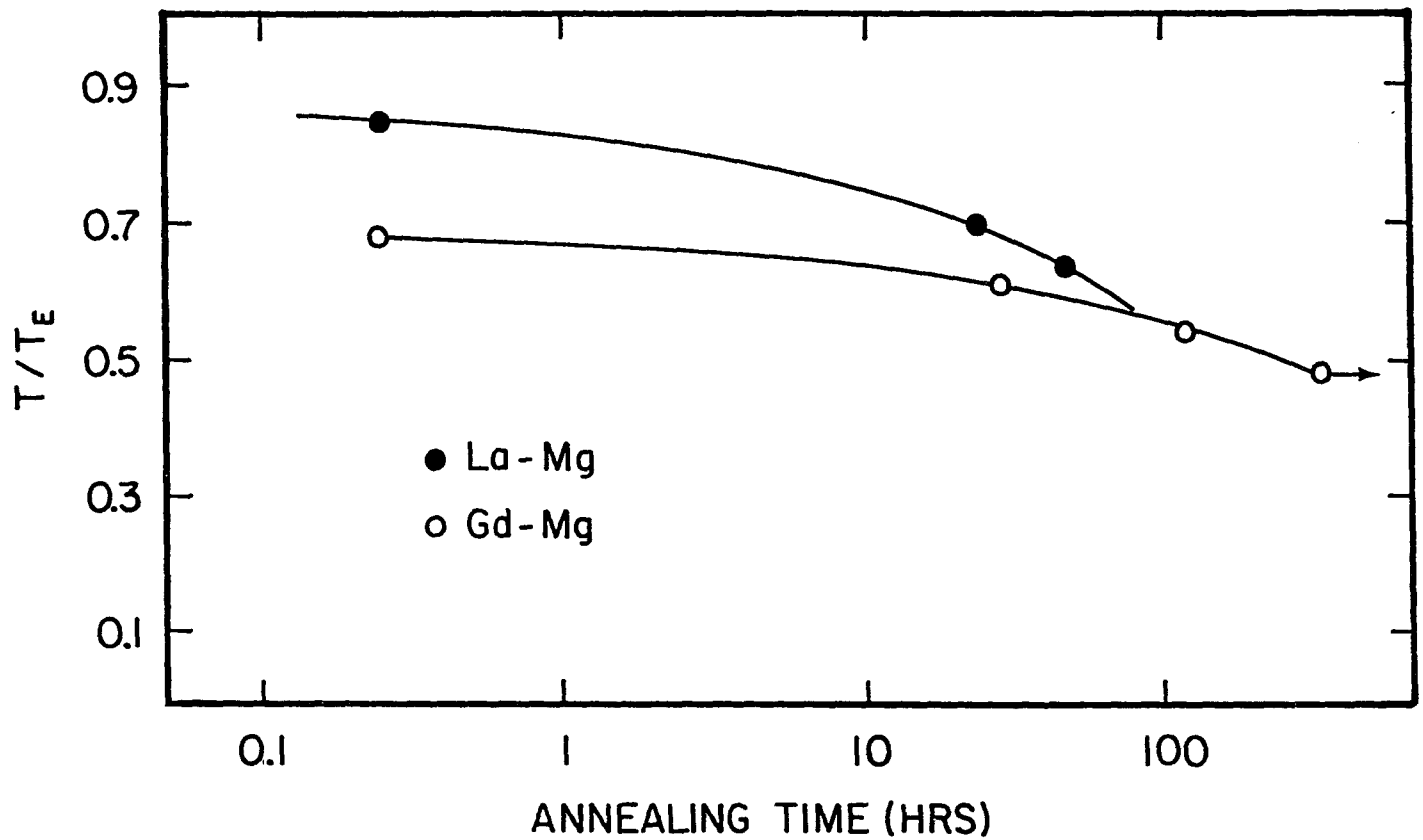

Figure 28. Reduced annealing temperature versus annealing time for Gd-Mg (this study) and La-Mg (Manfrinetti) alloys.

PART II. MAGNETIC STRUCTURE OF Mg-STABILIZED βGd AND βDy

βGd PROPERTIES

Magnetic Properties

The magnetic susceptibility from 4 to 30 K has been measured for four βGd alloys as a function of applied magnetic field. Static susceptibility, χ, was measured for all the alloys between 0.5 and 1.4 T while one of the alloys, at 28% Mg, was measured at lower fields, 0.05 and 0.005 T. In addition AC susceptibility, χ_{ac}, was measured for all the samples with B_o = 0.025 G.

High field

The 28% alloy is representative of the other alloys and its χ per mole of Gd is shown in Fig. 29 for B > 0.5 T. Above 120 K the alloy is paramagnetic. On cooling the alloy orders into a weak ferromagnetic state. The paramagnetic region, the ordering temperature and the magnetically ordered region are best discussed separately.

Paramagnetic region Above the 120 K the βGd alloys behave as normal paramagnets. A plot of the inverse susceptibility (Fig. 29) for the alloys is linear above T_c following the Curie-Weiss law. χ^{-1} is independent of applied field suggesting minimal ferromagnetic impurities (i.e., αGd). The effective paramagnetic moment per Gd atom, p_{eff}, is calculated from the slope, and the temperature intercept gives θ_p, the paramagnetic Curie temperature. These values are summarized for all the alloys in Table III.

The p_{eff} for βGd remains constant at about 8.5 μ_B independent of Mg concentration. The theoretical Gd 4f contribution, $g\{J(J+1)\}^{0.5}$, is 7.94 μ_B about 0.6 μ_B less than the measured values. The excess moment is due to polarization of the conduction electrons and is also found in pure Gd

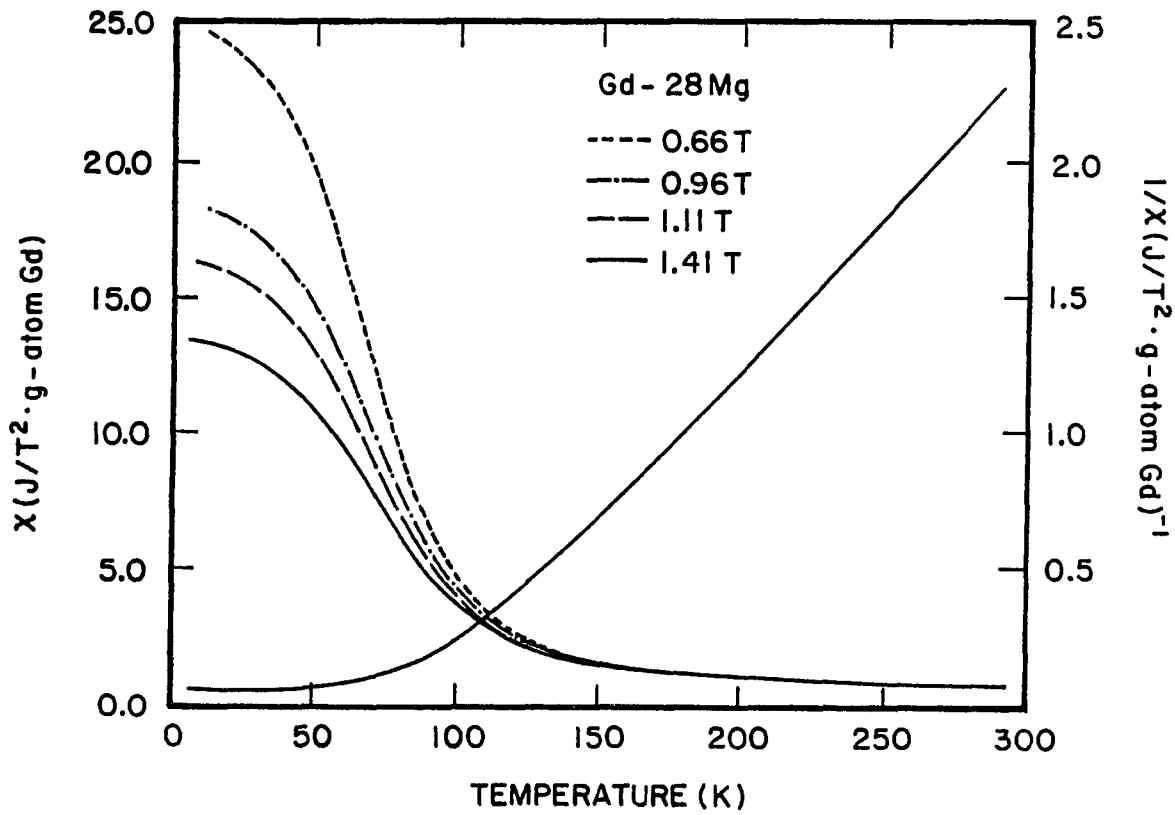

Figure 29. Magnetic susceptibility for the Gd-28Mg alloy, which is typical of all the Gd alloys.

and in Gd alloys. θ_p decreases with increased Mg content due to the increased amount of magnetic dilution.

Magnetic ordering The alloys order in what appears to be a ferromagnetic state at T_c some 20-30 K less than the value of θ_p. The Curie temperatures were determined from Arrott (σ^2 vs χ^{-1}) plots (Fig. 30) as the temperature where spontaneous magnetization was first observed. There was no evidence of a second transition in any of the "single phase" alloys that could be associated with a second phase. However, the same analysis was done for a known two phase alloy at 22% Mg, and the Arrott plot in this case shows two transitions with the higher T_c being for αGd. the fact that only one magnetic transition can be seen for the βGd alloys is further evidence that the dendritic "single phase" microstructures discussed previously are in fact very close to one phase alloys.

Table III. Summary of magnetic behavior in βGd

Alloy	C[a]	p_{eff} (μ_B)	θ_p (K)	T_c (K)	T_f (K)
Gd-23Mg	90.72	8.52	111.3	75	42.5
Gd-26Mg	90.68	8.52	103.0	71	46.0
Gd-28Mg	89.31	8.45	88.5	66	43.5
Gd-29Mg	90.18	8.49	89.7	62	45.5

[a]Curie-Weiss constant in $J \cdot K/T^2 \cdot$g-atom Gd.

A linear extrapolation to 0% Mg (Fig. 31) indicates an ordering for pure bcc Gd to be about 145 K. This is significantly lower than that of hcp Gd, 294 K. An extrapolation over such a long composition range is tenuous, so a series of saturated hcp αGd alloys were made by quenching from the eutectoid temperature. As can be seen there is an excellent linear relationship between these alloys up to 12% Mg suggesting that the bcc extrapolation may be valid. On the other hand, if the hcp line is

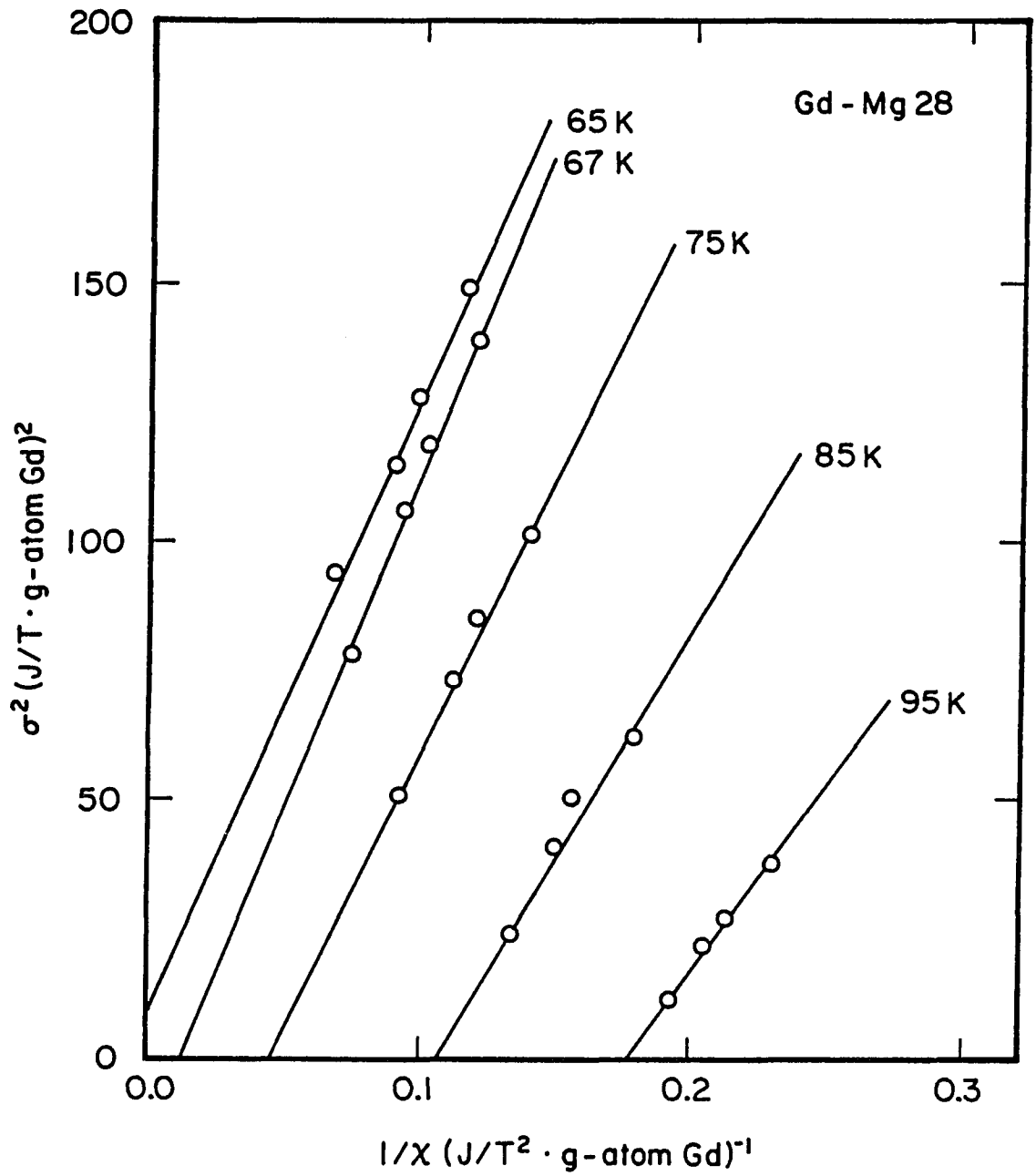

Figure 30. Arrott plot for Gd-28Mg. T_c = 66 K.

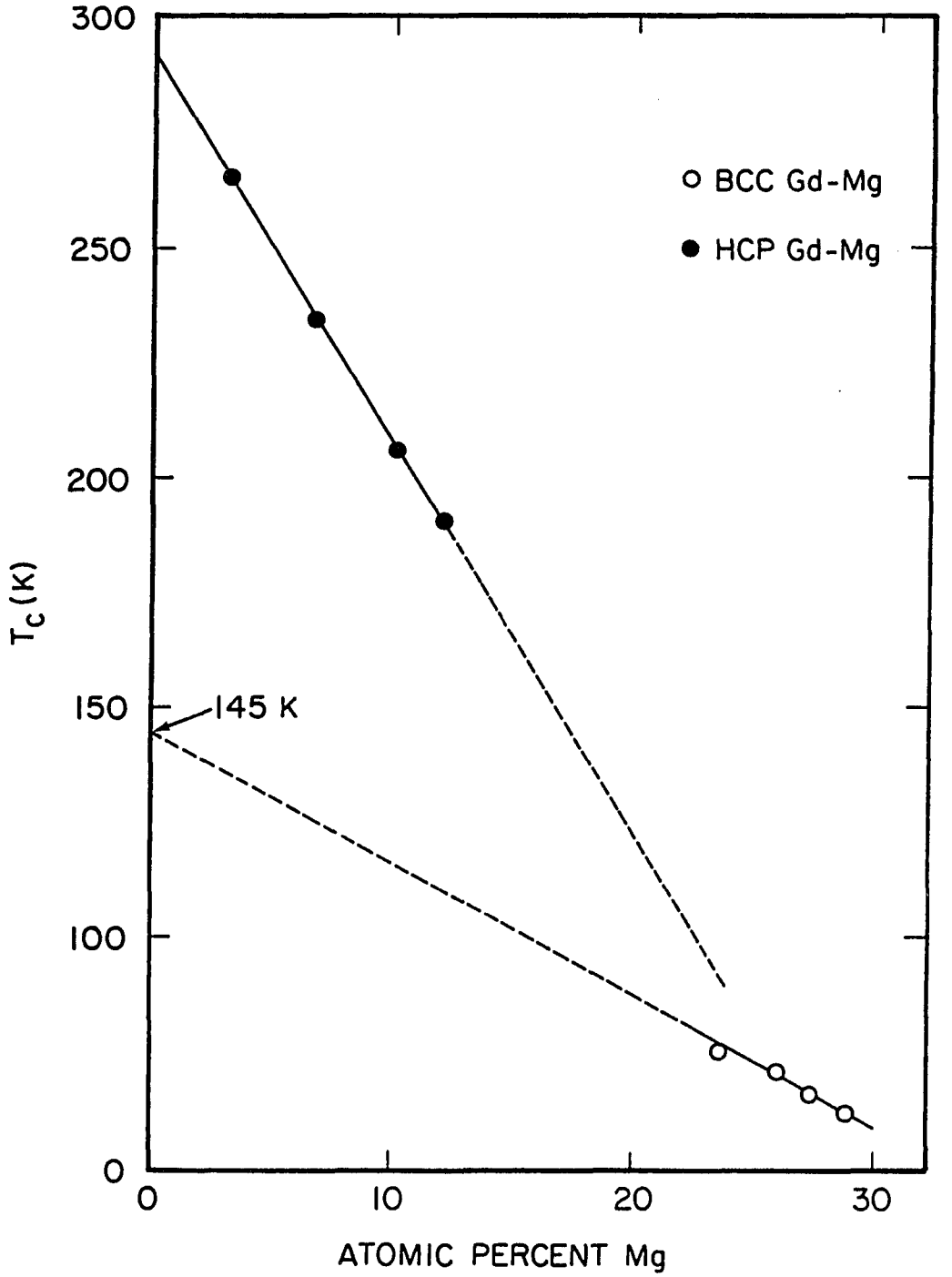

Figure 31. Curie temperature versus composition for bcc and hcp Gd-Mg alloys.

extended to meet the bcc data, one might conclude that the bcc curie temperatures are just an extension of the hcp Mg composition effect although it would no longer be linear.

Magnetic region From the magnetization, σ (in molar units), curves in Fig. 32 it is apparent that the 28% alloy is not yet saturated. This effect is seen more clearly in a plot of $\sigma_{4.2}$ vs. the internal field (i.e., corrected for demagnetization, Fig. 33). For all the alloys, even at 1.4 T the magnetization has not leveled off. The hcp alloys mentioned above have higher spontaneous moments at 77 K than the bcc phase at 4.2 K suggesting that a different degree of ordering may be occurring in the two phases. Whether the cause is due to Mg concentration or crystal structure effects cannot be determined from this measurement. The moment does increase as Mg concentration decreases suggesting that Mg additions change the number of Gd-Gd nearest neighbors, and their separation has an effect on the 4f-4f interactions via the conduction electrons (i.e., RKKY interactions). The maximum moment per Gd atom is only about 4.0 μ_B almost a factor of 2 lower than the 7 μ_B one would expect for Gd ions in a good ferromagnetic state.

Low field

Evidence for a magnetic disordering transition can be seen from χ measured at lower field for the 28% alloy (Fig. 34). In this measurement the sample was cooled to 5 K in zero field (ZFC), and χ was measured on heating with B= 0.005 or 0.05 T. When 120 K was reached (above θ_p) the sample was cooled this time in the measuring field (FC), and χ was measured on cooling. χ at low temperature for the ZFC branch is dramatically lower than that of the FC branch.

This type of irreversibility is characteristic of spin glass systems

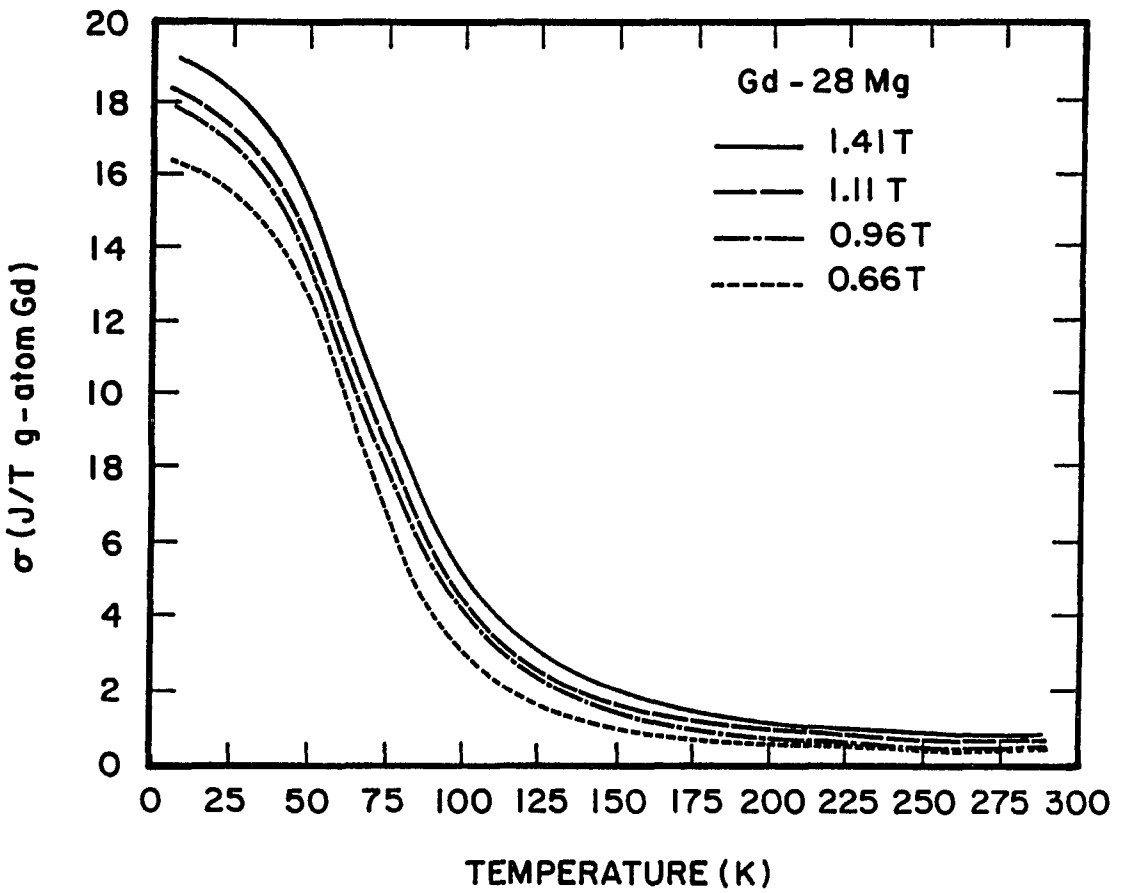

Figure 32. Magnetization versus temperature for Gd-28Mg.

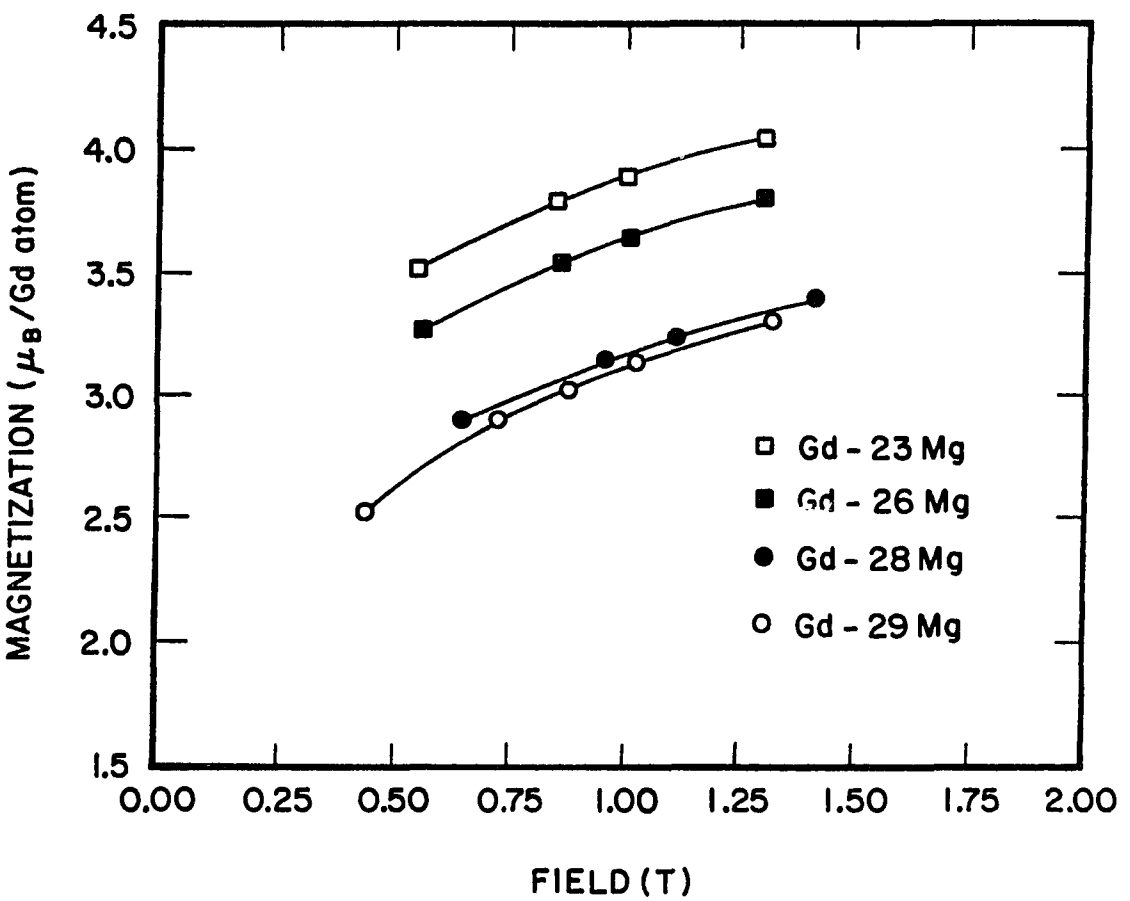

Figure 33. Magnetization at 4.2 K versus applied field for Gd-28Mg.

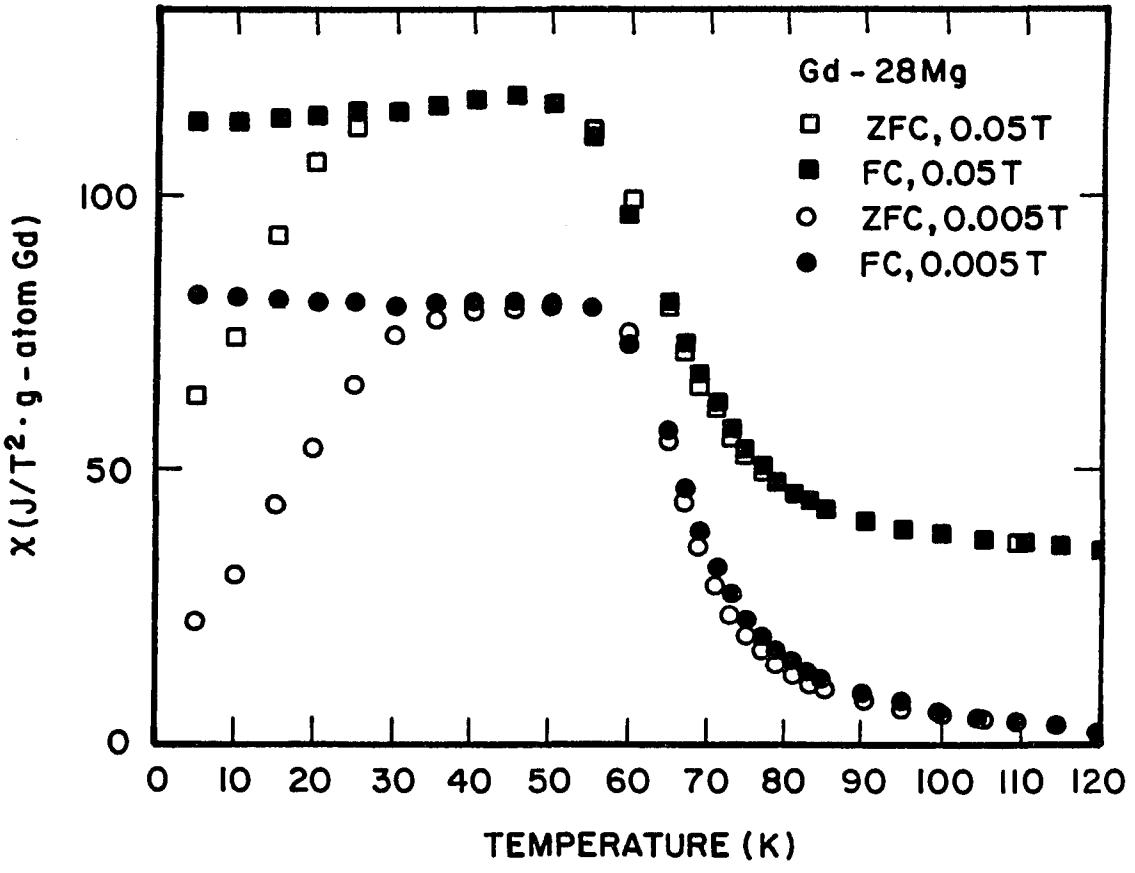

Figure 34. Field cooled (FC) and zero field cooled (ZFC) magnetic susceptibility for Gd-28Mg.

where the magnetic moments start to become frozen in some random arrangement below a critical temperature T_f marked by the divergence of the FC and ZFC branches. In the ZFC branch this spin freezing process destroys the spontaneous magnetization from the Curie transition. However if the sample is cooled in an external field as in the FC branch the moments freeze in a preferred orientation (that of the ferromagnetic alignment) with no drop in χ at T_f.

The spin disorder state created by zero field cooling can be destroyed by application of an external field and is observable by a reduction of T_f with increasing field. If T_f is taken as the divergent point of the FC and ZFC branches, one can see from Fig. 34 that T_f decreases from 50 K to 35 K when B is increased form 0.005 T to 0.05 T. The χ data for higher fields as in Fig. 29 were all ZFC measurements, and no downturn in χ exists showing that B=0.8 T is sufficient to completely revert the sample from the spin disorder state to the higher T ordered state.

In addition to the irreversibility at T_f there is a hysteresis at T_c. The χ's are equal for both branches in the paramagnetic state and at the maximum after ordering. However near the Curie temperature the cooling curve has a higher χ than the heating curve with the maximum difference occurring 5-8 K above T_c (Fig. 34).

T_f was determined for each alloy by low field (0.025 G) AC susceptibility as opposed to extrapolating low field static χ data to zero field. χ_{ac} is shown for the four alloys in Fig. 35, all measured on heating. The 28% alloy was measured on both heating and cooling below the maximum with no difference in χ_{ac}. Normally T_f is marked by a sharp cusp in χ_{ac}, but for these alloys the high temperature branch is lost due to

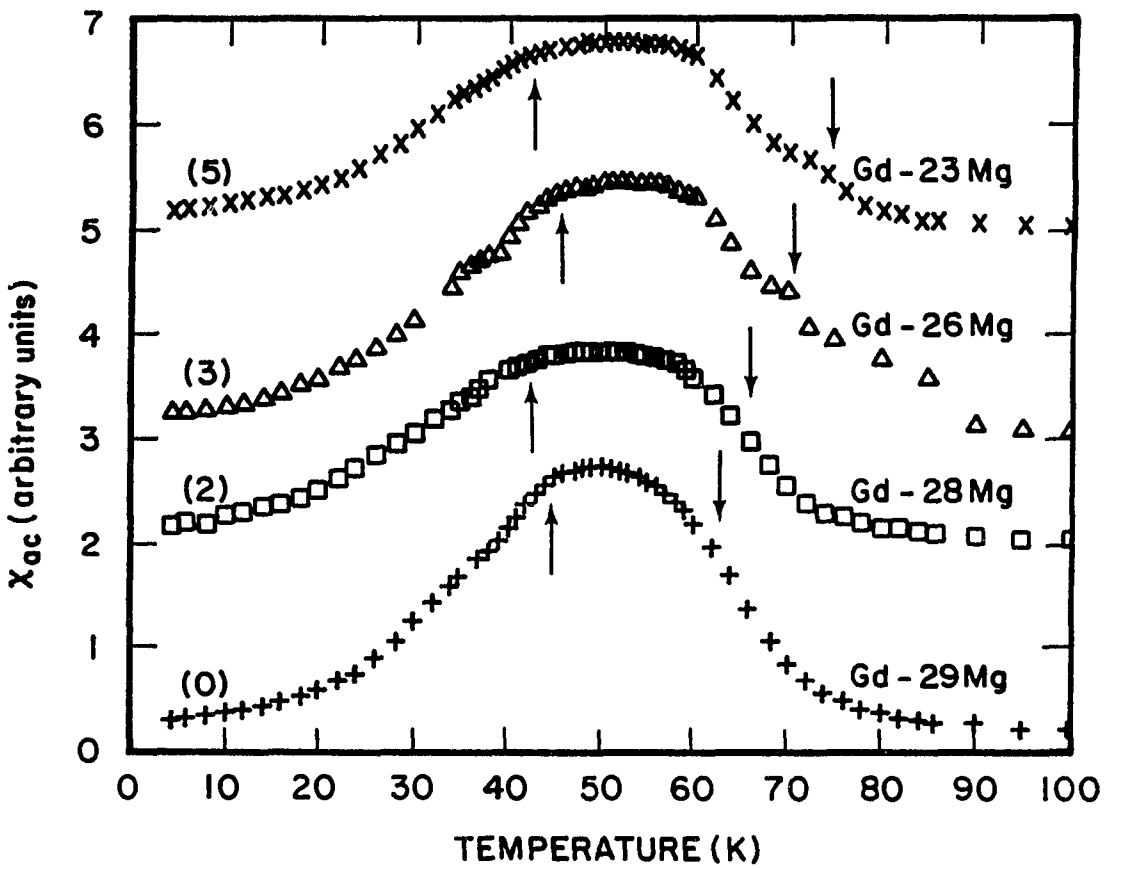

Figure 35. Ac magnetic susceptibility for Gd-Mg alloys. The number in parentheses is the amount of offset. The down arrows denote T_c's from Arrott plots and the up arrows denote T_f.

the ferromagnetic transition. Lacking a cusp, T_f was defined as the intersection between a linear extrapolation of the low temperature side of χ_{ac} with a horizontal line defined by the χ_{ac} maximum (see Gd-28Mg, Fig. 35). The results are plotted in a magnetic phase diagram along with the T_c's in Fig. 36. The tendency is for T_f to increase with Mg composition, the reverse of the T_c dependence. Although a pure spin glass behavior was never observed it is predicted by Fig. 36 for alloys containing up to 66% Gd which would be an unparalled large concentration of magnetic material for a spin glass.

Heat Capacity

The heat capacity has been measured for four bcc Gd-Mg alloys from 1.5 to 5 K (Fig. 37). Each curve is a combination of consecutive runs of approximately 50 points per run such that for each alloy there are at least 200 data points. The large amount of data points were taken to insure reproducibility and to enhance statistical fitting procedures.

Reproducibility was only achieved if the sample was electropolished before cooling the sample in the cryostat. Similar behavior was reported for pure Gd by Hill et al.[20] which was attributed to thin layers of ferromagnetic Gd_2O_3 on the surface that electropolishing removes.

The total heat capacity, C, does not follow a simple composition dependence. The effect of composition on C depends on the additive effects of the electronic, lattice and magnetic contributions. As Mg concentration increases, the Curie point decreases, and one would expect a higher magnetic contribution. At the same time the dilution of Gd with divalent Mg would cause a decrease in the electron concentration which for ferromagnetic βGd may cause a decrease in the electronic specific heat as

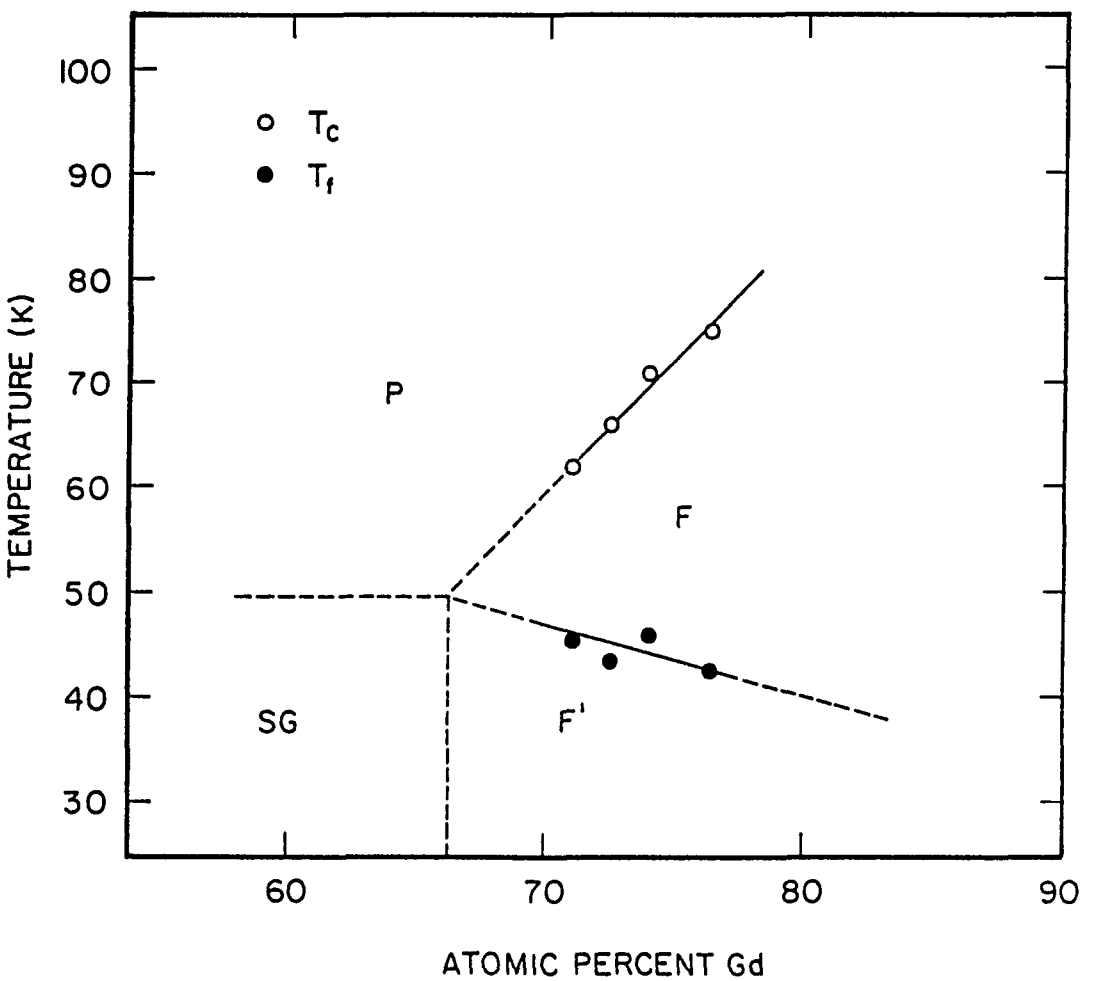

Figure 36. Magnetic phase diagram for the Gd-Mg system where P, F, F′ and SG are paramagnet, ferromagnet, mixed ferromagnet/spin glass and spin glass, respectively.

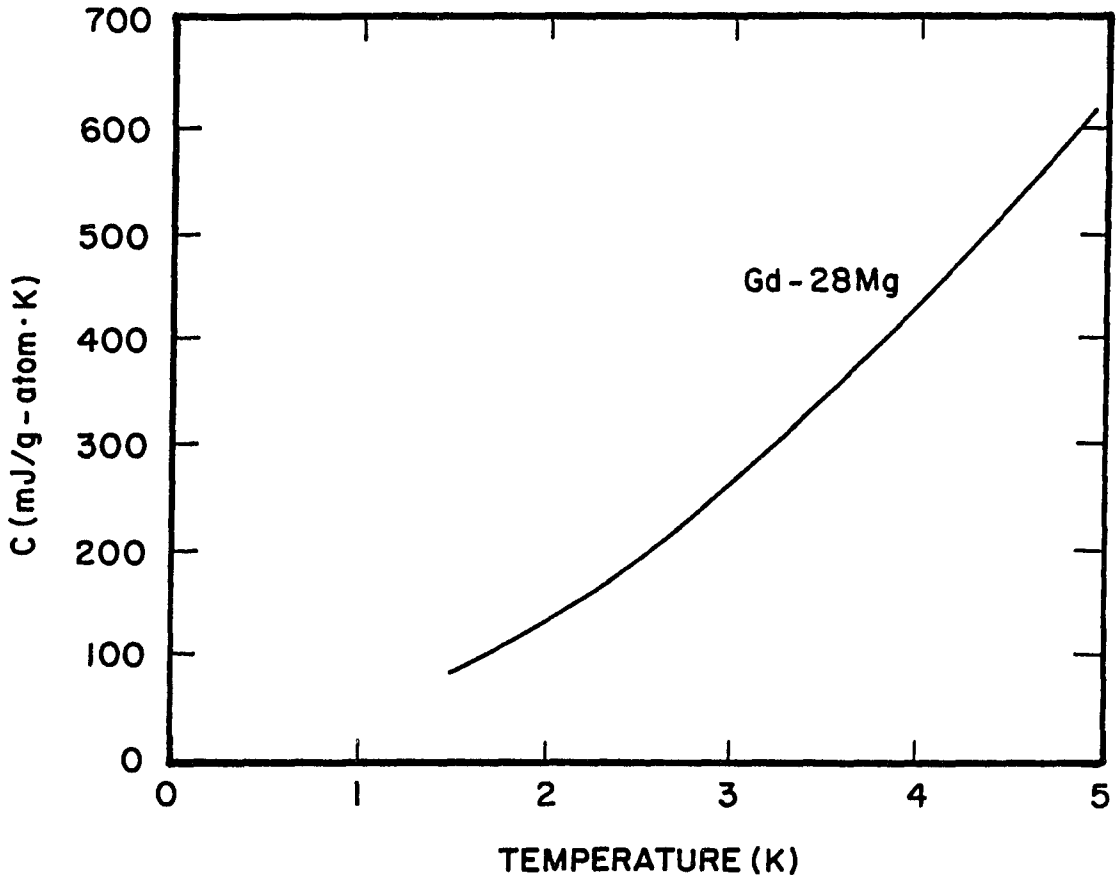

Figure 37. Heat capacity of Gd-28Mg.

suggested by band structure calculations.[21] One might also expect the lattice term to decrease with Mg additions due to solid solution stiffening, however this term might be dependent on the differences in the quench from alloy to alloy. The sum of these competing terms causes a complex composition dependence.

The strong curvature in the standard C/T vs. T^2 plot (Fig. 38) is evidence of a large magnetic term that overpowers the electronic and lattice terms. Even at the lowest temperatures (< 2K) the curvature still persists preventing the normal extrapolation to obtain the electronic coefficient, γ. The problem then becomes how to separate the three contributions to gain insight to the magnetic and electronic structure.

At low temperatures the C of a typical rare earth metal can be written as

$$(1) \qquad C = C_e + C_l + C_m + C_h$$

where C_e, C_l, C_m and C_h are the electronic, lattice, magnetic and hyperfine contributions respectively. The temperature dependence of C_e is linear, and C_l is a series of odd powers in T usually shortened to just T^3 for $T < \Theta_D/50$ where Θ_D is the Debye temperature. C_h goes as $1/T^2$.

The temperature dependence of C_m, even for pure materials is not definite though in general one can write

$$(2) \qquad C_m = DT^n \exp(-E_g/T)$$

where n varies with the type of magnetism involved, D is a constant, and E_g is an energy gap in the spin wave spectrum associated with the magnetic anisotropy of the crystal. Classically, n=1.5 for a ferromagnet and 3.0 for an antiferromagnet although these numbers are only valid at temperatures far below the ordering temperatures.

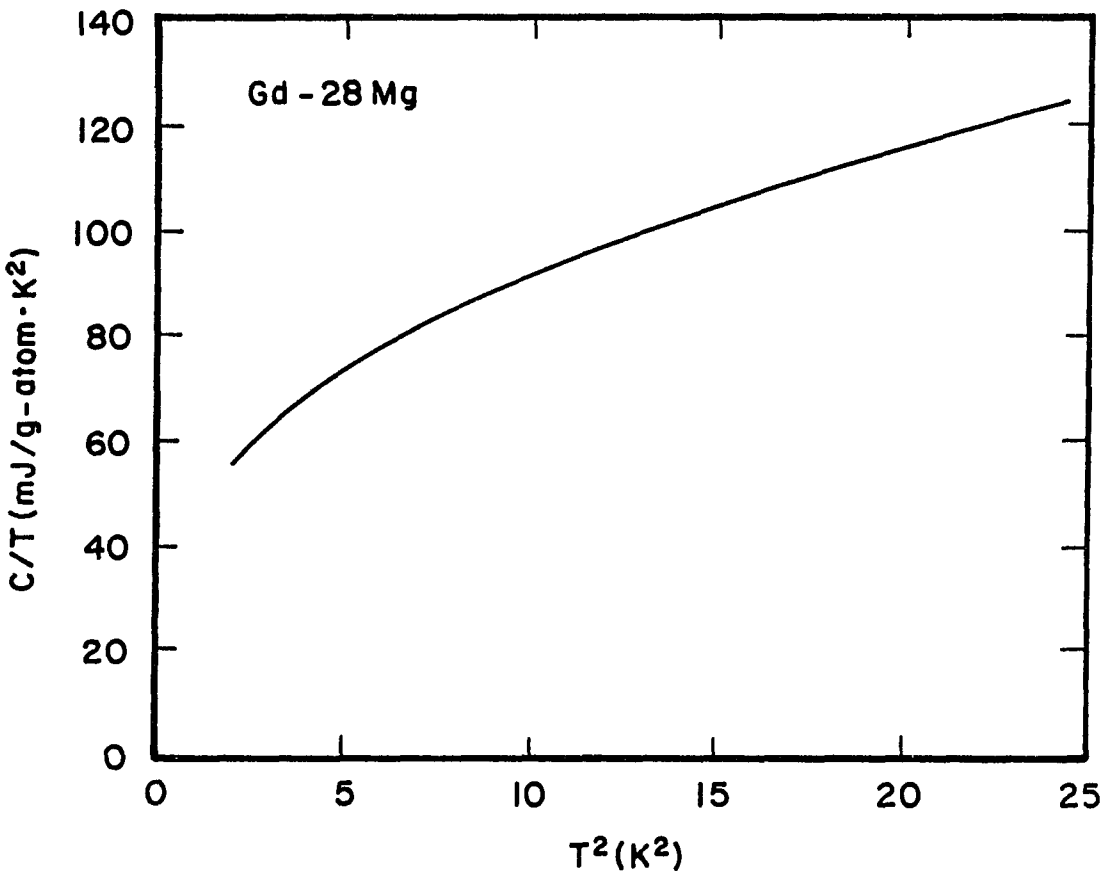

Figure 38. C/T versus T^2 for Gd-28Mg.

The complete temperature dependence can then be written as

$$(3) \qquad C = AT + BT^3 + DT^n\exp(-E_g/T) + C_h$$

where B is related to Θ_D and $A=\gamma$ (where γ is the electronic specific heat) in the absence of any other linear excitations. For Gd alloys some simplifications can be made. In its normal state Gd has no orbital angular momentum contribution (L=0) which means first that $C_h=0$. In addition, no orbital angular momentum would imply minimal anisotropy which would make E_g zero as well. The final equation would read

$$(4) \qquad C = AT + BT^3 + DT^n$$

The separation of the heat capacity into its components for the rare earths is not an easy task. Historically, a number of methods have been attempted with varying degrees of success. Lounasmaa and Sundstrom[22] chose to make an estimate of γ based on an average value of the nonmagnetic rare earth metals and also assumed a constant Θ_D (that of Lu) for all the heavy rare earths. In this way they could reduce equation (1) to just the magnetic term which could be easily analyzed. Morrison and Newsham[23] suggest a series of graphical extrapolations taking into account the relative magnitude of the specific terms in different temperature ranges. If limiting slopes were used, they claimed that two or three iterations would give consistent results. More recently, Hill et al.[20] for pure Gd assumed n=1.5 based on neutron scattering experiments of Stevens and Krukewich[24] and Sedaghat and Cracknell.[25] This reduces eq. (4) to a linear equation that could be fitted with standard least squares techniques.

Because it has been well established today that γ is not uniform across the lanthanide series,[20,26,27,28] Lounasmaa's and Sundstrom's method was not attempted. The graphical method of Morrison and Newsham

was attempted, but even after 20 iterations the parameters had not yet converged satisfactorily. The n=1.5 approximation is only good if the Curie temperature is far from the measurement range. For pure Gd, T_c=294 K, this is a good assumption; for the Gd-Mg alloys, T_c=80 K, it is not as good. Nevertheless least squares fits were tried with n=1.5, but nonphysical (e.g. A < 0) values for A or B were required for good fits suggesting n > 1.5.

A constrained non-linear statistical routine was tried next to fit the whole model [equation (4)]. This type of program searches for a minimum is the residual sum of squares subject to constraints specified by the operator such as A > 0 or n < 2. The program tended to go the limit of the constraints finding no local minima in the parameter ranges specified. That is, the best fit using equation (4) does not necessarily correspond to physical meaning.

What was discovered was that the fit was very sensitive to the value chosen for n. For example, if B was fixed at 0.35 mJ/g-atom K^4 (Θ_D=177 K), changing n from 1.50 to 1.65 would change A from -7 to +11 mJ/g-atom K^2 while changing D only from 50 to 35 mJ/g-atom K^{n+1}. This computer program had too much latitude in choosing n to get its best fit, so if n could be somehow fixed, a proper fit could be obtained.

To get a good value for n one has to know what C_m looks like, so a theoretical alloy was modeled. From band theory[21] γ should be between 5 and 10 mJ/g-atom K^2. One would expect some stiffening of the lattice due to Mg additions and some softening due to changing Gd from hcp to bcc. Since pure hcp Gd has Θ_D=169 K, the Debye temperature for the model alloy should be between 150 and 200 K. The theoretical heat capacity was thus examined with γ = A = 8 mJ/g-atom K^2, B=0.35 mJ/g-atom K^4 (Θ_D=177 K),

n=1.6 and D=38 mJ/g-atom $K^{2.6}$ with the estimates of D and n coming from previous fit attempts where A = 8 and B=0.35. The contribution of each term based on the above model are in Table IV.

Although the percentage of the total heat capacity for C_e and C_l increase and decrease with increasing temperature, respectively, the magnitude of C_m on a percentage basis goes through a maximum around 3 K and is remarkably constant. Between 2.25 K and 4.00 K the electronic and lattice term changes, on a percentage basis, in opposite directions at nearly the same rate. The result is that they cancel each other out, and that C_m/C varies at most 0.5%, within the experimental error. One can then write

$$C = K' C_m \qquad 2.25 < T < 4.00 \tag{5}$$

or

$$C = KT^n. \tag{6}$$

Taking a logarithm of both sides gives

$$\ln(C) = \ln(K) + n \ln(T) . \tag{7}$$

A plot of ln(C) vs ln(T) for a representative alloy are in Fig. 39. The curves for the other alloys are similar, and are almost linear especially between 2.25 K and 4.00 K. n was determined from a least squares fit of the logarithmic data. These n's were then used in equation (4) which was subsequently fit to the entire data of each alloy using a linear least squares method. Table V summarizes the results. The error limits are the least square standard deviations.

A plot of n vs. %Mg (Fig. 40) shows that n is decreasing with Mg content as would be expected. Decreasing Mg raises the Curie temperature

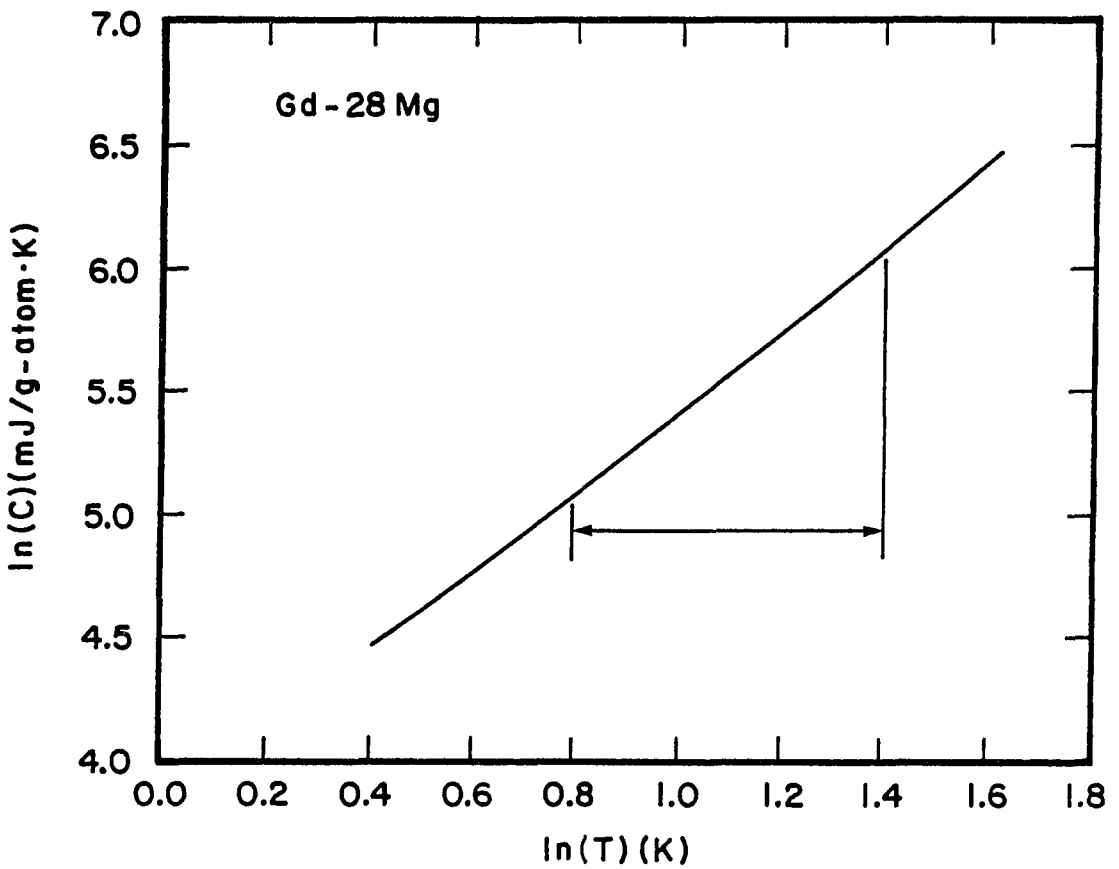

Figure 39. Ln(C) versus ln(T) for Gd-28Mg. The bracket marks the temperature range from which n was determined.

which would tend to bring n closer to the classical value of 1.5. The relationship is not linear, but the curve is bending in such a way to approach a value near 1.5. The Debye temperatures calculated from the B parameter show no clear composition dependence, but the values are reasonable in light of the previous discussion. Because the contribution of C_l is small relative to the magnetic and electronic contributions at these temperatures, Θ_D can only be known within 4 or 5 K. Taking this error into account, the Θ_D's are nearly constant.

Table IV. Relative contribution (%) of the heat capacity terms in βGd model

T	C_e	C_l	C_m
1.50	14.0	1.4	84.6
1.75	13.0	1.7	85.4
2.00	11.9	2.1	86.0
2.25	11.1	2.5	86.4
2.50	10.5	2.9	86.6
2.75	10.0	3.3	86.8
3.00	9.5	3.7	86.8
3.50	8.6	4.6	86.8
4.00	7.9	5.6	86.5
4.50	7.4	6.5	86.1
5.00	6.9	7.5	85.6

Values for A range from 4.79 to 8.06 (Fig. 41) increasing with decreasing Mg content, however a change of this magnitude cannot be explained by electron concentration effects. Leung et al.[21] predict γ for ferromagnetic bcc Gd to be as high as 11.4 mJ/g-atom K^2, but does not predict a large decrease in γ with Mg composition in a rigid band model. The χ measurements indicate the strong possibility of spin glass excitations in these materials which would contribute a linear term (see Discussion) to the overall heat capacity not accounted for in C_m. It seems likely, therefore, that the parameter A is a combination of γ and a

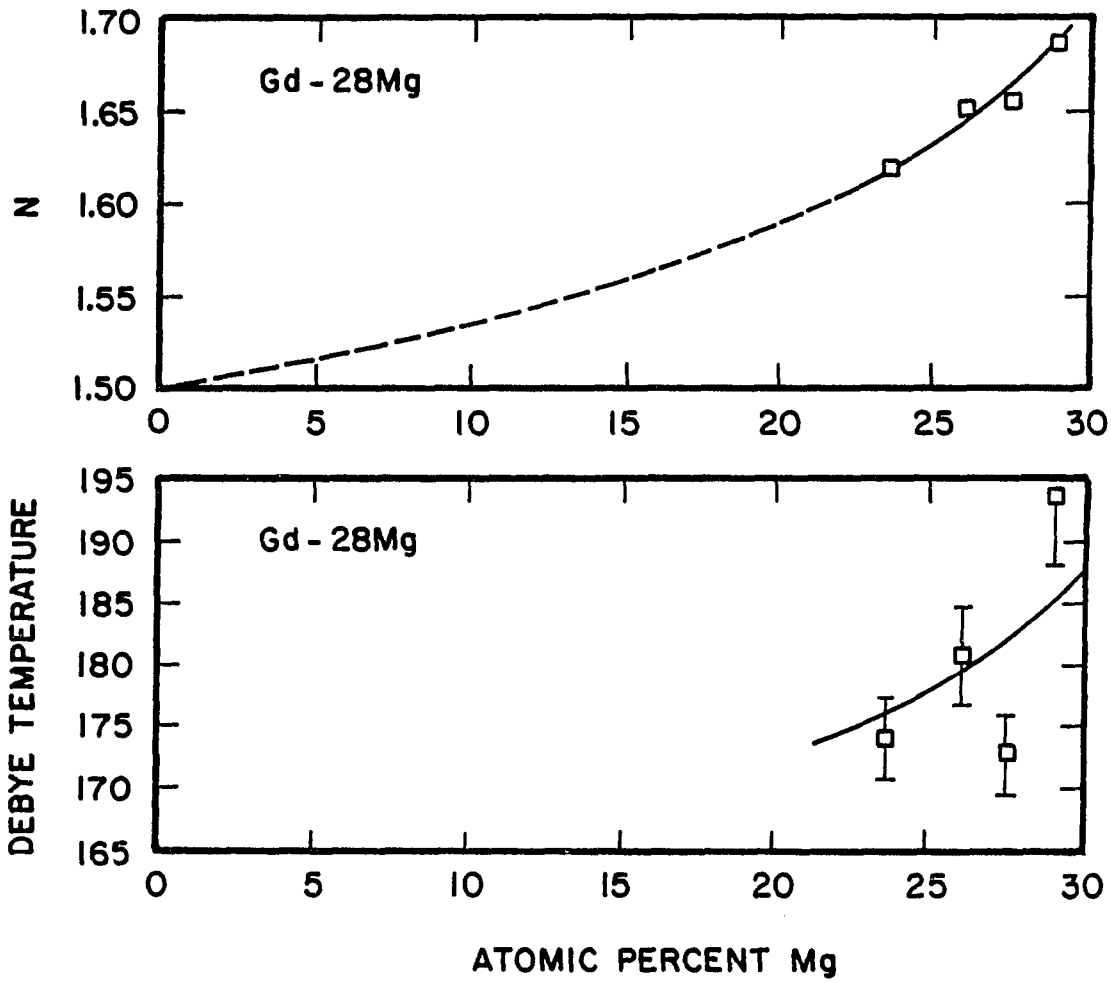

Figure 40. n and Θ_D versus composition for Gd-Mg alloys. The error bars for n are twice the size of the symbols.

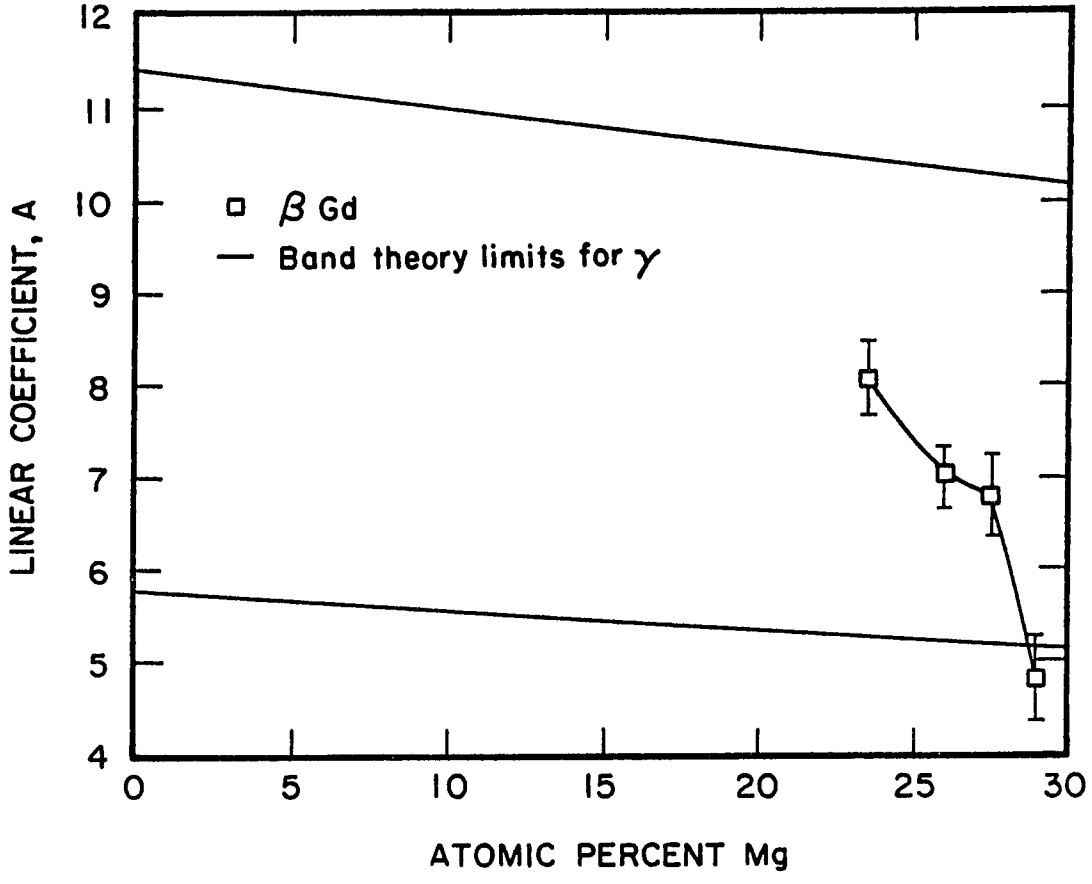

Figure 41. Linear heat capacity coefficient versus composition for Gd-Mg alloys. The solid lines mark the limits of γ predicted by Leung et al. with the slope being the expected composition dependence of γ from their theory.

spin glass term.

Table V. Summary of heat capacity coefficients for $^{\beta}$Gd in mJ units

Alloy	A	B	D	n	Θ_D (K)
Gd-23Mg	8.06 ± 0.39	0.37 ± 0.02	37.5 ± 0.3	1.620 ± 0.002	174 ± 4
Gd-26Mg	7.02 ± 0.33	0.33 ± 0.02	39.3 ± 0.2	1.651 ± 0.002	181 ± 4
Gd-28Mg	6.79 ± 0.48	0.37 ± 0.02	38.1 ± 0.3	1.656 ± 0.002	173 ± 5
Gd-29Mg	4.79 ± 0.44	0.27 ± 0.02	35.5 ± 0.3	1.688 ± 0.003	193 ± 5

β-Dy PROPERTIES

Magnetic Susceptibility

As for Gd alloys χ for the βDy alloys was measured for B_o up to 1.4 T (Fig. 42). The alloys follow Curie-Weiss behavior with θ_p ranging form 31 to 35 K (Table IV, p. 59). The effective moment calculated from the Curie-Weiss law gives p_{eff} between 10.8 and 10.9 μ_B. The theoretical moment for Dy is 10.64 μ_B, so there is only a small amount of conduction electron polarization.

Table VI. Summary of magnetic behavior in βDy

Alloy	C[a]	p_{eff} (μ_B)	θ_p (K)	T_f (K)
Dy-27Mg	149.10	10.92	31.4	30.0
Dy-28Mg	147.s6	10.86	35.1	31.0
Dy-29Mg	145.91	10.80	31.6	30.5

[a]Curie-Weiss constant in $J \cdot K/T^2 \cdot$g-atom Dy

High field

The type of magnetic ordering for βDy is different than for the βGd alloys. Even though $\theta_p > 0$, the alloys do not order ferromagnetically. Second, there is a maximum in χ that persists up to B=1.4 T. Arrott plots like Fig. 43 confirm no spontaneous magnetization down to 20 K where χ starts to decrease suggesting antiferromagnetic or spin glass ordering. The maxima vary little with composition in contrast to the T_c's of βGd which had a clear composition dependence, and the maxima are independent of applied field strength.

Low field

At low fields the maxima are better defined and less rounded. Fig. 44 shows FC χ(T) for the 27% alloy. The leveling of χ below 15 K is

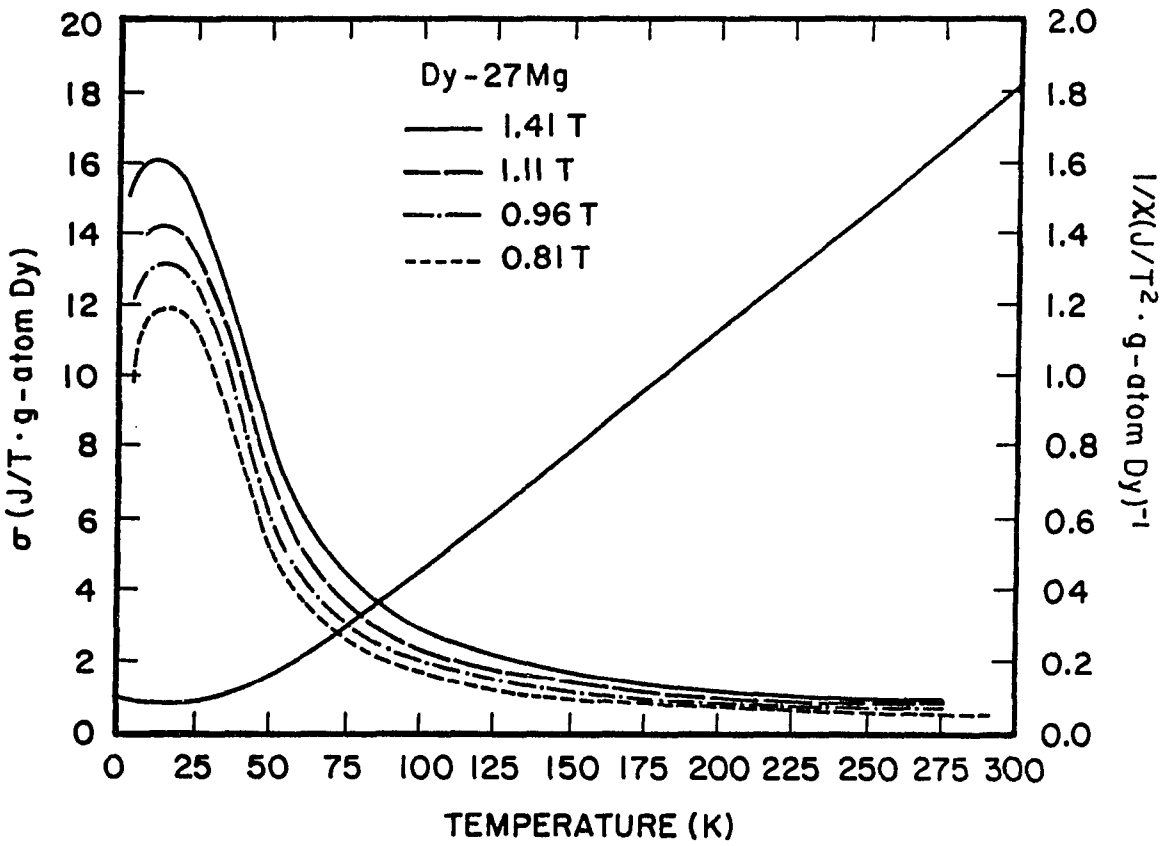

Figure 42. Magnetic susceptibility for Dy-27Mg.

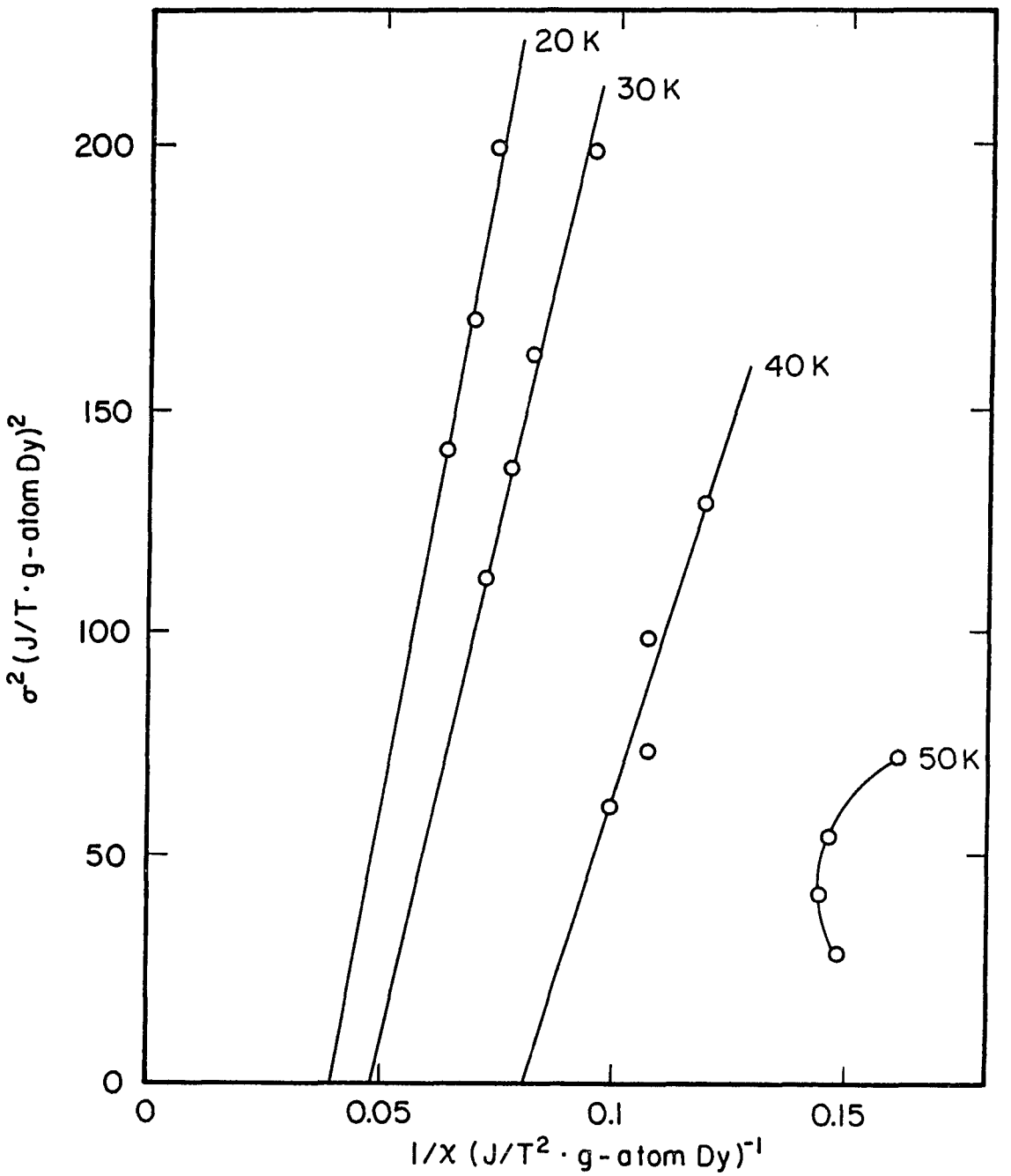

Figure 43. Arrott plot for Dy-27Mg. Note that there is no spontaneous magnetization.

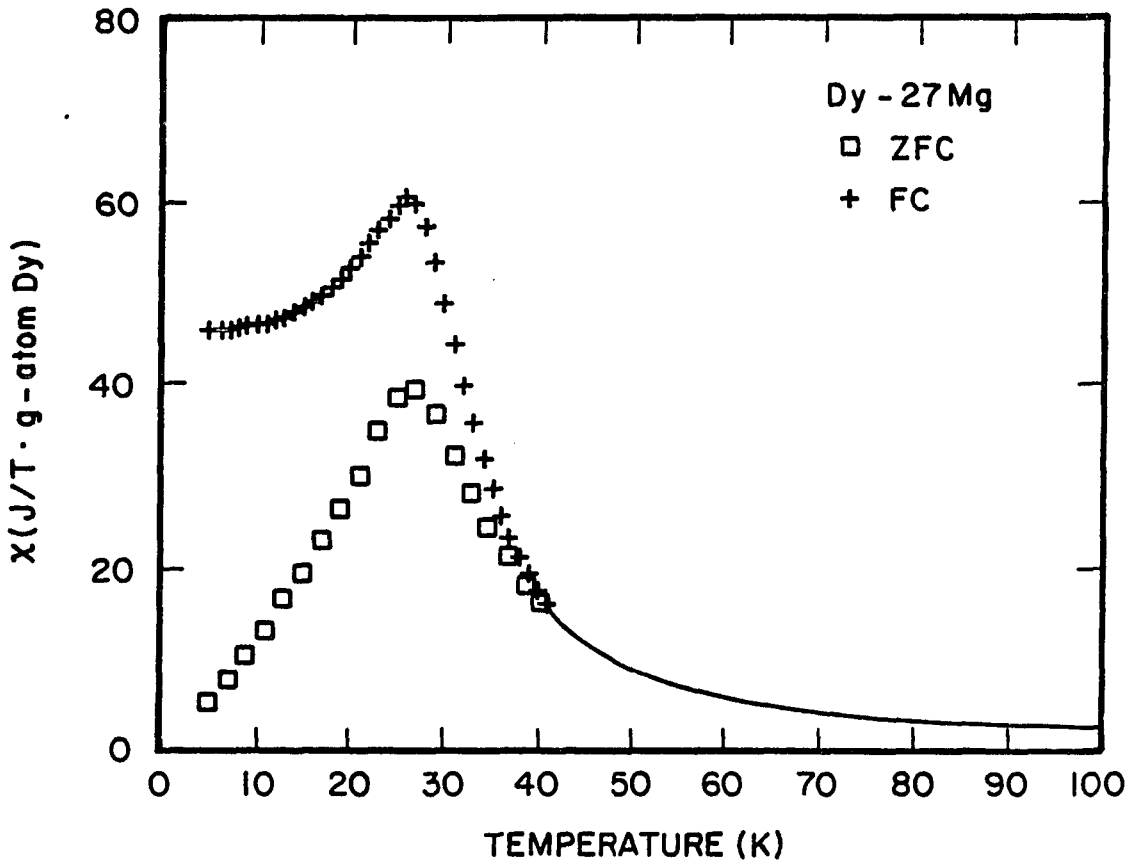

Figure 44. Field cooled (FC) and zero field cooled (ZFC) magnetic susceptibility for Dy-27Mg.

typical of antiferromagnetic ordering for polycrystalline materials. If the sample is ZFC a large drop in χ is seen, but the maximum remains at the same temperature. There are two other features to be examined closely. First, the splitting of the FC and ZFC branches occurs above the ordering maximum which is unusual. If the field cooling irreversibilities are of spin glass nature, one would expect that this state would be favored at lower temperatures than an assumed antiferromagnetic state. Second, the leveling off in χ does not exist for the ZFC branch. A nearly linear decrease in χ down to 5 K is similar to the disorder transition in βGd. There seems to be both spin glass and antiferromagnetic transitions going on with nearly the same ordering temperature. The field splitting above the cusp is more complex and may be the effect of competition between the two types of ordering. The maximum at 0.005 T is 10 K higher than for the high field measurements, and as the field is increased to 0.2 T the maximum becomes more rounded and begins to shift to lower temperatures (Fig. 45).

The χ_{ac} (Fig. 46) for the three βDy alloys show similar behavior. A cusp in χ_{ac} is sharp and well defined and could represent spin glass ordering. T_f, given by the maximum in χ_{ac} (Table VI), is the same within 1 K for all the compositions with the average at 30.5 K and does not show any obvious composition dependence.

Heat Capacity

The heat capacity up to 80 K has been measured for two of the alloys (Fig. 47). Above 70 K the scatter due to experimental limitations becomes too great for confident measurement. There is, however, a broad maximum between 40 and 50 K due to the magnetic ordering. The magnitude of the

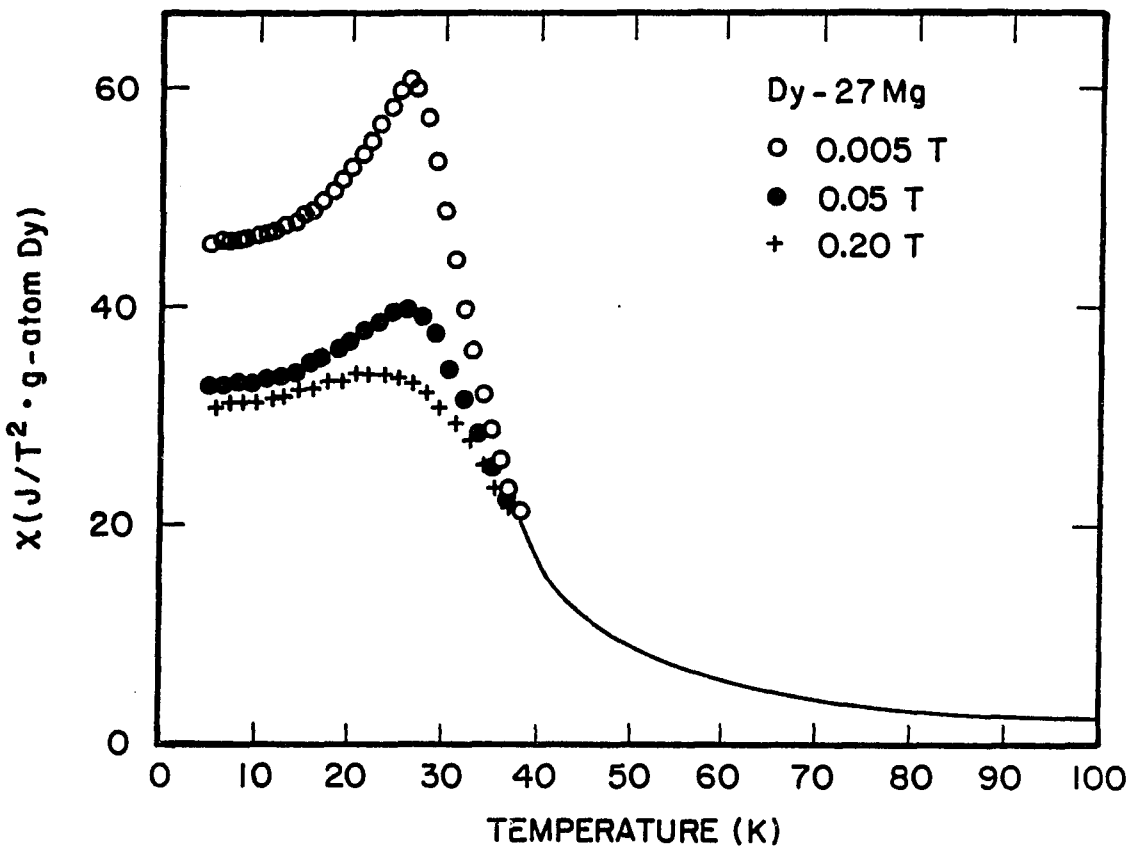

Figure 45. Field cooled magnetic susceptibility of Dy-27Mg as a function of field.

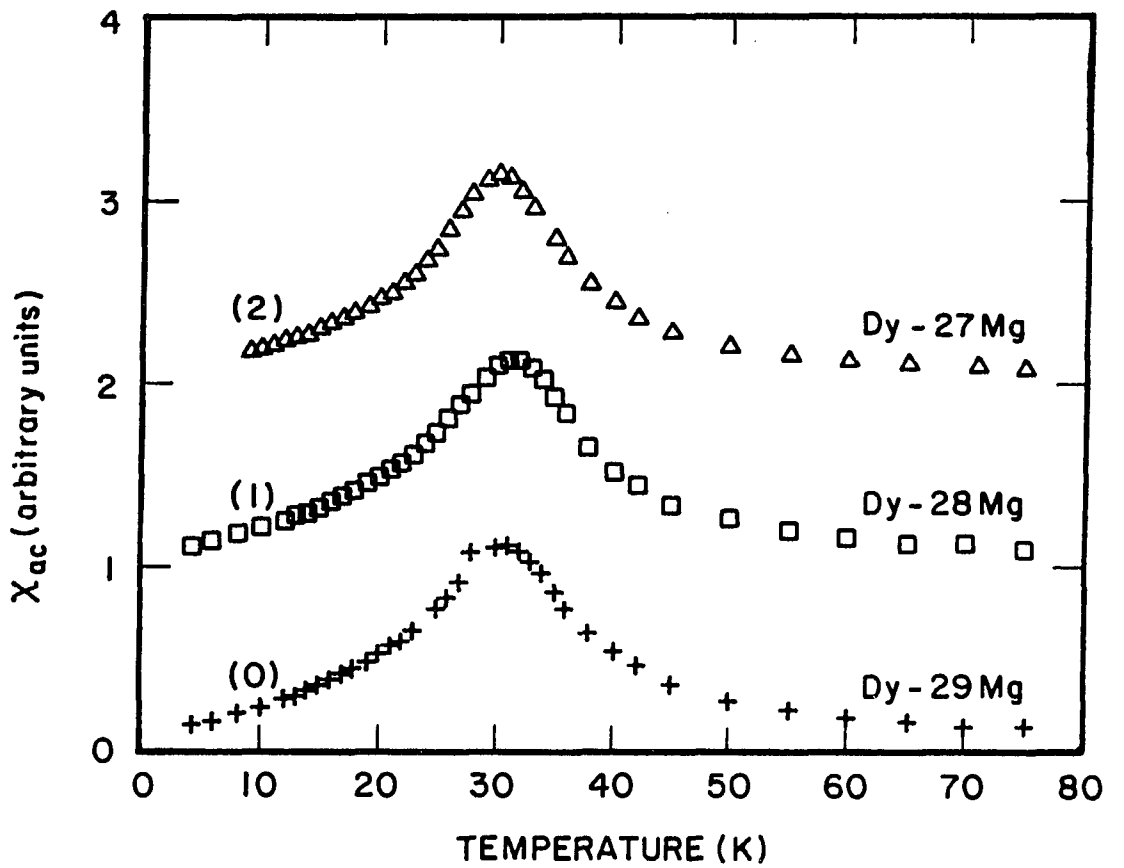

Figure 46. The ac magnetic susceptibility for three bcc Dy-Mg alloys. The offset is in parentheses. The cusp indicates T_f.

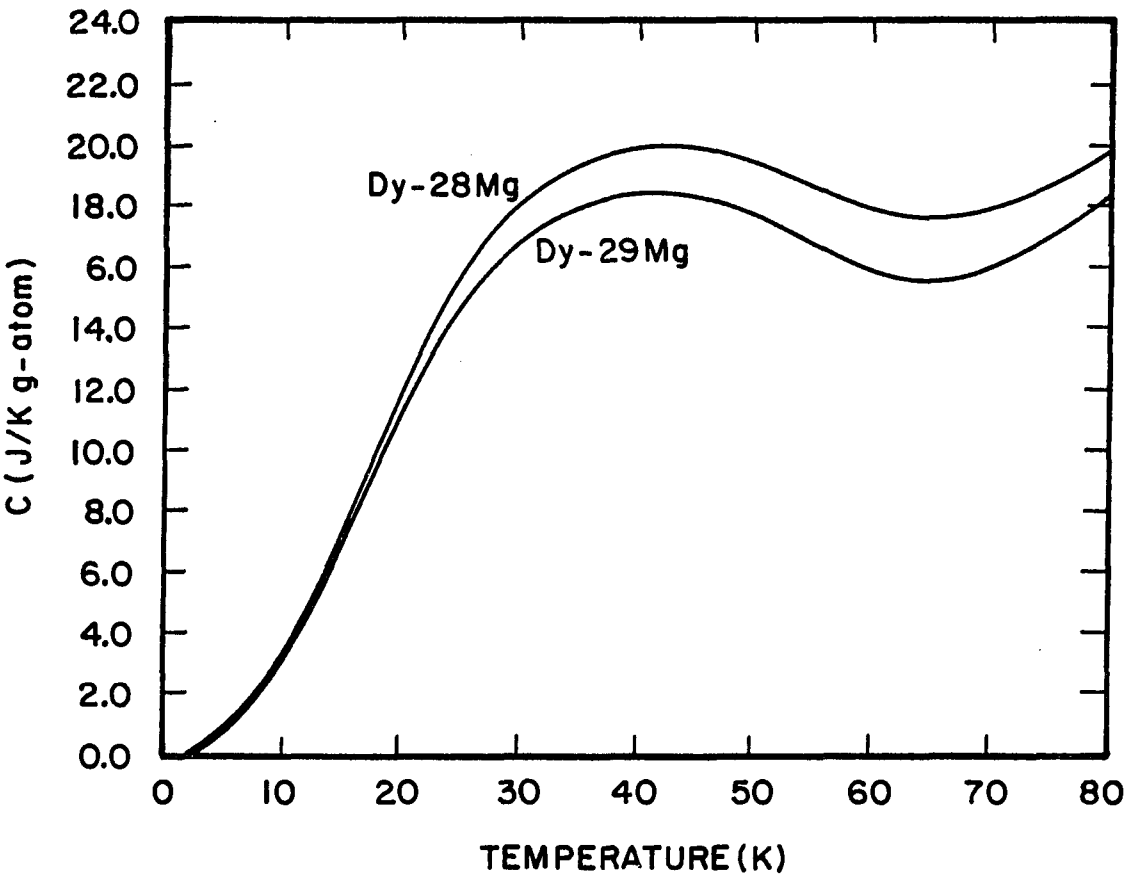

Figure 47. Heat capacity for two Dy-Mg alloys.

lattice contribution is increasing rapidly in this temperature range, and it should account for about 50% of the total heat capacity. Therefore, the actual maximum in C_m will be somewhat lower. The standard C/T vs T^2 plot (Fig. 48) for T < 10 K shows a distinct curvature, but not as much as the Gd alloys. It is apparent that C_m does not go as T^3 (a straight line on this plot) unless there is severe damping, so spin glass ordering looks more favorable than antiferromagnetic ordering.

For Dy there is a hyperfine contribution so there are at least four terms contributing to the total heat capacity: electronic, lattice, hyperfine and magnetic. The hyperfine contribution arises from the two isotopes, Dy^{161} and Dy^{163}, both with I = 5/2 giving six hyperfine levels each.

Following the analysis of Hill[29] for pure Dy, the Hamiltonian is

$$H = AI_z + P\{I_z^2 - I(I+1)/3\} \tag{8}$$

where A and P are constants associated with the given isotope. The energy associated with each level can be calculated directly from this Hamiltonian which can then be used to calculate the expected C_h. In the high temperature limit C_h can be represented as

$$\frac{C_h^n}{R} = c_2^n T^{-2} + c_3^n T^{-3} + \ldots \tag{9}$$

where c_h^n is the contribution of the n^{th} isotope and

$$c_2^n = \frac{1}{3}A_n^2 I(I+1) + \frac{1}{45}P_n^2 I(I+1)(2I+3)(2I-1) \tag{10}$$

and

$$c_3^n = -\frac{1}{15} A_n^2 P_n I(I+1)(2I+3)(2I-1).$$

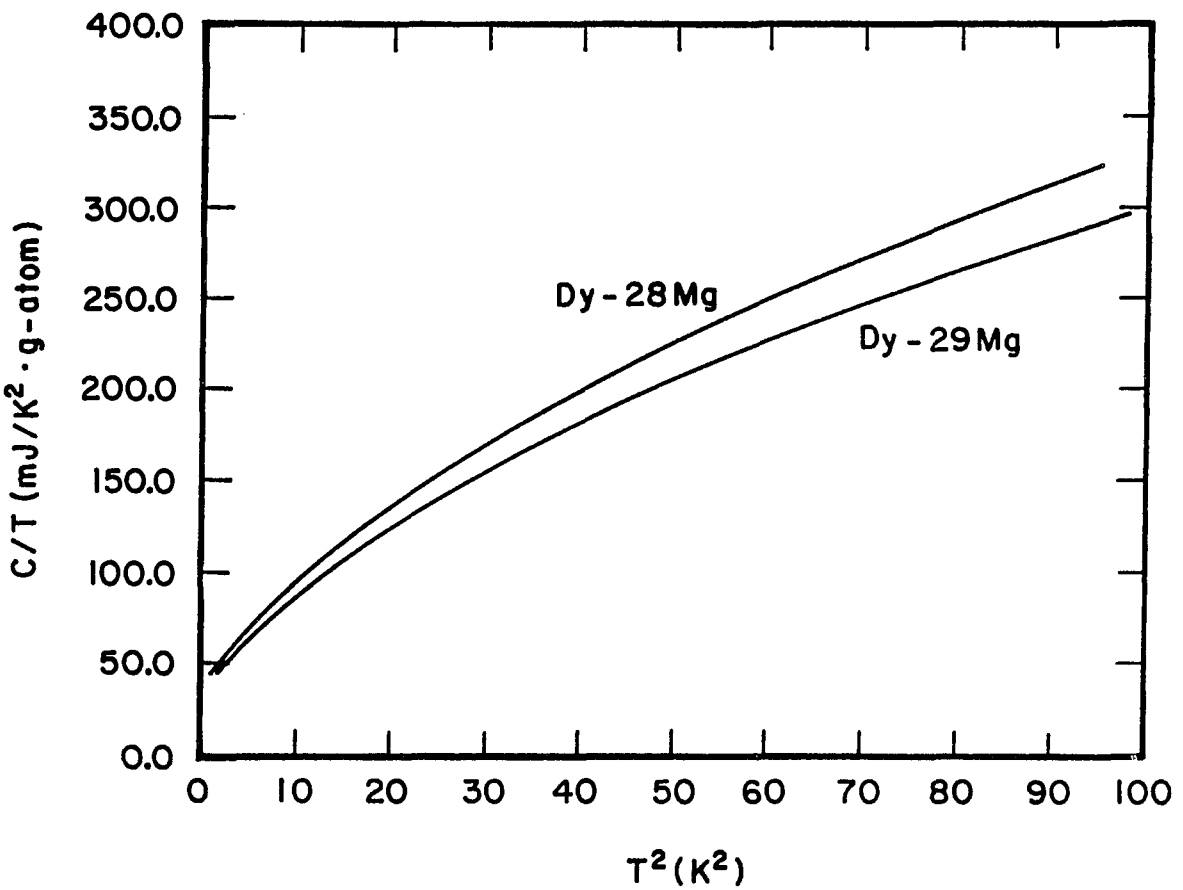

Figure 48. C/T versus T^2 for two Dy-Mg alloys.

The total hyperfine contribution can be written as

$$(11) \qquad C_h = f(a^{161}C_h^{161} + a^{163}C_h^{163})$$

where f is the atomic fraction of Dy in the alloy, and a^n is the isotopic abundance. Values for A_n and P_n were obtained from NMR measurements: A_{161}, $2P_{161}$, A_{163} and $2P_{163}$ = 830, 388, 1163 and 410 MHz, respectively.[30] The isotopic abundances were measured in this laboratory on Dy metal of similar stock, a^{161} = 0.1854 and a^{163} = 0.2522.[31] Using these values C_h can be approximated by

$$(12) \qquad C_h = f(28.235T^{-2} - 1.6177T^{-3})$$

for mJ/g-atom·K units. Rigorous calculations were done from (8) using a computer program provided by Hill[29] (Appendix E). The difference between (8) and (12) is only 0.2% at 1.6 K and falls to 0.025% at 5 K. Although the differences are well within experimental error, the rigorous calculation was chosen to represent C_h.

Ln(C) versus ln(T) plots, following the βGd analysis, predict a power law for C_m where $2 < n < 3$. However, the large linear region below 5 K like on the βGd plots are not available for the Dy alloys, so a definite choice could not be made confidently. Thus fitting was tried in two different ways.

The first method was to assume a power law dependence for C_m. Because the exponent would be close to 3 (the lattice term) an estimate of Θ_D was chosen to represent the T^3 term. The value of Θ_D should not differ much between βGd and βDy, so the arbitrary value of 180 K was selected. This value is a rough average of βGd alloys, and it is to be treated as an estimate only. The hyperfine and lattice estimates were subtracted from

the total heat capacity, and the remaining contributions were fit by trial and error to the form $AT + BT^n$ for $T < 5$ K. The best fit for both alloys occurs for n=2.2; the corresponding values for A and B are given in Table VII.

The values for A are different for both alloys and are much larger than to be expected for an electronic contribution alone. The presence of a linear heat capacity term for spin glasses has been long known, and the excess linear term is attributed to spin glass behavior. The $T^{2.2}$ term is empirical with no sound theoretical basis. However, some researchers have claimed a T^2 dependence in addition to the linear term for spin glasses. A plot of $(C-C_h-C_l)/T$ vs. $T^{1.2}$ (Fig. 49) shows that the fit is good even up to 10 K where damping of the magnetic term starts to take place.

Table VII. Summary of heat capacity coefficients for βDy in mJ units

	Alloy	A	B	D	Θ_D (K)
Method I	Dy-28Mg	19.15	18.25	0.33[a]	180[a]
	Dy-29Mg	17.64	16.42	0.33	180
Method II	Dy-28Mg	15.34	20.92	1.35[b]	
	Dy-29Mg	12.72	19.77	1.11	

[a]Value fixed before fitting.

[b]Includes both lattice and antiferromagnetic terms.

Because Θ_D was chosen arbitrarily, an effort was made to test this assumption. One of the alloys (at 28%) was reanalyzed for Θ_D = 170 and 190 K to see the effects. For Θ_D = 170 K, A increased 2.4% while B decreased 1.9%. For Θ_D = 190 K, the change in A and B was -1.9% and +1.4%, respectively. There was virtually no change in the standard deviations. Since the choice of Θ_D has only minimal effects on both A and B, the original choice of 180 K was retained.

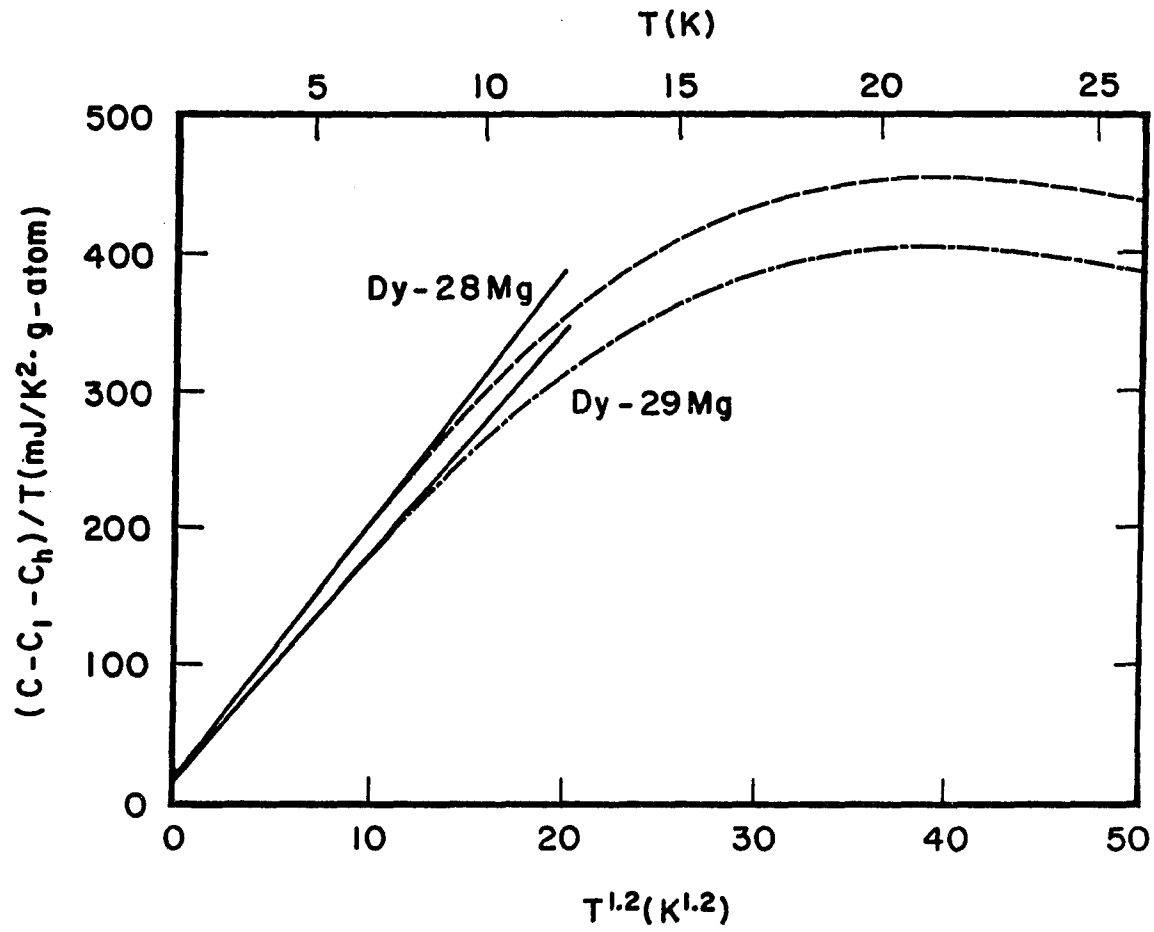

Figure 49. C/T versus $T^{1.2}$ for two Dy-Mg alloys. The straight lines are the <5 K least squares fit.

The second method was based on the assumption that the alloys were in a mixed antiferromagnetic-spin glass state. The heat capacity corrected for the hyperfine contribution was fit to the form $AT + BT^2 + DT^3$ for $T < 5$ K. A contains both the electronic term and the linear spin glass term, B would represent the spin glass T^2 term and D would represent C_l in addition to any antiferromagnetic excitations. The coefficients are also in Table VII.

The T^3 term is 2 to 3 times what would be expected for $\Theta_D = 180$ K (D = 0.33). The remaining part of the T^3 would then be attributed to antiferromagnetism. The linear term is 25 to 30% lower than in the first method, but it is still too large to be attributable entirely to the electronic heat capacity. The large coefficient of the T^2 term is indicative of its significance and favors the spin glass hypothesis.

A plot of $C'(T) = C-C_h-C_l$ (Fig. 50) shows a maximum near 28 K for all three alloys. The lattice contribution was estimated using the Debye function. Although this function surely fails at higher temperatures, it should be a reasonable estimate up to 30 or 40 K. The maxima in C' corresponds well to the χ_{ac} cusps, but generally are 2-4 K lower. The C' maxima can be shifted to higher T, matching or exceeding the χ_{ac} temperatures if a smaller lattice correction is used. The Debye function overestimates C_l especially as the temperature increases. What can be said confidently is that the maximum in C_m lies somewhere between 30 and 45 K.

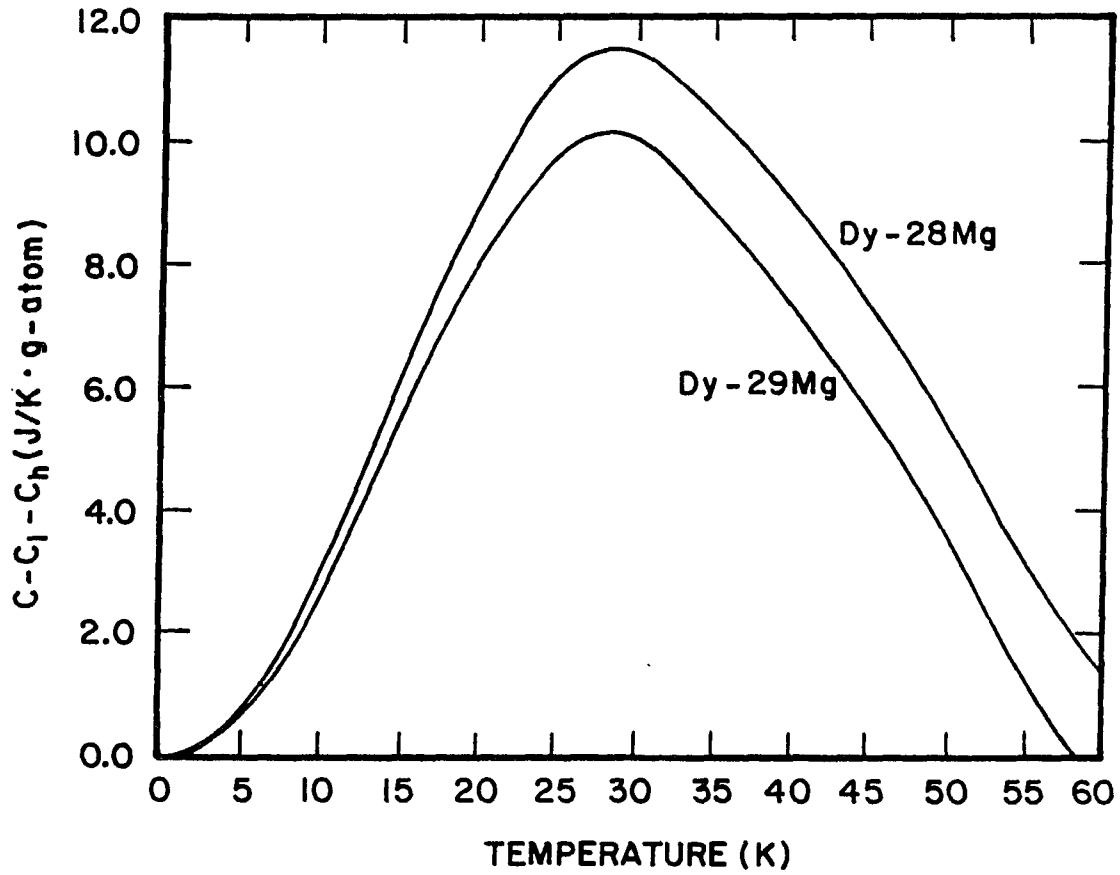

Figure 50. Heat capacity less the hyperfine and lattice contributions for two Dy-Mg alloys.

DISCUSSION

Spin Glass Review

Both the ^{64}Gd and ^{66}Dy alloys show field cooling effects in χ and unusual heat capacity behavior which may be explained by a spin glass state. It therefore seems appropriate to review the spin glass state including how it is recognized, its basis in theory, and some classical spin glass systems. A good comprehensive review of spin glass subject is given by Maletta and Zinn.[32]

A spin glass state is usually defined as a randomized array of spin moments caused by competing exchange interactions. Contrary to ferromagnetism or antiferromagnetism (Fig. 51), when a spin glass material is cooled below a critical spin freezing temperature T_f, the moments do not line up in an ordered arrangement, but freeze into a random network not unlike the atomic arrangements in common glasses. This transition is marked by a cusp in χ (Fig. 51c) at T_f. The spin glass differs from the paramagnetic state in that at long times there is a probability that a given spin will be in the same orientation where it is first observed. This condition holds even if the system is perturbed by a magnetic field. In a paramagnet which is also a collection of random spins the direction of the spins are always changing.

Experimental characteristics

Spin glasses can be detected by a number of different investigative techniques. The most common include heat capacity, magnetic susceptibility (both static and ac), time dependent magnetization and neutron diffraction. The latter two were not used in this study, but they should be discussed briefly.

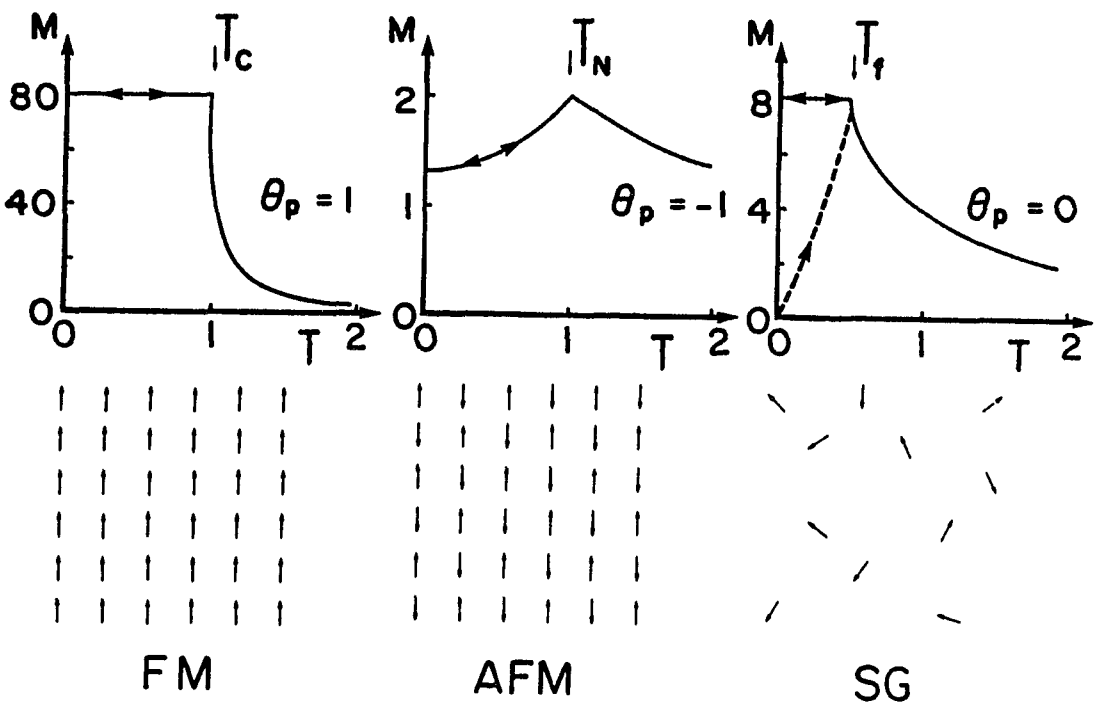

Figure 51. Comparison of the magnetization measured in a small applied field for a ferromagnet (FM), an antiferromagnet (AFM) and a spin glass (SG). The dashed line indicates the zero-field-cooled behavior of the spin glass. The curves are schematic and the units arbitrary, but the same average magnitude of the exchange interaction is chosen for all three. Values of the paramagnetic Curie-Weiss temperature θ_p are indicated. At the bottom the corresponding ordering of the magnetic moments is sketched schematically (after Ref. 33).

Neutron diffraction is a powerful tool in that it is sensitive to magnetic ordering. Magnetic ordering is observable in neutron diffraction by the appearance of magnetic superstructure lines. A spin glass has no long range order and therefore no magnetic diffraction peaks distinguishing spin glasses from ordered structures.

Spin glasses are also marked by magnetization relaxation phenomena. This time dependent behavior is a consequence of the long time probability that a given spin will remember its orientation. If the spin glass is disturbed by a field, and then the field is removed, there will be a measurable time period where the spins return to their former orientations. This relaxation goes as ln(t) for most systems. Another consequence of this time varying behavior is that χ_{ac} is frequency dependent.

The most prevalent measurement is the magnetic susceptibility. χ_{ac} at close to zero field features a sharp, field dependent cusp at T_f. Static χ measurements have a cusp only if cooled in zero field (Fig. 50). If the spin glass is cooled in a field the partial alignment of moments caused by the field is frozen in and is observable as a plateau in χ. If the applied field is strong enough, then the spin glass state is destroyed and no cusp is observed even for zero field cooling.

Below T_f the FC branch is reversible on thermal cycling, but the ZFC branch is only sometimes reversible depending on the magnitude of the measuring field. (This may be a consequence of the time relaxation effects. The ZFC branch may be reversible if enough time is allowed.) If the sample is heated above T_f, the particular spin glass state is lost, and the subsequent spin glass state on further cooling depends on the magnetic history.

The history dependent irreversibilities are a fundamental property of the spin glass state, but in themselves do not uniquely define the spin glass ordering. These same kind of irreversibilities can be associated with superparamagnetic clustering or domain wall effects.

Associated with the freezing transition is a magnetic term in the heat capacity. Most authors report a broad maximum in C_m with the maximum occurring above T_f as high as $1.3T_f$. No anomaly is observed at the freezing temperature. The temperature dependence below the transition is not much better understood. Mean field theory predicts a linear dependence as $T \rightarrow 0$. A linear heat capacity has been found in some systems, but only the classical dilute ones such as CuMn. Most authors report a nearly linear behavior with some positive deviation. More recently there has been a trend to report C_m as $AT + BT^2$ where the T^2 accounts for the positive deviations. The T^2 term improves the degree of fit and isolates the linear term, but it has no basis in theory as yet.

Theory

The theory for spin glass systems has only been established in the last 13 years. The basic precept for the theory is that in a spin glass material there is a competition between antiferromagnetic (AF) and ferromagnetic (FM) exchange interactions. If the energy of the FM and AF states are similar, then a given spin has a choice of which way to line up. The preferred orientation does not have to be exclusively FM or AF. For a given distribution of exchange interactions that a spin sees there may be several configurations which are energetically equal, i.e. there are degenerate states. At T_f a spin can be "frustrated" in trying to choose one state over the others and the result is an intermediate state and a randomized collection of spins as the material is cooled below T_f.

The application of a magnetic field disturbs this balance and gives rise to the irreversibilities in χ and the relaxation effects.

Edwards and Anderson[34] (EA) made the first attempt at explaining spin glass (SG) effects observed in CuMn by using mean field theory. They could predict a cusp in χ and in C, but only the χ cusp is observed experimentally. Sherrington and Kirkpatrick[35] (SK) made a big improvement in this model by proposing a system of pure but replicated spins each feeling a Gaussian distribution of exchange interactions centered at J_o with width J to solve the EA model. Not only did the SK solution predict a cusp in χ, but it also predicted $C \propto T$. The SK model also predicted (though partially incorrect) at certain compositions a FM to SG transition, that is reentrant spin glass behavior, for J_o/J slightly greater than 1.

De Almeida and Thouless[36] (AT) pointed out an instability (called the AT line) in the SK model caused by the breaking of symmetry of the replicated spins in the ferromagnetic state. Below the AT line a mixed FM/SG phase exists that would exhibit SG-like irreversibilities but with a spontaneous magnetization. Finally Gabay and Toulouse[37] (GT) predict two types of transitions from FM to SG (Fig. 52) consistent with the SK model. The first transition (called the GT line) involves a change from a colinear FM to a mixed canted F′ state where transverse spins are frozen at random while longitudinal spins retain FM ordering. A second transition occurs at a lower temperature analogous to the AT line where the replica symmetry breaking and irreversibilities occur. Cragg et al.[38] have pointed out however, that in real systems the two transitions may in fact be indistinguishable.

The theories are further supported by Monte Carlo calculations.

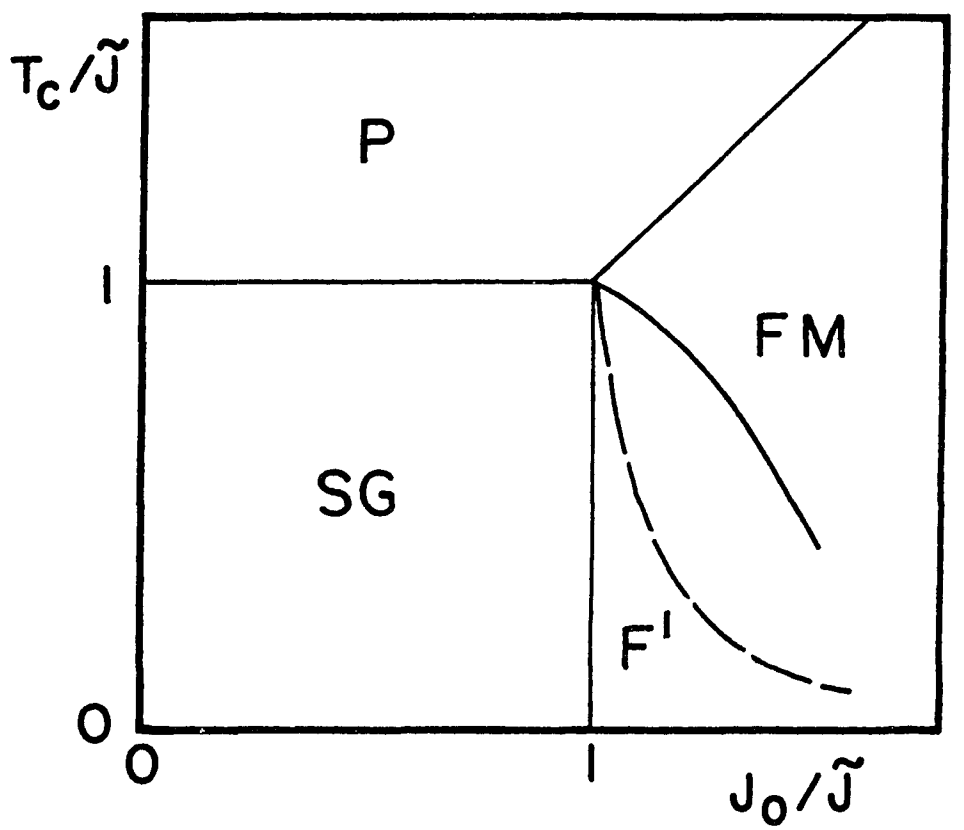

Figure 52. Theoretical magnetic phase diagram showing the GT (upper) and AT (lower) reentrant spin glass transitions (after Gabay and Toulouse). The ordinate is a temperature and the abscissa is a relative exchange interaction.

Binder and Schroder[39] find a cusp in χ that is rounded under an applied field in agreement with experiment. They also produce a maximum in C_m 25% higher than T_f again with surprising agreement with experiment. Kinzel[40] has shown that a GT-like FM to F′ transition is possible in his calculations.

Real systems

The early SG systems studied were dilute transition metals (<5%) with noble metal solvents: e.g. AuFe, CuMn, AgMn, PtMn and Pd(Fe_xMn_{1-x}). These systems have all been well characterized by magnetic susceptibility, heat capacity, neutron diffraction and relaxation experiment, but only experiments related to this study will be discussed. Cannella and Mydosh[41] reported sharp cusps in χ_{ac} for AuFe in the first published account of a SG system. These same cusps were reported by Nagata et al.[42] for CuMn in addition to field cooling irreversibilities. FC effects were also observed by Chamberlin et al.[43] in AgMn.

Similar effects have been reported in heavy rare earth (Gd, Tb or Dy) with nonmagnetic Y and Sc as solvents. SG phases have been reported in Sc systems with up to 24% solute.[44] Cusps in χ are observed in ScGd and ScTb alloys,[45] and field cooling dependencies are reported[46] in ScGd and YGd.

No agreement is found in the literature as to the form of C(T). The heat capacity of CuMn has been extensively investigated. Martin[47] reports a linear dependence for C(T) with additional positive curvature, while Wenger and Keesom[48] suggest a linear low T limit. Caudron et al.[49] prefer a $T^{1.2}$ dependence. Fogle et al.,[50] however, felt that the form $AT + BT^2$ gave the best fit to their data. The heat capacity of PtMn[51] also has this form. Thomson and Thompsom[52] reanalyzed the data of Fogle et al. and Martin among others (and for PdMn) and claimed that they all were really

$T^{1.5}$. Meschede et al.[53] measured a linear dependence for the insulating SG $Eu_xSr_{1-x}S$, but conceded that a T^2 term would improve the fit. A $T^{1.5}$ dependence was measured[54] for a-$GdAl_2$ (a- denotes amorphous) and was explained by ferromagnetic clustering. A $T^{1.7}$ dependence is reported for ScGd by Caudron et al.[49]

Overall the linear dependence seems well founded at least in the low temperature limit where higher order terms disappear quickly. Experiments also suggest a higher order term (absorbed by the fractional exponent in some cases) most likely corresponding to a second type of excitation. The linear term is unique in that a ferromagnet requires a $T^{1.5}$ dependence while an antiferromagnet requires a T^3 dependence. The occurrence of a linear term in the magnetic specific heat is good evidence of spin glass behavior.

If the amount of magnetic material is increased is some of the systems, reentrant spin glass behavior (after GT) is observed. In Au-18%Fe a FM to SG transition is observed by loss of spontaneous magnetization[55] and by a ferromagnetic rise in χ_{ac} followed by a plateau and a steady drop after T_f.[56] In PdMn systematic substitution of Fe for Mn cause a change from a SG state to an F′ state and finally to a FM state.[57] A FM to SG transition is observed in $Eu_{0.5}Sr_{0.5}S$ by both χ_{ac} and neutron diffraction.[58] Other reentrant spin glass phases include a-$Gd_{0.37}Al_{0.63}$ and a-GdCu,[59] Fe_xCr_{1-x}[60] and $(Fe_xMn_{1-x})_{75}P_{16}B_6Al_3$.[61,62] Coexistence of antiferromagnetism and spin glass disorder was confirmed in $Fe_{0.55}Mg_{0.45}Cl_2$ by neutron diffraction.[63,64]

βGd

The βGd alloys show evidence of reentrant spin glass behavior. Some type of ferromagnetic ordering is present as illustrated by the Arrott plots (Fig. 30). The field cooling effects (Fig. 34) are typical of spin glasses. The loss of spontaneous magnetization in χ_{ac} curves is similar to that observed by Maletta[58] for $Eu_{0.5}Sr_{0.5}S$ and Manheimer et al.[61] for $(Fe_xMn_{1-x})_{75}P_{16}B_6Al_3$ where the transition from ferromagnetism to spin glass is well established by other means as well. Although χ shows spin glass features, in themselves they are not conclusive.

The Gd-Mg system does seem to have the right ingredients for spin frustration caused by competing exchange interactions. Ferromagnetic exchange interactions should dominate the system as apparent by the appearance of spontaneous magnetization and a large positive θ_p. However, some antiferromagnetic interactions are likely to exist in light of the low spontaneous moment measured in high field and the lack of saturation.

The compound GdMg, CsCl structure, has been studied by two different groups both reporting unusual behavior. GdZn and GdCd are both good ferromagnets with T_c just below that of pure Gd (268, 270 and 294 K, respectively) and reach saturation (~7μ_B) easily. GdMg which has the same structure and electron concentration has a much lower T_c (121 K), is difficult to saturate[65,66] and reaches values ~6μ_B suggesting that GdMg has some antiferromagnetic ordering as well. Neutron diffraction cannot be made on Gd alloys due to high neutron absorption, but neutron diffraction has been done on TbMg[65,67] which is similar to GdMg though with a lower θ_p. These results indicate a structure of ferromagnetic sheets that are coupled antiferromagnetically producing a noncolinear

ferromagnet. Of importance to this discussion is that the type of antiferromagnetic coupling could not be uniquely determined with the investigators suggesting 2 or 3 equal alignments, an important ingredient for spin glass formation. Aleonard et al.[68] determined this same type of structure for the RMg compound with R = Dy, Ho and Er as well.

Buschow and Oppelt[66] discussed the possibility of disorder in GdMg structure, i.e. some Mg and Gd atoms interchange positions causing a disruption in the magnetic interactions. They claim a RKKY calculation shows a gradual change in θ_p from a strong positive value for perfect ordering to negative values for complete disorder illustrating a mechanism to produce antiferromagnetic ordering. Buschow later ruled out this possibility by neutron diffraction on NdMg, but the argument is appropriate for the βGd alloys of this study. A disordered CsCl structure is essentially a random bcc solid solution which is the same as βGd except that βGd has a lower concentration of Mg which means that some intermediate θ_p should be expected which decreases with increasing Mg concentration. This behavior is confirmed from χ^{-1} plots (Fig. 29 and Table II).

Buschow and Schinkel[69] decided that the antiferromagnetic interaction in GdMg is more fundamental in nature by studying the pseudobinary $(Gd_{1-x}La_x)Mg$. Just a 10% dilution of Gd by La induces a change from ferromagnetic ordering to antiferromagnetic ordering, so they asserted that a small antiferromagnetic interaction must be pre-existing in GdMg. A study of $Gd(Mg_xZn_{1-x})$[66] shows that T_c increases with increasing Zn concentration or with decreasing lattice parameter. The same phenomenon is observed in the $(Gd_{1-x}La_x)Mg$ system indicating that the strength of the antiferromagnetic interaction depends on the interatomic distance as might

be expected for RKKY interactions. There is evidence that the RKKY coupling in rare earth CsCl structure is carried in large part by 5d electrons.[70] Because this band is narrow, one would expect that the interaction would be sensitive to lattice parameter.

The distinction between the ordered CsCl structure and the random bcc structure is as follows. In the CsCl structure the Gd nearest neighbor is always a Mg ion and the second nearest neighbor is always another Gd ion. This gives rise to the ferromagnetic sheet structure in the rare earth Mg compounds. The antiferromagnetic interaction is between sheets or longer range. In a random bcc solution the nearest neighbor can be either a Mg ion or a Gd ion. The second nearest neighbor can also be either Mg or Gd. This uncertainty will disrupt the formation of the sheets with the finite probability that locally one ion may couple ferromagnetically and the next ion may order antiferromagnetically. If the interactions of all the atoms are considered then it is conceivable that the antiferromagnetic and ferromagnetic states may be equivalent for certain ions, but probably not for all depending of course on the environment surrounding the Gd ion in question. This competing interaction gives rise to the spin glass like behavior in the βGd alloys.

This picture favors a transition where a ferromagnetic phase transforms into a F′ state on cooling. A colinear ferromagnetic structure remains partially intact, but some of the spins freeze out of the ferromagnetic alignments because of the competition between AF and FM orderings.

Two transitions are measured with χ and χ_{ac} measurements indicating that such a disordering transition is present. T_f decreases with applied field showing that a field can overcome the spin frustration and force

some kind of periodic order. The lack of saturation in the FM state can be explained by the fact that even with the removal of spin frustration there will still be a strong tendency for AF coupling as in the Mg compounds.

The mixed F′ state at low T is also supported by the heat capacity data. The strong magnetic term is evidence of a remaining magnetic order. The temperature dependence which goes from $T^{1.6}$ to $T^{1.7}$ as Mg increase is reminiscent of a $T^{1.5}$ dependence for ferromagnetic magnon excitations. As the Mg concentration is decreased the AF interactions lessen and one would expect the material to become more like a true ferromagnet ($T_f \rightarrow 0$) with n approaching 1.5 as is indicated in Fig. 40. Increasing the Mg concentration should make βGd more spin glass like (higher T_f). A higher order term of approximately T^2 has been established for CuMn and PtMn spin glasses above, but these spin glass excitations interact with the ferromagnetic excitations giving an intermediate result but tending toward T^2.

The existence of the linear term in C can also be explained by a F′ state. In a simple model the linear coefficient at a given composition can be divided into three terms

$$A = \gamma + \lambda\gamma + \eta \qquad (13)$$

where λ is a ferromagnetic enhancement factor and η is the spin glass term. γ is proportional to the density of states at the Fermi level, and therefore, it is sensitive to changes in band structure. γ can be considered a base electronic contribution combining both the ferromagnetic phase, the spin glass phase, and any common enhancements that would effect both types of ordering equally such as electron-phonon coupling. If a

rigid band structure is assumed over the concentration range, then there will be an electron concentration effect that will decrease γ as Mg concentration increases, but this effect is small (refer Fig. 41).

In a ferromagnet there is often an enhancement, λ, of the electronic term due to spin waves. For pure Gd, this value may be as high as 1.[27] λ will depend on Mg concentration in two ways. First, as the amount of ferromagnetic phase decreases (Mg increasing), there will a decrease in λ proportional to the amount of ferromagnetic phase lost. Second, as the amount of ferromagnetic alignment decreases, the interactions necessary for electronic enhancement will be disrupted causing a further decrease in λ. These two effects will be additive leading to a strong negative dependence of A with increasing Mg.

Finally there is the spin glass term η. Since the alloys become more spin glass like at increased Mg concentration, one would expect η to increase with Mg concentration. But since the observed value of A drops rapidly with increasing Mg content (Fig. 41), this must be small as the negative dependence of the first two terms dominate. If the solid solution could be extended to higher Mg concentrations, then a leveling or an upturn in A might be observed as λ goes to zero In conclusion, the above analysis of the concentration dependence of A indicates that the dominant term is $\lambda\gamma$.

βDy

Much of the same arguments used for βGd can be applied to βDy. DyMg has a weak net positive interaction (θ_p = 25 K), and it orders antiferromagnetically. The θ_p's for the βDy alloys are on the order of 30 K indicating a slight increase of the ferromagnetic exchange interaction

by randomizing the bcc lattice.

This seems to be the opposite effect of the Gd-Mg system, but it is the same. In both DyMg and GdMg, the ordering is a system of ferromagnetic sheets with the antiferromagnetic coupling of the sheets larger in DyMg than for GdMg. In the GdMg system, a randomized lattice disrupting the ferromagnetic coupling and introducing antiferromagnetic exchanges explains the observed spin glass ordering. The spin glass behavior observed in the Dy-Mg system can also be explained by a randomization of the lattice, but in this case the antiferromagnetic ordering would be disrupted and stronger ferromagnetic exchanges would be introduced. Increasing the average ferromagnetic exchange relative to the average antiferromagnetic exchange interactions would introduce increased competition, and βDy would become a spin glass candidate.

χ_{ac} measurements show sharp cusps for all the compositions. The cusp, however, could be indicative of either spin glass behavior or antiferromagnetism although the cusps are quite sharp, whereas AF cusps tend to be broader. Classical antiferromagnets usually show a leveling at some intermediate χ value especially for polycrystalline samples corresponding to a mixture of the parallel and perpendicular susceptibilities. But at zero field this magnetization may be small. By themselves, the χ_{ac} are not conclusive.

High field measurements show no spontaneous magnetization ruling out any sort of ferromagnetic phase. The χ curves at these fields show a maximum even at 1.5 T, a field that would normally destroy a spin glass structure. This property favors antiferromagnetism.

For intermediate fields, a spin glass like irreversibility is observed for the FC 27% alloy (Fig. 44). This irreversibility is unusual

in that the curves are normally the same down to the maximum and then they split. The FC branch for this alloy reaches a much higher value, but the maximum remains at the same temperature. In addition, the field cooled branch now looks like a classical curve for an antiferromagnet. The coexistence of antiferromagnetism and spin glass behavior has been confirmed[64] for $Fe_{1-x}Mg_xCl_2$, but the split in this material is below a well defined Neel temperature.

Baberschke et al.[71] have measured χ for ScDy and ScTb alloys containing about 5% Dy (Tb) and they report a similar splitting between ZFC and FC branches at temperatures higher than the χ maxima. An extensive study of the field dependence was also done where the maxima remained constant up to 0.06 T before shifting to lower T similar to the results in this study. The field study also allowed them to interpret their results as a resolution of the AT and GT type transitions with the splitting being the GT transition. This explanation fits the current data as well except for the extreme increase in χ for the FC branch. It is more likely that there is a large antiferromagnetic component along with the spin glass ordering and that both order at approximately the same temperature. The application of a the small field may be just enough to make the antiferromagnetic state perferred for some of the Dy atoms.

The heat capacity is more revealing. At T_f there is a broad maximum in C_m like that of classical spin glasses. The sharp cusp that would be associated with antiferromagnetic ordering is not present implicitly, but could be covered up by a larger spin glass heat capacity. The position of the maximum is not clear, but it is within the accepted limits. The exact position of the maximum depends on the lattice correction and the amount and nature of any antiferromagnetic ordering in addition to the spin glass

ordering.

The low T heat capacity gives the same information whether the first or second analysis is actually correct. The linear term is large and cannot be attributed to the electronic coefficient alone. Recently Hill and Gschneidner[26] have accurately measured $\gamma = 4.9$ mJ for pure Dy. Even allowing a factor of 2 will not account for the large linear term of βDy. The largest portion of the linear term must therefore be due to spin glass excitations.

Both analyses give a significant T^2 term which is indicative of spin glasses. If no T^3 term is included a $T^{2.2}$ term is required to give an adequate fit. This term would then be a combination of the T^2 spin glass excitation and T^3 antiferromagnetic excitations. If a T^3 term is included a significant antiferromagnetic contribution is indicated, and the same conclusion is reached: a combination of antiferromagnetism and spin glass behavior is present.

Conclusions

It has been demonstrated that the βGd and βDy systems exhibit mixed spin glass order. A pure spin glass phase should not be expected because of the high content of magnetic material in the alloys that increase the probability of normal modes of magnetic coupling. In the case of βGd strong ferromagnetic exchange interactions dominate, but there is a GT type of transition from the ferromagnetic phase to a mixed ferromagnetic-spin glass phase. The βDy alloys are dominated by antiferromagnetic interactions, and only one transition appears to occur from the paramagnetic state to a mixed antiferromagnetic-spin glass state.

Very little can be said about the properties of a pure bcc Gd or Dy

structure. The mixture of exchange interactions caused by Mg dilution makes any extrapolation of magnetic properties suspect. Mg, however, is unique among the Group II metals in introducing the mixed interactions as GdMg has evidence of antiferromagnetic coupling and a low T_c while GdZn and GdCd are both good ferromagnets with T_c's close to that of pure Gd. Cd is a bcc stabilizer for La, and like Mg, should be a stabilizer for Gd and Dy as well. Since Cd additions are not as likely to affect the type of ordering, Cd stabilized βGd and βDy should resemble the pure bcc metals more than the Mg counterparts. A study of binary Gd-Cd and Dy-Cd alloys would lend itself better to extrapolation, and it would yield more information about pure bcc Gd and Dy that can be more readily compared to theory. Pseudobinary alloys of the type $Gd_{1-x}(Cd_{1-y}Mg_y)_x$ would be interesting systems to study the onset of spin glass behavior.

REFERENCES

1. Gibson, E. D.; Carlson, O. N. Trans. Am. Soc. Metals 1960, 52, 1047.
2. Miller, A. E.; Daane, A. H. Trans. Met. Soc. AIME 1964, 230, 568.
3. Spedding, F. H.; Cress, D.; Beaudry, B. J. J. Less-Common Met. 1973, 31, 1.
4. Manfrinetti, P. Ames Laboratory, Ames, IA, private communication.
5. Croat, J. J. Ph. D. Thesis, Iowa State University, Ames, IA, 1972.
6. Stierman, R. J. Ph. D. Thesis, Iowa State University, Ames, IA, 1982.
7. Tsang, T-W. E. Ph. D. Thesis, Iowa State University, Ames, IA, 1977.
8. Teatum, E. T.; Gschneidner, K. A.; Waber, J. T. Los Alamos National Laboratory Report, LA-4003, 1968.
9. Manfrinetti, P.; Gschneidner, K. A. J. Less-Common Met. 1986, 123, 267.
10. Bruzzone, G.; Merlo, F. J. Less-Common Met. 1976, 44, 259.
11. Griffin, R. B.; Gschneidner, K. A. Metall. Trans. 1971, 2, 2517.
12. Bruzzone, G.; Merlo, F. J. Less-Common Met. 1974, 38, 137.
13. Mason, J. T.; Chiotti, P. Metall. Trans. 1970, 1, 2119.
14. Delfino, S.; Saccone, A.; Cacciamani, G.; Ferro, R. Z. Metallkd. 1985, 76, 7.
15. McMasters, O. D.; Gschneidner, K. A. J. Less-Common Met. 1974, 38, 137.
16. Gschneidner, K. A.; Calderwood, F. W. Rare-Earth Information Center Report IS-RIC-PR-7, December, 1983.
17. Moffat, W. G. "The Handbook of Binary Phase Diagrams", Genium Publishing Co., Schenectady, NY, 1986.
18. Katgerman, L. J. Mat. Sci. Lett. 1983, 2, 444.
19. Herchenroeder, J. W.; Manfrinetti, P.; Gschneidner, K. A. Physica B, 1985, 135, 445.
20. Hill, R. W.; Collocott, S. J.; Gschneidner, K. A.; Schmidt, F. A. J. Phys. F 1987, 17, 1867.
21. Leung, T. C.; Wang, X. W.; Harmon, B. N. Physica B 1988, 149, 131.

22. Lounasmaa, O. V.; Sundstrom, L. J. Phys. Rev. 1966, 150, 399.

23. Morrison, J. A.; Newsham, D. M. T. J. Phys. C 1968, 1, 370.

24. Stevens, W. N. R.; Krukewich, K. J. Phys. F 1973, 3, 1229.

25. Sedaghat, A. K.; Cracknell, A. P. J. Phys. C 1971, 4, 3215.

26. Hill, R. W.; Gschneidner, K. A. to be published in J. Phys. F.

27. Tsang, T-W. E.; Gschneidner, K. A.; Schmidt, F. A.; Thome, D. K. Phys. Rev. B 1985, 31, 235.

28. Ikeda, K.; Gschneidner, K. A.; Takeshita. T.; Jones, D. W.; Farrant, S. P. Phys. Rev. B 1985, 31, 5878.

29. Hill, R. W. Clarendon Laboratory, Oxford University, United Kingdom, private communication.

30. Berthier, Y.; Barak, J.; Barbara, B. Solid State Commun. 1975, 17, 153.

31. Crain, J. S.; Houk, R. S. Ames Laboratory, Ames, IA, private communication, 1986.

32. Maletta, H.; Zinn, W. "Spin Glasses" in "Handbook on the Physics and Chemistry of Rare Earths", Vol. 12, North-Holland Publishing, The Netherlands, 1988, Chapter 84.

33. Moorjani, K.; Coey, J. M. D. "Magnetic Glasses", Elsevier, The Netherlands, 1984.

34. Edwards, S. F.; Anderson, P. W. J. Phys. F 1975, 5, 965.

35. Sherrington, D.; Kirkpatrick, S. Phys. Rev. Lett. 1975, 35, 1792.

36. de Almeida, J. R. L.; Thouless, D. J. J. Phys. A 1978, 11, 983.

37. Gabay, M.; Toulouse, G. Phys. Rev. Lett. 1981, 47, 201.

38. Cragg, D. M.; Sherrington, D.; Gabay, M. Phys. Rev. Lett. 1982, 49, 158.

39. Binder, K.; Schroder, K. Phys. Rev. B. 1976, 14, 2142.

40. Kinzel, W. Phys. Rev. B 1979, 19, 4595.

41. Cannella, V.; Mydosh, J. A. Phys. Rev. B 1972, 19, 1633.

42. Nagata, S.; Keesom, P. H.; Harrison, H. R. Phys. Rev. B 1979, 19, 1633.

43. Chamberlin, R. V.; Harcliman, M.; Turkevich, L. A.; Orbach, R. Phys. Rev. B 1982, 25, 6720.

44. Sarkissian, B. V. B.; Coles, B. R. Comm. Phys. 1976, 1, 17.

45. Sarkissian, B. V. B. J. Phys. F 1977, 7, L139.

46. Wendler, R.; Pureur, P.; Fert, A.; Baberschke, K. J. Magn. Mag. Matls. 1984, 45, 185.

47. Martin, D. L. Phys. Rev. B 1979, 20, 368.

48. Wenger, L. E.; Keesom, P. H. Phys. Rev. B 1976, 13, 4053.

49. Caudron, R.; Costa, P.; Lasjaunias, J. C.; Levesque, B. J. Phys. F 1981, 11, 451.

50. Fogle, W. E.; Boyer, J. D.; Fisher, R. A.; Phillips, N. E. Phys. Rev. Lett. 1983, 50, 1815.

51. Sato, T.; Miyako, Y. J. Phys. Soc. Jap. 1982, 51, 2143.

52. Thomson, J. O.; Thompson, J. R. J. Phys. F 1981, 11, 247.

53. Meschede, D.; Steglich, F.; Felsch, W.; Maletta, H.; Zinn, W. Phys. Rev. Lett. 1980, 44, 102.

54. Coey, J. M. D.; von Molnar, S.; Gambino, R. J. Solid State Commun. 1977, 24, 167.

55. Crane, S.; Claus, H. Phys. Rev. Lett. 1981, 46, 1693.

56. Verbeek, B. H.; Mydosh, J. A. J. Phys. F 1978, 8, L109.

57. Verbeek, B. H.; Nieuwenhuys, G. J.; Stocker, H.; Mydosh, J. A. Phys. Rev. Lett. 1978, 40, 586.

58. Maletta, H.; Felsch, W. Z. Physik B 1980, 37, 55.

59. McGuire, T. R.; Mizoguchi, T.; Gambino, R. J., Kirkpatrick, S. J. Appl. Phys. 1978, 49, 1689.

60. Fincher, C. R.; Shapiro, S. M.; Palumbo, A. H.; Parks, R. D. Phys. Rev. Lett. 1980, 45, 474.

61. Manheimer, M. A.; Bhagat, S. M.; Chen, H. S. J. Magn. Mag. Matls. 1983, 38, 147.

62. Yeshurun, Y.; Salamon, M. B.; Rao, K. V.; Chen, H. S. Phys. Rev. Lett. 1980, 45, 1366.

63. Bertrand, D.; Bensamka, F.; Fert A. R.; Gelard, J.; Redoules, J. P.; Legrand, S. J. Phys. C 1984, 17, 1725.

64. Wong, P-Z; von Molnar, S.; Palstra, T. T. M.; Mydosh, J. A.; Yoshizawa, H.; Shapiro, S. M.; Ito, A. Phys. Rev. Lett. 1985, 55, 2043.

65. Aleonard, R.; Morin, P.; Pierre, J.; Schmitt, D. Solid State Commun. 1975, 17, 599.

66. Buschow, K. H. J.; Oppelt, A. J. Phys. F 1974, 4, 1246.

67. Will, G.; Schafer, W.; Buschow, K. H. J. "Proceedings of the 12th Rare Earth Research Conference", 1976, 41.

68. Aleonard, R.; Morin, P.; Pierre, J.; Schmitt, D. J. Phys. F 1976, 6, 1361.

69. Buschow, K. H. J.; Schinkel, C. J. Solid State Commun. 1976, 18, 609.

70. Weimann, G.; Bopp, H.; Elschner, B.; Buschow, K. H. J. Intl. J. Mag. 1973, 5, 1.

71. Baberschke, K.; Pureur, P.; Fert, A.; Wendler, R.; Senoussi, S. Phys. Rev. B 1984, 29, 4999.

ACKNOWLEDGEMENTS

The completion of a study of this magnitude is rarely the work of just one person, and I will not claim an exception here. Help and support has been given by many individuals of which only a few will be mentioned; I think that the readers will appreciate that I am keeping this list short.

I would like to thank Karl Gschneidner for letting me have my own head. This is the only way it could have worked. I would also like to thank: Pietro Manfrinetti for getting me started, Jack Moorman and Nile Beymer who provided valuable technical assistance that rescued me many times, "Cap" Capellen who did the search in research, Jinke Tang for his helpful discussions, Peter Klavins and Jerry Ostenson for help with the ac susceptibility measurements, and Wonchoon Lee who did the low field magnetic susceptibility measurements for me. A very special thanks goes to my wife Laurie who got me to this point and who sacrificed three years of her life for mine.

This material is based on work supported under a National Science Foundation Graduate Fellowship and by Ames Laboratory, operated for the U.S. Department of Energy by Iowa State University under contract No. W-7405-ENG-82. This work was supported by the Office of Basic Energy Sciences. The United States government has assigned the DOE Report number IS-T 1358 to this thesis.

APPENDIX A. SUPERCONDUCTIVITY IN γLA[1]

Superconductivity in γLa is of interest because the superconducting behavior of the dhcp α phase and the fcc β phase are known. Information on γLa allows comparison between three different crystalline phases -- dhcp, fcc, and bcc.

The superconducting transition temperature, T_c, for each alloy was determined from AC susceptibility, χ_{ac}, measurements (Fig. 53). The value taken for T_c is the temperature at 50% level of the change in χ_{ac}. The transition width, ΔT, is the range between the 10% and 90% levels.

A correlation exists between the amount of distortion in the γ phase as measured by the x-ray line broadening and the width of the superconducting transition. Fig. 53 shows plots of a typical x-ray diffraction line and χ_{ac} data for the 13 and 18 at.% Mg alloys. The 18% alloy has a sharp pattern and a corresponding narrow transition width, ΔT = 0.1 K. The 13% alloy, however, has a much broader x-ray peak and consequently a large transition width of ~0.6 K.

The T_c's are plotted as a function of composition in Fig. 54. A value for the T_c for pure γLa was obtained by extrapolating the data back to 0% solute. This method yielded 8.1 K and 7.9 K from the Cd alloys and Mg alloys respectively.

The extrapolation line is a least squares fit of the data ignoring the higher composition alloys due to a saturation effect. This saturation is best explained by looking at the La-Cd system (Fig. 5). Above the eutectoid composition of 13.5 at% Cd, T_c remains constant at 2.75 K. This

---

[1]Reproduced from reference 19.

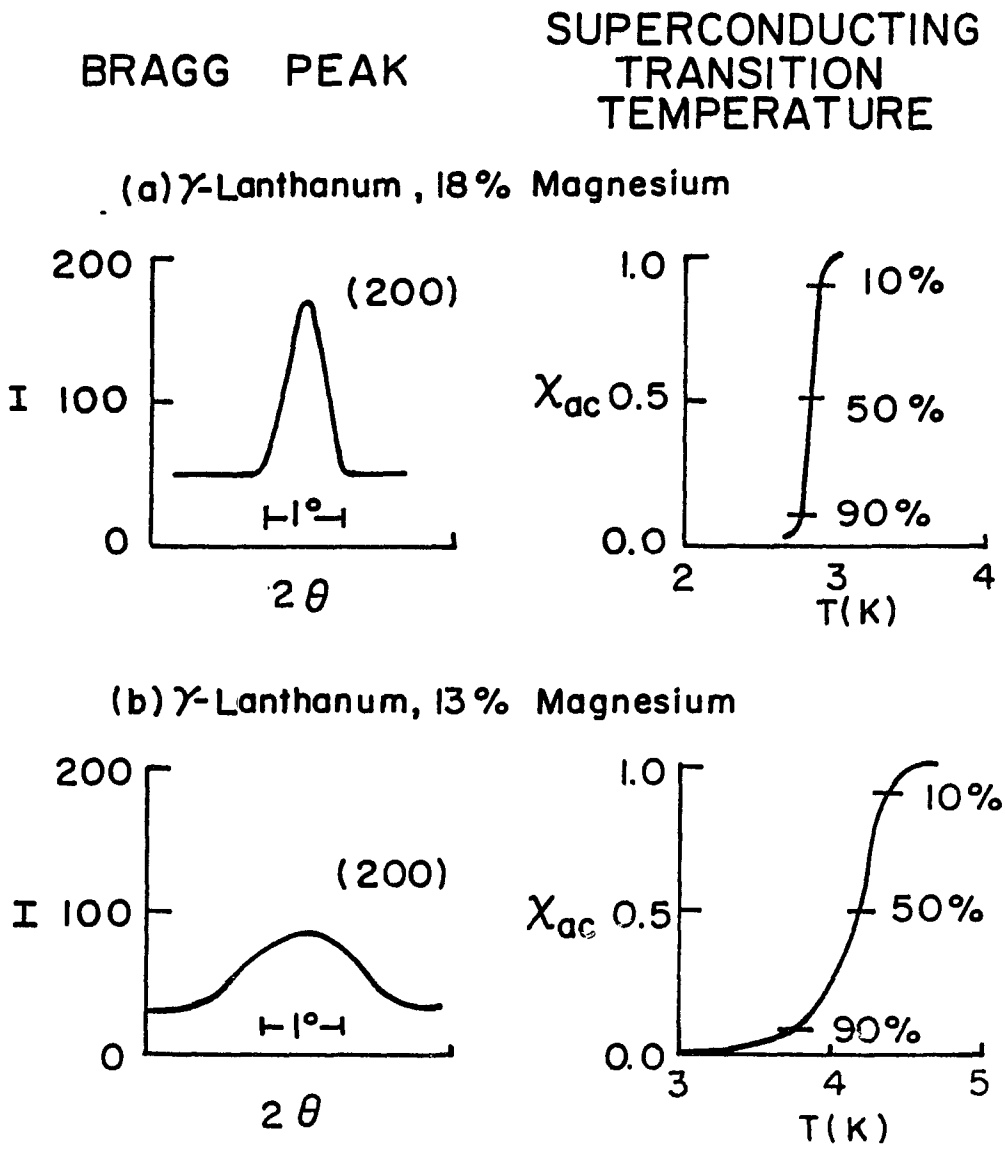

Figure 53. X-ray scan of the (200) Bragg peak [intensity (I) versus angle (2θ)] and the superconducting transition temperature (from a χ_{ac} versus T plot) for two γLa alloys containing (a) 18 at.% Mg and (b) 13 at.% Mg.

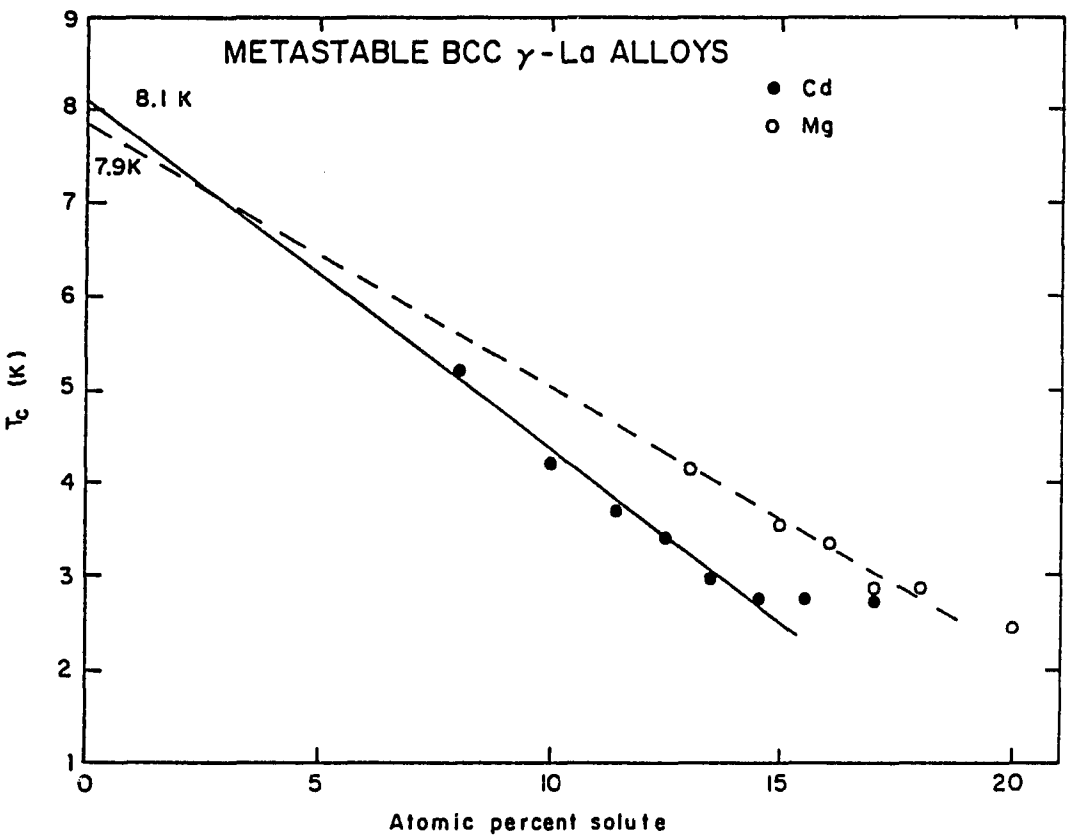

Figure 54. The superconducting transition temperature T_c versus composition for some bcc γLa alloys containing Mg or Cd as stabilizing agents.

means that the composition of the bcc phase remains constant although the overall alloy composition is increasing. This can be accommodated by a small amount of precipitation of the LaCd equilibrium compound. Therefore, the T_c values plotted at 15.5 and 17 at% Cd are not representative of γLa of those compositions, and thus these points were ignored. Similarily, the 20 at% point in the La-Mg system was also ignored.

These data suggest that if pure bcc La could be prepared at standard temperature and pressure, it would be a superconductor at 8 K. This would be the second highest elemental superconductor, only surpassed by Nb's 9.2 K transition.

The superconducting transition temperatures for the other La crystal structures are 5.0 K for the dhcp α phase and 6.1 K for the fcc β phase. The current results suggest that the bcc structure is significantly more favorable for superconductivity than the fcc structure, which is more favorable than the dhcp structure.

APPENDIX B. IMPURITY CONTENTS OF STARTING MATERIALS

Table B1. Semiquantatative analysis of common impurities for La-41985, Gd-3679 and Dy-42187c in ppm atomic

Element	La	Gd	Dy
Total Rare Earth	<7.4	9.8	6.7
H	a	311	643
C	139	79	121
N	59	11	34
O	69	216	499
F	18	<25	<25
Al	<0.5	4	<0.03
Si	3	2	0.25
Ca	1	<0.08	<0.5
Fe	18	26	15
Co	<0.04	<0.09	<0.03
Ni	0.96	1	<0.1
Cu	0.50	3	4.4
Mo	<0.5	<0.6	<0.6
Ta	1.5	3	<0.6
W	<0.8	5	<2.0

[a]No value reported.

Table B2. Semiquantitative analysis (ppm atomic) of ten highest impurities for sublimed Mg

Element	Amount
N	0.2
O	0.7
Cl	0.1
Ca	0.20
Zn	0.20
Sr	0.6
Eu	0.8
Lu	0.50
Ba	1
Hg	1

APPENDIX C. CALIBRATION OF FARADAY APPARATUS

Before use the Faraday susceptibility rig needed calibration. The force exerted on a magnetic sample is given by

$$(C1) \quad F = m\sigma_g \frac{dB_o}{dz}$$

where F is the force due to a uniform field gradient dB_o/dz perpendicular to the direction of the field B_o, σ_g is the gram magnetization and m is the sample mass. For a paramagnetic sample, $\sigma_g = B_o\chi_g$ where χ_g is the gram susceptibility which can be substituted into (C1),

$$(C2) \quad F = \frac{1}{2}m\chi_g \frac{dB_o^2}{dz}$$

since

$$(C3) \quad \frac{dB_o^2}{dz} = 2H \frac{dB_o}{dz}.$$

Measuring the magnetic field and the gradient proved to be difficult due to difficulty in measuring precise distances on the apparatus. Therefore, standards were used to calculate the system parameters from the equations above. Values for dB_o^2/dz for ten applied fields were obtained from equation (C2) using paramagnetic Pt and Pd standards (NBS) at room temperature. The values obtained at a single field for one metal standard were within 1% of the other standard. The average dB_o^2/dz at each field was taken as the true value.

Values at each field for dB_o/dz were obtained from ferromagnetic Ni at three temperatures 4.2, 77 and 293 K. The Ni used was from an electron beam-melted high purity nickel rod. To minimize shape effects, the Ni was swaged and drawn to a 10 mil diameter. The wire was annealed at 900°C for

25 minutes to remove the cold work. The actual sample was 0.2 inches long giving a length to diameter ratio of 20 which makes shape effects negligible. The average dB_o/dz at each temperature was averaged for each field to obtain a best value. The magnitude of the field was then calculated from the two gradients using equation (3). A complete listing of the calibrated values are in the following table.

Table C1. Summary of calibration for the Faraday susceptibility rig

Field	dB_o^2/dz (T^2/m)	dB_o/dz (T/m)	B_o (T)
1	3.202	3.163	0.506
2	5.450	4.155	0.656
3	8.343	5.139	0.812
4	11.774	6.166	0.963
5	15.789	7.088	1.114
6	20.225	7.995	1.265
7	25.006	9.839	1.414
8	29.729	9.529	1.563
9	33.483	9.849	1.700
10	36.844	9.960	1.848

APPENDIX D. DERIVATION OF T_o CURVES

Katgerman[16] has put forth a method of estimating T_o curves from phase diagrams using a regular solution model. The following derivation follows his arguments with the addition of details and special treatments for the La-M alloys.

Normally, T_o curves are used for rapid solidification from a liquid phase to a solid phase. In this study the transformation of interest is a solid to another solid, but the thermodynamics are the same. For convenience the high temperature solid will be called J and the low temperature solid S.

The free energy of the two phases in a binary alloy of elements A and B in a regular solution is given by

$$G^J = (1-x)G_A^J + xG_B^J + \Delta G_{mix}^{id} + Jx(1-x) \qquad \text{(D1)}$$

$$G^S = (1-x)G_A^S + xG_B^S + \Delta G_{mix}^{id} + Sx(1-x) \qquad \text{(D2)}$$

where x is the atomic fraction of metal B; G_A^J, G_B^J are the free energies of the high temperature solids A and B; G_A^S, G_B^S are the free energies of the low temperature solids A and B; ΔG_{mix}^{id} is the ideal free energy change from random mixing; and J and S are interaction enthalpies due to mixing.

At a fixed temperature in the two phase region, equilibrium requirements between J and S mean that

$$\bar{G}_A^J \Big|_{x=x_J} = \bar{G}_A^S \Big|_{x=x_S} \qquad \text{(D3)}$$

and

$$\bar{G}_B^J \Big|_{x=x_J} = \bar{G}_B^S \Big|_{x=x_S} \qquad \text{(D4)}$$

where $\overline{G}$ is the partial molar free energy of A or B with respect to either the solid J or S. x_S and x_J correspond to the low/high temperature solvus compositions (analogous to solidus/liquidus compositions).

For a regular solution

$$(D5) \qquad \overline{G}_B^J = G_B^J + RT\ln(x) + J(1-x)^2$$

$$\overline{G}_B^S = G_B^S + RT\ln(x) + S(1-x)^2$$

and

$$(D6) \qquad \overline{G}_A^J = G_A^J + RT\ln(1-x) + Jx^2$$

$$\overline{G}_A^S = G_A^S + RT\ln(1-x) + Sx^2$$

Combining D5 with D3 and D6 with D4 gives

$$(D7) \qquad 0 = \Delta G_B^{S\rightarrow J} + RT\ln\left(\frac{x_J}{x_S}\right) + J(1-x_J)^2 - S(1-x_S)^2$$

$$(D8) \qquad 0 = \Delta G_A^{S\rightarrow J} + RT\ln\left(\frac{1-x_J}{1-x_S}\right) + Jx_J^2 - Sx_S^2$$

where $\Delta G^{S\rightarrow J}$ is the free energy change corresponding to the transformation from S to J for the pure metals A or B. B, which is the alloying element, does not undergo a phase change for any metal in this study, so $\Delta G_B^{S\rightarrow J} = 0$. Using this simplification and solving D7 and D8 for J and S give

$$(D9) \qquad J = \frac{\Delta G_A^{S\rightarrow J} + RT\ln\left(\frac{1-x_J}{1-x_S}\right) - x_S^2(1-x_S)^{-2}RT\ln\left(\frac{x_J}{x_S}\right)}{x_S^2(1-x_J)^2(1-x_S)^{-2} - x_J^2}$$

and

$$(D10) \qquad S = \frac{\Delta G_A^{S\to J} + RT\ln\left(\frac{1-x_J}{1-x_S}\right) - x_J^2(1-x_J)^{-2}RT\ln\left(\frac{x_J}{x_S}\right)}{x_S^2 - x_J^2(1-x_S)^2(1-x_J)^{-2}}$$

Combining D1 and D2 with $\Delta G_B^{S\to J} = 0$ gives at alloy composition x_o

$$(D11) \qquad x_o = \frac{\Delta G_A^{S\to J}}{S - L}$$

For the La alloys, $\Delta G_A^{S\to J}$ is the fcc β to bcc γ (or the Pr α to β) transformation free energy which is known as a function of temperature. A computer program was used to calculate J and S using x_J and x_S from the appropriate phase diagram, and the subsequent T_o curve is calculated from D11.

APPENDIX E. CALCULATION OF HYPRFINE HEAT CAPACITY

```
      PROGRAM HYPERFINE

      real*8 e1(6),e3(6),b1,b3,c1,c3,d1,d3,x1,x3,chfs,C,T,climit,
     +       Mg_percent
      integer i,j
      character*10 infile
      data a1,a3,p1,p3/0.039834,0.055768,0.009263,0.009815/

      write(6,*) 'Enter input datafile.'
      read(5,*) infile
      write(6,*) 'Enter Mg percentage'
      read(5,*) Mg_percent
      open(unit=2,file=infile,status='old')
      infile(8:10)='hfs'
      open(unit=1,file=infile,status='new')
      do i = 1,6
        e1(i) = (i-3.5)*a1 + p1*((i-3.5)**2 - 35.0/12.0)
        e3(i) = (i-3.5)*a3 + p3*((i-3.5)**2 - 35.0/12.0)
      end do

      do j = 1,600
        read(2,*,err=1000) T, C
        b1=0.0
        c1=0.0
        d1=0.0
        b3=0.0
        c3=0.0
        d3=0.0
        do i = 1,6
          b1 = b1 + exp(-e1(i)/T)
          c1 = c1 + e1(i)*exp(-e1(i)/T)
          d1 = d1 + e1(i)**2*exp(-e1(i)/T)
          b3 = b3 + exp(-e3(i)/T)
          c3 = c3 + e3(i)*exp(-e3(i)/T)
          d3 = d3 + e3(i)**2*exp(-e3(i)/T)
        end do
        x1 = 8314.4 *(b1*d1 - c1**2)/(b1*t)**2
        x3 = 8314.4 *(b3*d3 - c3**2)/(b3*t)**2
        chfs = (1.0 - Mg_percent/100.0) * (0.1854*x1 + 0.2522*x3)
        C = C - chfs
        write(1,10) T, C, C/T, T*T
      end do
 1000 close(unit=1,status='keep')
   10 format(f15.5,2e13.5,f13.5)
      end
```